MIAMI UNIVERSITY
The Graduate School

Certificate For Approving The Dissertation

We hereby approve the Dissertation

Of

Jun-Xia Lu

Candidate for the Degree:

Doctor of Philosophy

_____

Director

Dr. Gary A. Lorigan

_____

Reader

Dr. Christopher A. Makaroff

_____

Reader

Dr. Richard T. Taylor

_____

Reader

Dr. Shouzhong Zou

_____

Graduate School Representative

Dr. Katia Del Rio-Tsonis

ABSTRACT

SOLID-STATE NMR STUDIES OF PHOSPHOLIPID MODEL MEMBRANES AND MEMBRANE-ASSOCIATED MACROMOLECULES

by Jun-Xia Lu

Cholesterol is commonly found in eukaryotic cell membranes and has implicated cellular functions. The synthetic peptide KIGAKI is a peripheral membrane protein that has greater antimicrobial activity than many natural-occurring antimicrobial peptides. Phospholamban (PLB) is an integral membrane protein that regulates the contraction and relaxation cycle of cardiac muscle cells in the heart by binding to Ca-ATPase. The three membrane-associated macromolecules and their interactions with the phospholipid membranes were studied.

The topology of magnetically oriented phospholipid bilayer model membranes (bicelles) was probed using a high-resolution ^{1}H-^{13}C heteronuclear dipolar solid-state NMR spectroscopy (SAMMY). Three different membrane-associated molecules (cholesterol, KIGAKI and PLB) were incorporated into the bicelles. The effects of these molecules on the membrane topology were compared and the SAMMY technique proved to be a fast and promising way to detect the different modes of interaction of these membrane-associated molecules with the bicelle membrane lipids.

The effect of cholesterol on the bicelles was further studied utilizing both solid-state ^{2}H NMR and the EPR spin labeling approach. The results indicate a higher molecular ordering of the lipids and a higher alignment transition temperature of the bicelles in the presence of cholesterol.

Antimicrobial peptides can interact directly with the bacterial membranes and disrupt the membranes without causing any harm to the host mammalian membranes. The interaction mechanism between KIGAKI and different membrane mimics with various

lipid compositions was analyzed using solid-state ^{2}H, ^{31}P NMR and relaxation studies from the membrane perspective. The results suggested a carpet interaction mechanism for KIGAKI.

Uniform ^{15}N-labeled PLB was expressed as a maltose fusion protein in *E. coli.* BL21 (RIL) (DE3) cells and purified with a combination of affinity chromatography and reverse phase C4 HPLC. Solid-state ^{15}N NMR studies concluded that PLB has two populations with different dynamic motions upon reconstitution into POPC bilayers and the difference is in the cytosolic segment of PLB. ^{15}N NMR studies of PLB on oriented membranes also indicated that the transmembrane segment of PLB aligns close to the bilayer normal, whereas the cytosolic segment aligns nearly perpendicular to the bilayer normal and closer to the membrane surface.

Solid-state NMR studies of phospholipid model membranes and membrane-associated macromolecules

A DISSERTATION

Submitted to the Faculty of
Miami University in partial
fulfillment of the requirements
for the degree of
Doctor of Philosophy
Department of Chemistry and Biochemistry

by

Jun-Xia Lu
Miami University
Oxford, Ohio
2007

Dissertation Director: Gary A Lorigan

Table of Contents

List of Tables

List of Figures

Acknowledgements

I would like to express my deepest gratitude to my advisor Gary Lorigan for his unbelievable patience and unconditional support to me for these five years. He brought me into the fascinating field of NMR research, showed me how to do research in a very challenging environment, and encouraged me to pursue my interest and career. He gave me full freedom in my research and only came to me when I was going to fall into a mistake.

I would like to thank Damodaran Achary. I learned so much from him. His knowledge and experience in NMR instrumentation helped me in the SAMMY and relaxation studies. Without him, I wouldn't be able to finish those projects. I also want to thank all of the members in the Lorigan group. Elvis Tiburu, Parish Dave, Thomas Cardon and Nisreen Nusair spent a lot of time introducing me to the research in the lab. I wish to thank Johnson Inbaraj, Shadi Abu-baker, Shidong Chu and Hari Ghimire. The discussion with them was always very helpful for me. Also I want to thank my friends in Dr. Makaroff's lab, Ling Jiang, Meghan, Kinsley, Sriram, Pat, Lara and Xiaohui for letting me work happily in their lab, and explain new concepts to me whenever I ask. Peter Hu and other students in Dr. Crowder's lab also helped me a lot when I came to use the instruments in their lab.

I would like to thank Dr. Blazyk who collaborated with our lab in the antimicrobial peptide project. The research on the antimicrobial peptide is a major part of my dissertation. I thank Dr. Veglia who provided us the phospholamban gene and allowed me to work in his lab for two weeks. I wish to thank my committee professors Dr. Makaroff, Dr. Taylor, Dr. Zou and Dr. Del Rio-Tsonis for listening to my presentations, reading my dissertations and giving wonderful suggestions. Dr. Makaroff also spent time guiding me in the protein expression and purification and writing different letters for me. I thank you for your support.

Finally, I want to thank my parents and grandparents. They always trusted me and felt proud of me. They are the people who nurtured me and taught me who I was and who I will be. I know they sacrificed so much for me to obtain my Ph. D. degree.

Chapter 1

Introduction

1.1 Membrane bilayers and membrane-associated molecules

Complex biological membranes are mainly composed of lipids and membrane associated macromolecules such as cholesterol, proteins etc. (*1*). The lipids are mainly phospholipids, forming a bilayer structure. Membrane-associated macromolecules floating or embedded in the complex bilayer structure modify the membrane properties and functions (*1*). The most common membrane structure model is the fluid-mosaic model (Figure 1.1).

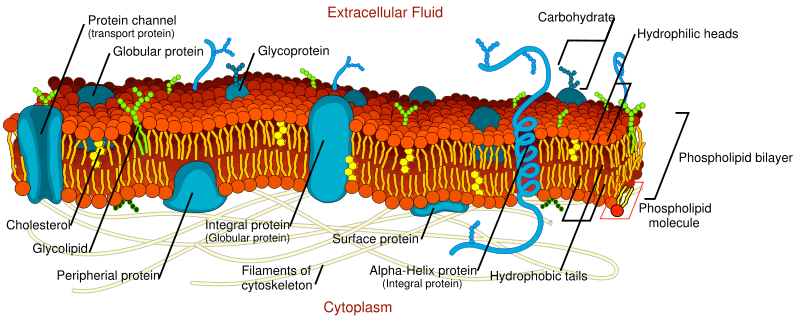

Figure 1.1 Illustration of a cell membrane (by Mariana Ruiz wikipedia.org).

The membrane is fluid and semi-permeable. The lipids in the bilayers are quite dynamic and possess a variety of motions with a hierarchy of correlation times in the nanosecond to microsecond time scale, including the trans-gauche isomerization of lipids acyl chains, the axial rotation of the lipids, and the lateral diffusion of the lipids (*2, 3*). The dynamics of the lipids and the fluidity of the membrane can be adjusted by varying the membrane compositions. For example, cholesterol concentration in the mammalian cell varies depending upon different locations and stages of cell development (*4*). The addition of cholesterol in biological membranes are reported to decrease the close packing of the phospholipids and increase the fluidity of the membrane (*5, 6*).

There are two kinds of membrane-associated proteins. Peripheral membrane proteins associate with the membrane on the bilayer surface, while integral membrane proteins run across the membrane bilayers one or several times. One third of the total number of proteins are membrane proteins and they are responsible for molecular

transportation across the membrane, signal transduction and many other properties and functions of biological systems (*1*). Therefore, membrane proteins have been important drug targets (*7, 8*). In the literature, enormous attention has been focused on the structure of membrane proteins and their interactions between different membrane proteins and with lipid bilayers or other ligands (*9-11*).

1.2 Model membranes

A real biological membrane is quite complicated. The simplified model membrane is often utilized in NMR spectroscopic studies. Model membranes can be made simply by mixing certain phospholipids followed by proper hydration (*12*). Model membranes can be categorized into two kinds: micelles and bilayers (Figure 1.2). Short-chain detergents such as SDS (Sodium dodecyl sulfate) can form the micelle complexes when SDS is above a certain concentration in an aqueous solution (*13*). Micelles have a hydrophobic interior and hydrophilic surface and can help dissolve hydrophobic molecules into the solution (*13*). Micelles are a widely used media for studying the structure of integral membrane proteins in solution NMR, because the fast rotation of micelles can help average the anisotropic NMR interactions and give sharp NMR resonances (*14*). Many membrane protein structures such as G-protein coupled receptors (*15*), potassium channels (*16*), and the major coat protein of filamentous bacteriophage M13 (*17*) etc. have been obtained utilizing solution NMR, where short chain phospholipids such as DPC (dodecylphosphocholine) and SDS are used to form the micelles. It is not always desirable to reconstitute a membrane protein into a micelle for structural studies. Some membrane proteins are not stable in micelles. Micelles have a higher membrane curvature when compared to natural bilayer membranes. Upon reconstitution into the micelles, membrane proteins may not maintain their native structural conformations and function (*14*). Conversely, bilayer model membranes made up of long chain phospholipids have also been used to incorporate membrane proteins since it has a structure much closer to the natural membrane when compared to micelles (Figure 1.2) (*18*). The bilayer can be in the form of vesicles or aligned membranes on a glass plate substrate depending on the method used to make the sample. Bilayers have reduced motion with a dynamic range perfect for solid-state NMR studies (*19-21*).

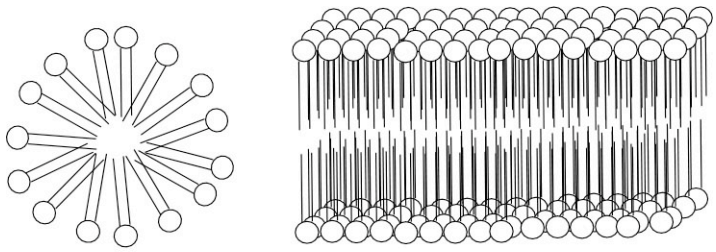

(a) Micelle (b) Bilayers

Figure1.2 Schematic drawing of model membrane structures.

Another unique membrane system (Bicelles) has also emerged for protein structure studies (*22*). Bicelles are made of both long chain phospholipids and short chain phospholipids with combined characteristics of both micelles and bilayers (*23, 24*). They have relatively fast tumbling motion and high water content similar to micelles (*25*). The bilayer structure segment of bicelles facilitates the reconstitution of the membrane protein into the native conformation. Bicelles undergo various temperature-dependent phase transitions. Bicelles can be aligned only above the gel to liquid-crystalline phase transition temperature (T_m) (*26, 27*), which provides another approach to obtain high-quality NMR spectra (*24*). Bicelles have been a nice media with a dynamic range good for both solution and solid-state NMR studies (*22, 28, 29*).

1.3 Solution NMR and solid-state NMR

NMR spectroscopy studies the nucleus with a non-zero nuclear spin value ($I \neq 0$). In a static magnetic field B_0, the nucleus interacts with B_0 and the nuclear energy level will split. This is called the nuclear Zeeman interaction. The energy separation between two continuous energy levels determines the corresponding frequency (Larmor frequency). Additionally, the nucleus also experiences magnetic and electric fields originating from the nuclear electronic structure and nearby nuclei. These local fields modify the nuclear Zeeman interaction and cause a shift in the frequency in a NMR spectrum. The chemical shielding of the nucleus ($\hat{H}_{CS}$), the nuclear dipole-dipole coupling ($\hat{H}_{DD}$), the through bond scalar coupling ($\hat{H}_J$), and the quadrupolar interaction ($\hat{H}_Q$) are the four major nuclear spin interactions that modify the nuclear Zeeman

interaction ($\hat{H}_{Zeeman}$) (*30*). In the absence of a radio frequency pulse, the total nuclear spin interaction Hamiltonian can be expressed as (1):

$$\hat{H}_{total} = \hat{H}_{Zeeman} + \hat{H}_{CS} + \hat{H}_{DD} + \hat{H}_{J} + \hat{H}_{Q} \quad (1)$$

Chemical shielding, nuclear dipole-dipole coupling, through bond scalar coupling and quadrupolar interaction are also called the internal nuclear spin interactions since they are originated from the sample itself. These interactions are molecular orientation dependent. In solid-state NMR, the through bond scalar coupling is usually not observed, because the scalar coupling is small when compared to other internal nuclear spin interactions.

1.3.1 The molecular orientation dependence of internal nuclear spin interactions

1) Chemical shielding anisotropy

Chemical shielding is caused by the electron cloud surrounding the nuclear spin. The external magnetic field B_0 induces currents in the electron clouds in the molecule, which will generate an induced field. The nuclear spin senses the combined effect of these two magnetic fields. Chemical shielding is related to the molecular structure. The chemical bonds and the electronic environment are not the same in different directions within the molecule. Therefore, chemical shielding is anisotropic and orientation dependent. The chemical shielding tensor has three principle components σ_{11}, σ_{22}, and σ_{33}. The chemical shift of a nucleus (υ_{CS}) in a specific orientation can be defined by:

$$\upsilon_{CS} = \sigma_{11}\cos^2\phi\sin^2\theta + \sigma_{22}\sin^2\phi\sin^2\theta + \sigma_{33}\cos^2\theta \quad (2)$$

where ϕ and θ are angles relating the principle axes of the chemical shielding tensor to the direction of the magnetic field B_0 (Figure 1.3(A)).

2) Dipolar coupling

A nuclear spin can also feel a magnetic field caused by a nearby nuclear spin. This is the source of the direct dipolar interaction. The dipole-dipole coupling d_{ij} is related to the distance between the two nuclei r_{ij} and the angle Θ_{ij} between the internuclear vector connecting the two nuclei and the external magnetic field (3).

$$d_{ij} \propto \frac{\left(3\cos^2\Theta_{ij} - 1\right)}{r_{ij}^3} \quad (3)$$

The dipolar coupling is equal to zero when the angle $\Theta_{ij} \cong 54.74°$(the magic angle).

3) Quadrupolar interaction

A nucleus with a spin > ½ possesses an electric quadrupole moment, which interacts strongly with the electric field gradients generated by the surrounding electron clouds. For a given nucleus the electric quadrupolar interaction is directly proportional to the electric field gradient. The electric field gradient is determined by the molecular structure, which is anisotropic. Thereby, the electric quadrupolar interaction has orientation dependence (*30*).

In the solution state, the rapid molecular isotropic tumbling motion averages these internal spin interactions, resulting in a relatively sharp NMR resonance peak. In solid-state NMR, the broad resonance line shape is often observed because of all these internal spin interactions mentioned above. The static powder sample has a distribution of molecular orientations. Molecules in different orientations give resonances at slightly different frequencies, since spin interactions are orientation dependent. Therefore, the NMR spectrum of a static powder sample is a superposition of all these peaks. Although the broad spectra make the interpretation a demanding task, the static powder spectra provide additional molecular structure information because the internal spin interactions depend upon the structure and orientation of the molecules with respect to the magnetic field. Furthermore, solid-state NMR is a method of choice to study samples such as zeolites, membrane proteins and bilayer membranes, which are solid or gel-like and not applicable to solution NMR studies.

1.3.2 High resolution solid-state NMR

There are several strategies to improve solid-state NMR resolution. For the static powder sample, high-resolution solid-state NMR spectra can be achieved by aligning all the sample molecules to a single orientation (*31*). For example, the orientations of the ^{15}N chemical shift tensor principal components σ_{11}, σ_{22}, σ_{33} in the molecular frame (Figure 1.3(A)) has been determined from model peptides and verified in the protein studies, where σ_{33} is almost aligned with the N-H bond (~17° angle), σ_{11} is about 20° from the peptide plane, and σ_{22} is perpendicular to σ_{11} and σ_{33} (*32*). A broad powder spectrum will be obtained for a site-specific ^{15}N-labeled peptide sample incorporated into phospholipid

bilayers, indicating a random orientation of the ^{15}N nucleus with respect to the static magnetic field B_0 (Figure 1.3(B) top). However, the sharp resonance spectra can be achieved upon incorporation of the peptide into magnetically oriented bicelle model membranes or mechanically oriented bilayer model membranes on glass plates (*33*). If B_0 is along the σ_{33} direction, the solid-state ^{15}N NMR spectrum displays a resonance near the σ_{33} position (equation (2), Figure 1.3(B) bottom). In a peptide with a single helical structure, the orientation of N-H bonds is very close to the peptide helical axis. Since σ_{33} is almost aligned with the N-H bond, a ^{15}N NMR spectrum with a sharp resonance near the σ_{33} position indicates a helix structure aligned parallel with respect to the magnetic field. Conversely, if B_0 is perpendicular to the σ_{33} direction and along the σ_{11}/σ_{22} plane, the ^{15}N NMR spectrum displays a sharp resonance near the σ_{11} and σ_{22} position (Figure 1.3(B) middle) (*34*).

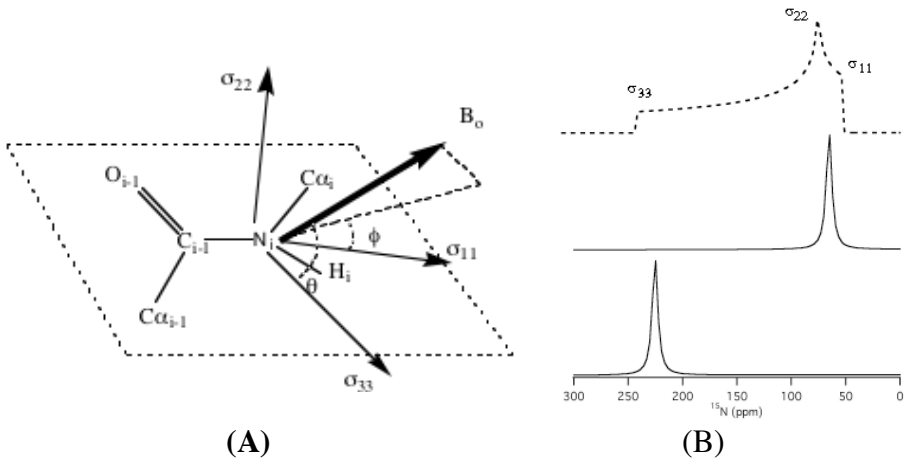

(A) (B)

Figure 1.3 (A) Representation of the ^{15}N CSA principal axis in the molecular frame, ϕ is the angle between the project of B_0 on the σ_{11}/σ_{22} plane and σ_{11}, and θ is the angle between B_0 and σ_{33}. (B) Simulated ^{15}N solid-state NMR spectra of backbone ^{15}N-labeled peptide. The dotted line represents a ^{15}N solid-state NMR spectrum of random oriented peptide in a hydrated lipid bilayer. The solid line represents ^{15}N spectra of peptides in oriented bilayer samples (*35*).

Another approach to obtain high resolution solid-state NMR spectra is to mechanically rotate the sample at a magic-angle of 54.74° (kHz speed). The rotation can

mimic the effect of isotropic molecular motion. It can average out the chemical shielding anisotropic interactions to the isotropic positions ($\upsilon_{iso} = (\sigma_{11} + \sigma_{22} + \sigma_{33})/3$) and reduce the dipolar coupling interaction significantly, improving the solid-state NMR spectral resolution (*36*). For example, ^{31}P nuclei in different lipid headgroups have very close chemical shift isotropic positions and a broad chemical shielding anisotropy, making it impossible to distinguish them in the static solid-state NMR spectrum. Magic-angle sample spinning was carried out to give high-resolution ^{31}P NMR spectra and to distinguish different ^{31}P nuclei in the lipid headgroups in Chapters 4 and 5.

1.3.3 Probing the molecular motions utilizing solid-state NMR

One of the most important advantages of NMR is its ability to probe molecular motions, over a wide range of timescales. The orientation dependence and molecular motion dependence of the spin interactions are correlated. A fast molecular motion usually suggests an average of the spin interactions in all directions (*ergodic hypothesis*) (*37*).

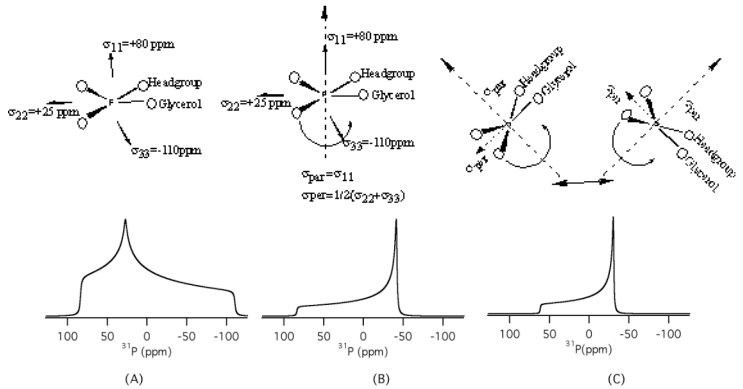

Figure 1.4 Simulated ^{31}P NMR spectra for the phosphodiester moiety of a membrane describing various motional states, with the phosphodiester (A) static; (B) ordered with rapid axial rotation; and (C) disordered with rapid axial rotation. In the case of motional averaging of the chemical-shift tensor due to axial symmetry, σ_{par} refers to the chemical shift for the external magnetic field parallel to the unique axis, and σ_{per} to that for the field in the equatorial plane (*38*).

Let's first consider the lipid headgroups ^{31}P chemical shielding interaction as an example (Figure 1.4). If the lipids are in a solid dry powder state, the ^{31}P NMR displays a

spectrum with inhomogeneous broadening (Figure 1.4A). If the lipids form the hydrated bilayer membrane structure, the lipid molecules will have rapid axial rotation along the long molecular axis and relatively restricted motions in other directions such as molecular diffusion. In this case the ^{31}P NMR spectrum displays a wide horn shape, indicating an axial symmetry (Figure 1.4B). However, if the hydration is increased or smaller size vesicles are formed, the lipids will have faster molecular diffusion motions, the ^{31}P NMR spectrum will become narrower (Figure 1.4C). In extreme cases when small vesicles or micelles are formed, the fast molecular tumbling motion will average the ^{31}P NMR resonance to isotropic Lorentzian lineshapes.

The molecular motions also modulate the dipolar coupling values and the quadrupolar splittings. In the case of fast isotropic molecular motions, the dipolar coupling values are averaged to zero; and the quadrupolar interactions are also averaged to zero to a first approximation when the nuclear quadrupolar interaction is not too large. The dynamics of the phospholipid membranes were studied in Chapters 2 and 3. Chapter 2 probed the perturbation of the membrane-associated molecules to bicelles by observing changes in the lipids ^{13}C-^{1}H dipolar coupling values in the aligned bicelle membranes. Chapter 3 investigated the bicelle lipids molecular ordering utilizing perdeuterated lipids and ^{2}H quadrupolar interaction.

Molecular motions have a range of timescales. The molecular vibrations can be observed in the picosecond range while molecular macroscopic diffusion could take many seconds (*37*). Figure 1.5 shows a summary of NMR timescales in comparison to the timescales of selected lipids and protein motions. NMR lineshape perturbations usually are sensitive to motions in the millisecond to microsecond timescale, which only covers a relatively small dynamic range (*2*). NMR spin-lattice relaxation, on the other hand, is sensitive to faster molecular motions in nanosecond to picosecond range (*2*). In a thermal equilibrium state, the populations of spins are given by Boltzmann distribution. In a NMR experiment, radio frequency pulses disturb the equilibrium of the system. Relaxation is the process by which equilibrium is regained through interaction of the spin system with the molecular environment (*37*). Relaxation is determined by the transition probabilities between different energy states. Spin transitions are facilitated by fluctuating local magnetic fields and different nuclear spin interactions (mentioned

above); therefore, NMR spin transitions are related to the molecular motions (*37*). NMR relaxation has been used in this dissertation to study the membrane lipids molecular motion as complementary to the ^{31}P and ^{2}H NMR lineshape perturbation study.

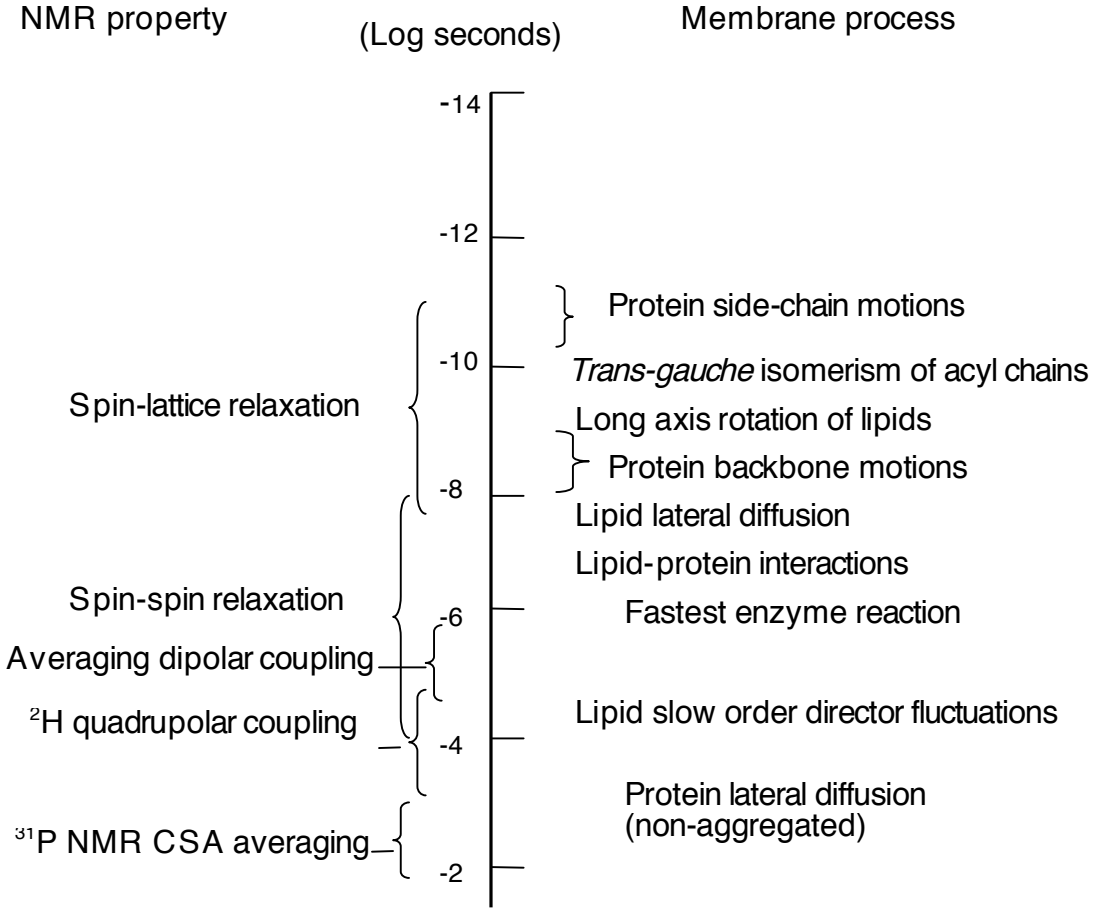

Figure 1.5 Summary of different timescales of NMR experiment and membrane motions (*2, 19*).

1.4 Outline of the research

Bicelles have been demonstrated to be useful model membrane systems to study membrane proteins (*28, 39, 40*). Therefore, it attracts great attention to understand its structural and dynamic properties (*22*) (*41*). The membrane topology of bicelles in the liquid-crystalline phase was studied in Chapter 2 using high-resolution ^{1}H-^{13}C heteronuclear dipolar solid-state NMR spectroscopy (*42*).

The membrane topology of the bicelles was compared upon incorporation of three different membrane-associated molecules (cholesterol, the peripheral membrane peptide

KIGAKI (full sequence KIGAKIKIGAKIKIGAKI) and the integral membrane protein phospholamban) individually to understand the perturbations of these molecules to the bicelle model membrane system. Chapter 2 has been published and was taken from the paper "Probing Membrane Topology by ^{1}H-^{13}C Heteronuclear Dipolar Solid-State NMR Spectroscopy" *J. Magn. Reson.* (2006) 178, 283-287 without further modification.

Cholesterol plays an important role in modifying the membrane fluidity and lipid dynamics (*5, 15*). The effects of cholesterol on bicelles were further analyzed utilizing both solid-state ^{2}H NMR and EPR spectroscopy in Chapter 3. A combination of both techniques can provide more comprehensive information since solid-state NMR and EPR spectroscopy are sensitive to molecular motions with different time scales (*43*). Chapter 3 has been published and was taken from the paper "The Effects of Cholesterol on Magnetically Aligned Phospholipid Bilayers: A Solid-State NMR and EPR Spectroscopy Study" *J. Magn. Reson.* (2004) 168: 18-30 without modification.

Bilayer model membrane is also commonly utilized in the solid-state NMR study of membrane proteins. Chapters 4, 5 and 6 utilized bilayer vesicles and mechanically oriented bilayer model membranes.

Antimicrobial peptides can interact directly with the bacterial membranes and disrupt the membranes at a concentration without causing any harm to the host mammalian membranes (*44*). Bacterial membranes and mammalian membranes are significantly different in their lipids compositions (*44*). Antimicrobial peptides interact directly with biological membranes without requirements for specific receptors on the membranes. Three major models have been proposed to describe the interaction of the antimicrobial peptide with the membranes (*45*). They are the barrel stave model, the toroidal wormhole model, and the carpet model (Figure 1.6) (*45, 46*). The antimicrobial peptide KIGAKI has demonstrated a higher antimicrobial activity than the naturally occurring antimicrobial peptide magainin and an increased selectivity with bacterial membranes (*47*). In Chapters 4 and 5, ^{2}H and ^{31}P solid-state NMR and relaxation studies are applied to distinguish the interaction mechanism between the antimicrobial peptide KIGAKI and model bilayer membranes with different lipid compositions. Although the electrostatic interaction between cationic peptides and anionic bacterial membranes was

indicated as an important factor in the KIGAKI activity, our results further proved that the synergistic effects of the two main lipids PE and PG in the bacterial membranes

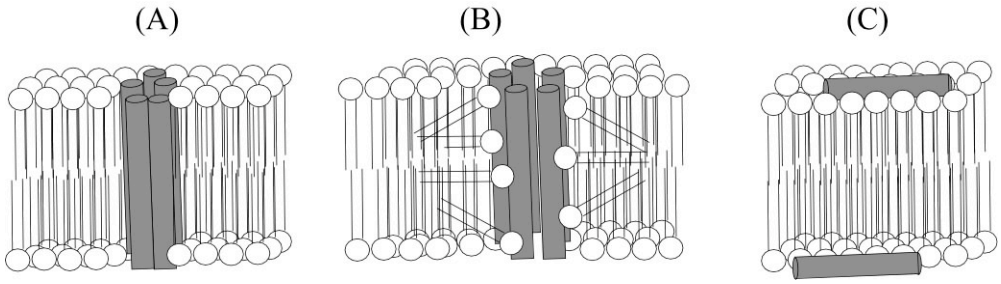

Figure 1.6 Antimicrobial peptide interaction mechanisms: barrel stave model (A), toroidal wormhole model (B) and carpet model (C) (*48*).

should not be neglected. KIGAKI may act as a peripheral membrane protein and disrupt the bacterial membrane using the carpet mechanism (Figure 1.6(C)). Chapter 4 was taken from the paper "Solid-State NMR Relaxation Studies of the Interaction Mechanism of Antimicrobial Peptides with Phospholipid Bilayer Membranes" *Biochemistry* (2005) 44, 10208-10217. Chapter 5 was published as "Exploring membrane selectivity of the antimicrobial peptide KIGAKI using Solid-State NMR spectroscopy" *Biochim. Biophys. Acta* (2006) 1758, 1303-1313.

Phospholamban (PLB) is a 52 amino-acid transmembrane protein that regulates the contraction/relaxation cycle of cardiac muscle cells in the heart by binding to Ca-ATPase (*49*). Although many studies have reported PLB structures, no consensus results have been obtained so far (*50, 51*). In Chapter 6, solid-state ^{15}N NMR studies on uniform ^{15}N-labeled PLB upon reconstitution into POPC model bilayers clearly indicated that PLB has two conformational populations giving one ^{15}N isotropic resonance and one broad ^{15}N anisotropic resonance. Comparing the solid-state ^{15}N NMR results obtained using ^{15}N site-specific labeled PLB, our research suggests that the cytosolic segment of PLB has a dynamic component besides a dominant rigid component. Solid-state ^{15}N NMR studies of PLB reconstituted into oriented bilayer model membranes were also carried out. The high-resolution NMR spectra of uniform ^{15}N-labeled PLB obtained from the oriented sample clearly demonstrated that PLB has two segments, one parallel and the other perpendicular with respect to the bilayer normal. The dynamic and orientation

studies in this research provide very useful information towards solving the PLB structure in a native-like bilayer membrane. Results in this chapter were used partially in two articles "The side-chain and backbone dynamics of phospholamban in POPC bilayers utilizing ^{2}H and ^{15}N solid-state NMR spectroscopy" *Biochemistry* (in progress) and "The structural topology of wild-type phospholamban in oriented bilayers using ^{15}N solid-state NMR spectroscopy" *Protein Science* (in progress).

1.5 References

(1) Alberts, B., Johnson, A., Lewis, J., Roberts, K., and P., W. (2002) *Molecular biology of the cell*, 4th ed., Garland Science, New York.

(2) Watts, A. (1998) Solid-state NMR approaches for studying the interaction of peptides and proteins with membranes. *Biochim. Biophys. Acta-Rev. on Biomem. 1376*, 297-318.

(3) Blume, A. (1993) Dynamic Properties, in *Phospholipids handbook* (Cevc, G., Ed.) pp 988, Marcel Dekker, INC., New York.

(4) Ohvo-Rekila, H., Ramstedt, B., Leppimaki, P., and Slotte, J. P. (2002) Cholesterol interactions with phospholipids in membranes. *Prog. Lipid Res. 41*, 66-97.

(5) Chiu, S. W., Jakobsson, E., Mashl, J., and Scott, H. L. (2002) Cholesterol-induced modifications in lipid bilayers: a simulation study. *Biophys. J. 83*, 1842-1853.

(6) Dufourc, E. J., Parish, E. J., Chitrakorn, S., and Smith, I. C. P. (1984) Structural and dynamical details of cholesterol lipid interaction as revealed by deuterium NMR. *Biochemistry 23*, 6062-6071.

(7) Hopkins, A. L., and Groom, C. R. (2002) The druggable genome. *Nature Reviews Drug Discovery 1*, 727-730.

(8) Hopkins, A. L., Polinsky, A., and Anthony, W. (2006) Knowledge and Intelligence in Drug Design, in *Annu. Rep. Med. Chem.* pp 425-437, Academic Press.

(9) Hilty, C., Wider, G., Fernandez, C., and Wuthrich, K. (2004) Membrane protein-lipid interactions in mixed micelles studied by NMR spectroscopy with the use of paramagnetic reagents. *Chembiochem 5*, 467-473.

(10) Epand, R. M. (1998) Lipid polymorphism and protein-lipid interactions. *Biochim. Biophys. Acta 1376*, 353-368.

(11) Doyle, D. A., Cabral, J. M., Pfuetzner, R. A., Kuo, A. L., Gulbis, J. M., Cohen, S. L., Chait, B. T., and MacKinnon, R. (1998) The structure of the potassium channel: Molecular basis of K+ conduction and selectivity. *Science 280*, 69-77.

(12) Prosser, R. S., Losonczi, J. A., and Shiyanovskaya, I. V. (1998) Use of a novel aqueous liquid crystalline medium for high- resolution NMR of macromolecules in solution. *J. Am. Chem. Soc. 120*, 11010-11011.

(13) Sanders, C. R., and Landis, G. C. (1995) Reconstitution of membrane-proteins into lipid-rich bilayered mixed micelles for NMR-studies. *Biochemistry 34*, 4030-4040.

(14) Sanders, C. R., Hoffmann, A. K., Gray, D. N., Keyes, M. H., and Ellis, C. D. (2004) French swimwear for membrane proteins. *ChemBioChem 5*, 423-426.

(15) Yeagle, P. L., Choi, G., and Albert, A. D. (2001) Studies on the structure of the G-protein-coupled receptor rhodopsin including the putative G-protein binding site in unactivated and activated forms. *Biochemistry 40*, 11932-11937.

(16) Yu, L., Sun, C., Song, D., Shen, J., Xu, N., Gunasekera, A., Hajduk, P. J., and Olejniczak, E. T. (2005) Nuclear magnetic resonance structural studies of a potassium channel-charybdotoxin complex. *Biochemistry 44*, 15834-15841.

(17) Papavoine, C. H., Christiaans, B. E., Folmer, R. H., Konings, R. N., and Hilbers, C. W. (1998) Solution structure of the M13 major coat protein in detergent micelles: a basis for a model of phage assembly involving specific residues. *J. Mol. Biol. 282*, 401-419.

(18) Hallock, K. J., Wildman, K. H., Lee, D. K., and Ramamoorthy, A. (2002) An innovative procedure using a sublimable solid to align lipid Bilayers for solid-state NMR studies. *Biophys. J. 82*, 2499-2503.

(19) Watts, A. (1998) Solid-state NMR approaches for studying the interaction of peptides and proteins with membranes. *Biochim. Biophys. Acta 1376*, 297-318.

(20) Lu, J., Damodaran, K., Blazyk, J., and Lorigan, G. A. (2005) Solid-state nuclear magnetic resonance relaxation studies of the interaction mechanism of

antimicrobial peptides with phospholipid bilayer membranes. *Biochemistry 44*, 10208-10217.

(21) Dave, P. C., Tiburu, E. K., Damodaran, K., and Lorigan, G. A. (2004) ^{31}P and ^{2}H Solid-State NMR Spectroscopic Studies of the Transmembrane Domain of the Membrane-Bound Protein Phospholamban. *Biophys. J. 86*, 1564-1573.

(22) Sanders, C. R., and Prosser, R. S. (1998) Bicelles: a model membrane system for all seasons? *Structure 6*, 1227-1234.

(23) Sanders, C. R., and Schwonek, J. P. (1992) Characterization of magnetically orientable bilayers in mixtures of dihexanoylphosphatidylcholine and dimyristoylphosphatidylcholine by solid state NMR. *Biochemistry 31*, 8898-8905.

(24) Vold, R. R., and Prosser, R. S. (1996) Magnetically oriented phospholipid bilayered micelles for structural studies of polypeptides. Does the idea bicelle exist? *J. Magn. Reson. 113*, 267-271.

(25) Vold, R. R., Prosser, R. S., and Deese, A. J. (1997) Isotropic solutions of phospholipid bicelles: A new membrane mimetic for high-resolution NMR studies of polypeptides. *J. Biomol. NMR 9*, 329-335.

(26) Whiles, J. A., Brasseur, R., Glover, K. J., Melacini, G., Komives, E. A., and Vold, R. R. (2001) Orientation and effects of mastoparan X on phospholipid bicelles. *Biophys. J. 80*, 280-293.

(27) Cardon, T. B., Tiburu, E. K., and Lorigan, G. A. (2003) Magnetically aligned phospholipid bilayers in weak magnetic fields: optimization, mechanism, and advantages for X-band EPR studies. *J. Magn. Reson. 161*, 77-90.

(28) Bax, A., and Tjandra, N. (1997) High-resolution heteronuclear NMR of human ubiquitin in an aqueous liquid crystalline medium. *J. Biomol. NMR 10*, 289-292.

(29) Tiburu, E. K., Moton, D. M., and Lorigan, G. A. (2001) Development of magnetically aligned phospholipid bilayers in mixtures of palmitoylstearoylphosphatidylcholine and dihexanoylphosphatidylcholine by solid-state NMR spectroscopy. *Biochim. Biophys. Acta-Biomembr. 1512*, 206-214.

(30) Haeberlen, U. (1976) *High Resolution NMR in Solids: Selective Averaging*, Academic Press. INC, New York.

(31) Opella, S. J., and Waugh, J. S. (1977) Two-dimensional carbon-13 NMR of highly oriented polyethylene. *J. Chem. Phys. 66*, 4919-24.

(32) Wu, C. H., Ramamoorthy, A., Gierasch, L. M., and Opella, S. J. (1995) Simultaneous characterization of the amide 1H chemical shift, 1H-15N dipolar, and 15N chemical shift interaction tensors in a peptide bond by three-dimensional solid-state NMR spectroscopy. *J. Am. Chem. Soc. 117*, 6148-6149.

(33) Opella, S. J., and Marassi, F. M. (2004) Structure determination of membrane proteins by NMR spectroscopy. *Chem. Rev. 104*, 3587-3606.

(34) Kovacs, F. A., Denny, J. K., Song, Z., and R., Q. J. (2000) Helix tilt of the M2 transmembrane peptide from Influenza A visrus. *J. Mol. Biol. 295*, 117-125.

(35) Valentine, K. G., Mesleh, M. F., Opella, S. J., Ikura, M., and Ames, J. B. (2003) Structure, topology, and dynamics of myristoylated recoverin bound to phospholipid bilayers. *Biochemistry 42*, 6333-6340.

(36) Mehring (1983) *Principles of high resolution NMR in solids*, Springer-Verlag, New York.

(37) Levitt, M. H. (2001) *Spin Dynamics:Basics of Nuclear Magnetic Resonance*, John Wiley & Sons, Chichester, NewYork.

(38) Gorenstein, D. G. (1984) *Phosphorus-31 NMR:principles and applications*, Academic Press, Orlando, Fla.

(39) Howard, K. P., and Opella, S. J. (1996) High-resolution solid-state NMR spectra of integral membrane proteins reconstituted into magnetically oriented phospholipid bilayers. *J. Magn. Reson., Ser. B 112*, 91-94.

(40) De Angelis, A. A., Nevzorov, A. A., Park, S. H., Howell, S. C., Mrse, A. A., and Opella, S. J. (2004) High-resolution NMR spectroscopy of membrane proteins in aligned bicelles. *J. Am. Chem. Soc. 126*, 15340-15341.

(41) Vold, R. R., and Prosser, R. S. (1996) Magnetically oriented phospholipid bilayered micelles for structural studies of polypeptides. Does the ideal bicelle exist? *J. Magn. Reson. B. 113*, 267-271.

(42) Nevzorov, A. A., and Opella, S. J. (2003) A "Magic Sandwich" pulse sequence with reduced offset dependence for high-resolution separated local field spectroscopy. *J. Magn. Reson. 164*, 182-186.

(43) Seelig, J., and Niederberger, W. (1974) Two pictures of a lipid bilayer. A comparison between deuterium label and spin-label experiments. *Biochemistry 13*, 1585-1588.

(44) Blazyk, J., Wiegand, R., Klein, J., Hammer, J., Epand, R. M., Epand, R. F., Maloy, W. L., and Kari, U. P. (2001) A novel linear amphipathic beta-sheet cationic antimicrobial peptide with enhanced selectivity for bacterial lipids. *J. Biol. Chem. 276*, 27899-27906.

(45) Oren, Z., and Shai, Y. (1998) Mode of action of linear amphipathic alpha-helical antimicrobial peptides. *Biopolymers 47*, 451-463.

(46) Shai, Y., and Oren, Z. (2001) From "carpet" mechanism to de-novo designed diastereomeric cell-selective antimicrobial peptides. *Peptides 22*, 1629-1641.

(47) Jin, Y., Mozsolits, H., Hammer, J., Zmuda, E., Zhu, F., Zhang, Y., Aguilar, M. I., and Blazyk, J. (2003) Influence of tryptophan on lipid binding of linear amphipathic cationic antimicrobial peptides. *Biochemistry 42*, 9395-9405.

(48) Strandberg, E., and Ulrich, A. S. (2004) NMR methods for studying membrane-active antimicrobial peptides. *Concepts Magn. Resonance A 23A*, 89-120.

(49) Simmerman, H. K., J.H. Collins, J.L. Theibert, A.D. Wegener, and L.R. Jones. (1986) Sequence analysis of phospholamban: identification of phosphorylation sites and two major structural domains. *J. Biol. Chem. 261*, 13333-13341.

(50) Oxenoid, K., and Chou, J. J. (2005) The structure of phospholamban pentamer reveals a channel-like architecture in membrane. *Proc. Natl. Acad. Sci. USA 102*, 10870-10875.

(51) Traaseth, N. J., Buffy, J. J., Zamoon, J., and Veglia, G. (2006) Structural dynamics and topology of phospholamban in oriented lipid bilayers using multidimensional solid-state NMR spectroscopy. *Biochemistry 45*, 13827-13834.

Chapter 2

Probing Membrane Topology by High-Resolution ^{1}H-^{13}C Heteronuclear Dipolar Solid-State NMR Spectroscopy

Lu, J.X., Damodaran, K., and Lorigan, G. A., "Probing Membrane Topology by ^{1}H-^{13}C Heteronuclear Dipolar Solid-State NMR Spectroscopy" *J. Magn. Reson.* (2006) 178, 283-287.

2.1 Abstract

Membrane topology changes introduced by the association of biologically pertinent molecules with membranes were analyzed utilizing the ^{1}H-^{13}C heteronuclear dipolar solid-state NMR spectroscopy technique (SAMMY) on magnetically aligned phospholipid bilayers (bicelles). The phospholipids ^{1}H-^{13}C dipolar coupling profiles lipid motions at the headgroup, glycerol backbone, and the acyl chain region. The transmembrane segment of phospholamban, the antimicrobial peptide $(KIGAKI)_3$ and cholesterol were incorporated into the bicelles, respectively. The lipids ^{1}H-^{13}C dipolar coupling profiles exhibit different shifts in the dipolar coupling contour positions upon the addition of these molecules, demonstrating a variety of interaction mechanisms exist between the biological molecules and the membranes. The membrane topology changes revealed by the SAMMY pulse sequence provide a complete screening method for analyzing how these biologically active molecules interact with the membrane.

2.2 Introduction

Functioning cell membranes contain a large variety of biological additives. The interaction between biologically pertinent molecules and lipids plays a key role in modulating the physical characteristics of membranes, and directly determines the activity of cell membranes (*1, 2*). The most common method for probing these interactions utilizing solid-state NMR techniques has been a combination of both ^{2}H and ^{31}P NMR spectroscopy. In this communication, a recently reported high-resolution heteronuclear dipolar solid-state NMR spectroscopy technique (SAMMY) (*3*) is applied to magnetically aligned phospholipid bilayers (bicelles) (*4*) to detect and characterize natural abundant ^{13}C lipid motion perturbations induced by the association of biological molecules with the membrane bilayer.

The dipole-dipole interaction between two nuclei is related to the internuclear distance, the orientation of the dipolar interaction tensor with respect to the magnetic field, and the motion of the molecule. For phospholipid molecules in a hydrated bilayer sample, the heteronuclear dipolar coupling interaction between ^{13}C and the covalently bonded ^{1}H reflects the ordering and the motional rates of the individual segments of the lipid molecules (*5*). The addition of biologically pertinent molecules to membrane bilayers modulate the ordering and motions of the phospholipids (*5*). Therefore, the ^{1}H-^{13}C dipolar coupling of phospholipid bilayers reflects the interaction between the lipids and the molecules, and elucidates pertinent membrane-protein topology information.

In order to obtain a high-resolution solid-state NMR spectrum of a randomly dispersed bilayer sample, magic-angle spinning of the sample at relatively high speeds is needed which will simultaneously attenuate the anisotropic dipolar interactions. These dipolar interactions can be ascertained utilizing dipolar recoupling pulse schemes, such as FSLG-CP (*6, 7*), R-PDLF (*8*), DIPSHIFT (*9*) at a specific sample spinning speed. Alternatively, the PISEMA or SAMMY solid-state NMR pulse technique on an oriented membrane sample provides a direct way to obtain a high-resolution two-dimensional ^{1}H-^{13}C heteronuclear dipolar couplings (*10*). The SAMMY pulse sequence was chosen because it has a better signal to noise ratio, more reliable scale factors for all resonances and is much easier to setup, when compared to the PISEMA sequence (*3*). The bicelle alignment method was used because the membrane system can be easily aligned in a

solution NMR spectrometer above the gel to liquid crystalline phase transition temperature. The aligned bicelles make high-resolution NMR spectra possible without spinning the sample at the magic angle (*11*). Furthermore, the fully hydrated bicelles provide an environment close to physiologically relevant conditions (*4*). The experiments were carried out on a standard 500 MHz narrow bore using a soft SAMMY pulse sequence that does not require a high power amplifier, wide bore magnet, and magic-angle spinning capability. Thus, this method is potentially widely applicable to a wide range of users.

2.3 Results and discussion

Figure 2.1 exhibits the two-dimensional ^{1}H-^{13}C dipolar coupling/^{13}C chemical shift spectrum of aligned DMPC/DHPC bicelles with a DMPC to DHPC molar ratio of 3.5 at 37 °C utilizing the SAMMY pulse sequence. The Hartmann-Hahn contact time was 1 ms. The ^{1}H 90° pulse was 10.1 μs and the recycle delay was 3 s. The one-dimensional ^{13}C chemical shift spectrum of the same bicelle sample (shown at the top) was obtained separately using a standard cross-polarization sequence. The assignment of the ^{13}C chemical shifts of phospholipids is based on previous studies utilizing magic-angle sample spinning (MAS) NMR spectroscopy for a randomly dispersed bilayer sample (*6, 12*) and Sanders assignment on bicelles (*13*). The ^{13}C chemical shift values for the lipid acyl chain region are consistent with those obtained for the bilayers. However, at the lipids headgroup and glycerol regions the bicelles exhibit a slight shift in peak positions when compared to the bilayers. The C_{β}, GC_1 and GC_3 peaks become crowded together with much lower intensity for glycerol groups. It is difficult to distinguish between the GC_1 and GC_3 peaks. The spectrum of the aligned sample exhibits excellent linewidths with comparable spectral resolution as that of the randomly oriented sample. For bicelles, the bilayer normal of phospholipids are aligned with its long molecular axis perpendicular to the static magnetic field (*11, 14*).

In the one-dimensional ^{13}C spectrum, the ^{13}C chemical shifts originating from individual carbons of less abundant DHPC molecules may overlap with those from DMPC and affect the spectral resolution. In this research, no significant DHPC contribution was observed in the ^{13}C chemical shift dimension. However, in the two-

dimensional SAMMY spectrum, some ^{1}H-^{13}C dipolar coupling contours with small splitting values were observed, which is probably caused by DHPC molecules with relatively faster motion than DMPC molecules (*14*). It is possible in the future to use fully deuterated DHPC in preparing the bicelle samples to diminish the DHPC ^{13}C signals obtained by ^{1}H-^{13}C cross-polarization and reduce the number of ^{1}H-^{13}C dipolar coupling contours near the center of the SAMMY spectrum.

A number of doublets were observed in the ^{13}C chemical shift dimension in the two-dimensional SAMMY spectrum. These splittings were absent for the randomly dispersed bilayer sample obtained under MAS conditions. This observation is consistent with previous reports by Sanders (*13*). They explained that the splittings are introduced by the dipolar coupling of the isotopically dilute carbons to the headgroup ^{31}P, which is averaged out by the sample spinning at the magic angle for randomly oriented samples. The doublet at around 73 ppm, 67 ppm and 57 ppm exhibits the same apparent ^{1}H-^{13}C dipolar coupling values. These results confirm that each doublet originates from the same ^{13}C nucleus. Conversely, another doublet at around 174 ppm, corresponding to the DMPC carbonyl carbon for the *sn2* chain, exhibits a different phenomenon. Two different dipolar coupling values between ^{13}C and indirect coupled ^{1}H were revealed for the two peaks. Sanders implied that the splitting is also caused by ^{31}P-^{13}C dipolar coupling interactions (*13*). However, the two-dimensional ^{1}H-^{13}C dipolar coupling/^{13}C chemical shift spectrum suggests that this splitting may be caused by a slight difference in the chemical shift instead of by coupling to a third nucleus (e. g. ^{31}P). One possible reason for the slight difference in the chemical shift is that there are two populations of DMPC carbonyl carbons with slightly different molecular conformation or motions, which is consistent with the ^{13}C-^{1}H dipolar coupling difference.

In order to probe membrane perturbations induced by biological molecules, two-dimensional ^{1}H-^{13}C dipolar coupling/^{13}C chemical shift spectra were also obtained for DMPC/DHPC bicelle samples after incorporating the transmembrane segment of phospholamban (TM-PLB), the antimicrobial peptide $(KIGAKI)_3$ and cholesterol (Figure 2.2). Phospholamban is a transmembrane peptide that regulates cardiac contractility and spans the lipid bilayer (*15*). $(KIGAKI)_3$ is a positively charged peptide designed to have

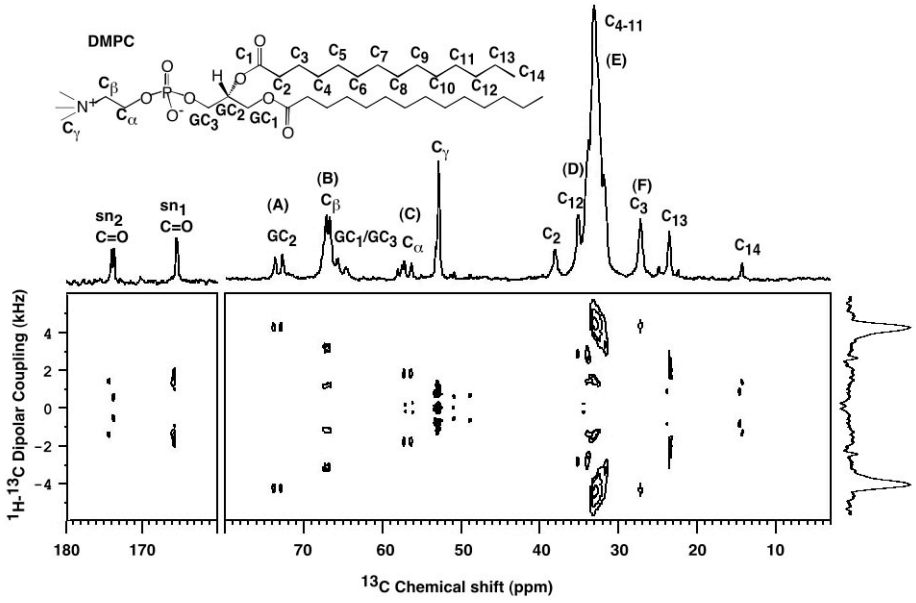

Figure 2.1 Two-dimensional ^{1}H-^{13}C dipolar coupling/^{13}C Chemical shift spectrum of a DMPC/DHPC bicelle sample (1:3 w/w phospholipids in 100mM HEPES buffer) utilizing the SAMMY pulse sequence on a Bruker 500 MHz narrow bore NMR spectrometer at 37 °C. The Hartmann-Hahn contact time was 1 ms. The ^{1}H 90° pulse was 10.1 μs and the recycle delay was 3 s. The spectra were collected with 200 increments in the t1 dimension and 1024 data points in the t2 dimension. 512 scans were accumulated for each t1 increment. The ^{1}H-^{13}C dipolar coupling value is the apparent dipolar coupling value without considering the scaling factor. The one-dimensional ^{13}C chemical shift spectrum was obtained using a standard cross-polarization sequence with proton decoupling. The carbon position labeling is defined in the inset with the DMPC structure. The resonance peaks corresponding to the carbonyl carbons of phospholipids (*sn1* and *sn2* acyl chains) are shown in the left panel. The slice on the dipolar dimension represents the ^{1}H-^{13}C dipolar coupling taken from GC_2 group. Labels A-F were used to indicate the spectral regions exhibited in Figure 2.2.

high antimicrobial activity and is known to strongly interact with the membrane surface (1, 16). The peptide concentrations used were approximately 0.3 mol% with respect to DMPC. For bicelles incorporated with $(KIGAKI)_3$, a reduction of the bicelle alignment temperature was observed by ^{31}P NMR spectroscopy (spectra not shown). The SAMMY experiment was carried out at 34 °C, at which the $(KIGAKI)_3$ bicelles are optimally aligned. Cholesterol is a main component of eukaryotic cell membranes, and is implicated in several diseases, such as heart disease and stroke (*2*). At very high concentrations (>10 mol%), cholesterol can alter the bicelle alignment temperature (*17*). 5 mol% cholesterol (respect to DMPC) was incorporated into the bicelles in order to maintain the bicelle alignment at 37 °C.

The two-dimensional strip plots in Figure 2.2 reveal the ^{13}C chemical shift values between 75 ppm and 55 ppm that represents the lipid glycerol and headgroup region, while the ^{13}C chemical shift range between 36 ppm to 25 ppm represents the lipid acyl chain region. The control peaks prepared with DMPC/DHPC only are shown in black. The individual lipid group dipolar coupling value is in the same range as that obtained on DMPC bilayers using a power-demanding separated local-field experiment (CT-DIPSHIFT) (*5*). The ^{1}H-^{13}C dipolar splittings decrease in both the lipid headgroup/glycerol region and the acyl chain region when TM-PLB (red) was incorporated into the bicelles, indicating that both the DMPC headgroup and the acyl chains experience a disordering effect. These results are consistent with previous ^{2}H and ^{31}P NMR experimental results on TM-PLB (*15*). A more pronounced reduction in the ^{1}H-^{13}C dipolar coupling was observed when $(KIGAKI)_3$ (blue) was added to the lipid bilayers. Close examination also reveals that the lipid headgroups and glycerol region exhibit displacements in the chemical shift. These results indicate that the surface peptide $(KIGAKI)_3$ disturbs the membrane surface and alters the lipid motions. However, the decreased dipolar couplings in Figure 2.2(D-F) suggest that it also perturbs the lipids acyl chain carbons. ^{2}H NMR order parameter experiments carried out on randomly dispersed POPC bilayers exhibited a decrease in the quadrupolar splitting values of each deuteron along the POPC lipids acyl chain upon incorporation of the antimicrobial peptide $(KIGAKI)_3$ (*18*). The ^{1}H-^{13}C SAMMY results presented here are consistent with ^{2}H order parameters. Different from TM-PLB and $(KIGAKI)_3$, only a slight increase in the ^{1}H-^{13}C

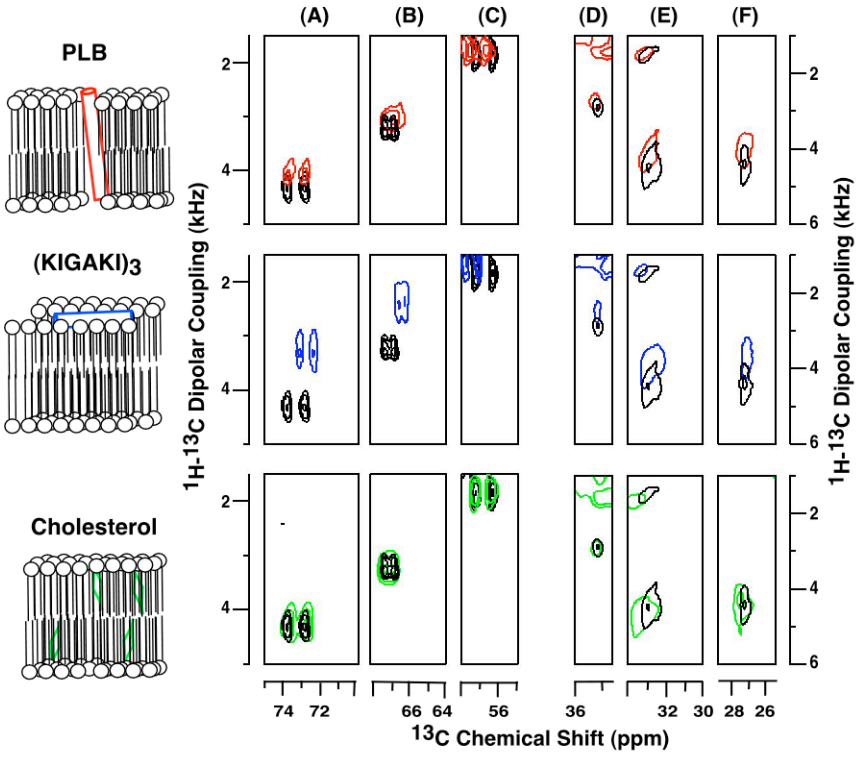

Figure 2.2 ^{1}H-^{13}C dipolar coupling profiles comparing control DMPC/DHPC bicelles (black) and bicelles containing the transmembrane segment of PLB (red), antimicrobial peptide $(KIGAKI)_3$ (blue) and cholesterol molecules (green) utilizing a soft SAMMY pulse sequence. The left three bilayer models show the proposed modes of interaction between the lipid bilayer and the biological added molecules. Contours from the lipid glycerol sites (A), headgroup ((B), (C)) and acyl chain region ((D), (E), (F)) are displayed. The bicelle dipolar coupling profile with $(KIGAKI)_3$ was obtained at 34 °C. All the other spectra were obtained at 37 °C.

dipolar coupling value in the middle (Carbons 4-11) of the DMPC acyl chain region with a definite deshielding in the chemical shift (Figure 2.2(E)) was observed upon addition of cholesterol (green) at 5 mol% to the bicelles. Meanwhile, the dipolar interaction in the glycerol, and headgroup regions of the lipids were nearly undisturbed. The cholesterol molecule has a rigid planar ring structure intercalated in the membrane and parallel to the lipid acyl chains. The addition of cholesterol can diminish the *trans-gauche* isomerization of the lipid acyl chains and increase order within the lipid acyl chains at higher concentrations (*17*). Similar deshielding effects in the lipids acyl chain region were also observed in lipid bilayers upon incorporation of cholesterol due to higher molecular ordering (*12*). Unlike the large headgroup of DMPC, cholesterol has only a small OH group positioned in the vicinity of the fatty ester groups of the phospholipids (*19*). This explains the reduced perturbation observed in the lipid glycerol and headgroup regions upon incorporation of cholesterol. In general, the changes in ^{1}H-^{13}C dipolar coupling values reflect a perturbation effect of these biological pertinent molecules upon association with the bilayer membranes. However, the characteristic of the perturbation may be a motional change or a conformational change or both.

2.4 Conclusion

In conclusion, the two-dimensional SAMMY pulse sequence (^{1}H-^{13}C dipolar coupling/^{13}C chemical shift) provides detailed information on membrane topology and an easy method to probe the structural perturbations induced upon the addition of biologically relevant molecules. The motional and ordering properties of the headgroup and the acyl chain regions of phospholipid bilayers are usually examined with a combination of ^{31}P and ^{2}H solid-state NMR spectroscopy and different deuterated lipids. ^{2}H NMR spectra usually exhibit poor resolution for acyl chain segments with very rigid molecular motions (top of the acyl chain, carbons 1-6) (*11*). The 2D ^{1}H-^{13}C dipolar coupling/^{13}C chemical shift experiment simultaneously revealed high-resolution spectra of the ^{13}C nuclei present in the phospholipid headgroups, glycerol sites, and the acyl chains. Currently, we are working towards complete assignment of the bicelle ^{1}H-^{13}C dipolar coupling/^{13}C chemical shift profile. Here biological pertinent molecules were incorporated at low concentrations into the bicelle samples with comparably large effects

on the values of ^{1}H-^{13}C dipolar coupling. The alignment of bicelle samples was verified by ^{31}P NMR spectroscopy (observed sharp ^{31}P peaks at $\sigma_{\perp}$ position). The observed change in the ^{1}H-^{13}C dipolar coupling values is not a result of the decrease in the orientational order of the bicelles. Instead, a combination effect is observed in which changes of the phospholipids conformation and motion is responsible for the deviation of the ^{1}H-^{13}C dipolar coupling values.

The SAMMY spectra were obtained utilizing a standard solution 500 MHz NMR spectrometer and naturally abundant ^{13}C phospholipids. Thus, this membrane topology method is widely applicable because it does not require isotopic labeling, magic angle spinning, or an expensive wide-bore solid-state NMR spectrometer. This research also extends the application of the bicelles from an ideal membrane system for structure determination of membrane proteins to a complete membrane topology method good for characterizing the interaction between membrane lipids and biological molecules.

Acknowledgements:

This work was supported by an American Heart Association Scientist Development grant (0130396N) and a National Institutes of Health grant (GM60259-01). The 500 MHz NB NMR was obtained from the state of Ohio's Hayes Investment Fund. We thank Dr. Elvis Tiburu and Prof. Jack Blazyk for kindly providing TM-PLB and the $(KIGAKI)_3$ peptide.

2.5 References

(1) Blazyk, J., Wiegand, R., Klein, J., Hammer, J., Epand, R. M., Epand, R. F., Maloy, W. L., and Kari, U. P. (2001) A novel linear amphipathic beta-sheet cationic antimicrobial peptide with enhanced selectivity for bacterial lipids. *J. Biol. Chem. 276*, 27899-27906.

(2) Ohvo-Rekila, H., Ramstedt, B., Leppimaki, P., and Slotte, J. P. (2002) Cholesterol interactions with phospholipids in membranes. *Prog. Lipid Res. 41*, 66-97.

(3) Nevzorov, A. A., and Opella, S. J. (2003) A "Magic Sandwich" pulse sequence with reduced offset dependence for high-resolution separated local field spectroscopy. *J. Magn. Reson. 164*, 182-186.

(4) De Angelis, A. A., Nevzorov, A. A., Park, S. H., Howell, S. C., Mrse, A. A., and Opella, S. J. (2004) High-resolution NMR spectroscopy of membrane proteins in aligned bicelles. *J. Am. Chem. Soc. 126*, 15340-15341.

(5) Middleton, D. A., Hughes, E., and Madine, J. (2004) Screening molecular associations with lipid membranes using natural abundance C-13 cross-polarization magic-angle spinning NMR and principal component analysis. *J. Am. Chem. Soc. 126*, 9478-9479.

(6) Dvinskikh, S. V., Castro, V., and Sandstrom, D. (2005) Efficient solid-state NMR methods for measuring heteronuclear dipolar couplings in unoriented lipid membrane systems. *Phys. Chem. Chem. Phys. 7*, 607-613.

(7) Dvinskikh, S. V., Zimmermann, H., Maliniak, A., and Sandstrom, D. (2003) Heteronuclear dipolar recoupling in liquid crystals and solids by PISEMA-type pulse sequences. *J. Magn. Reson. 164*, 165-170.

(8) Schmidtrohr, K., Nanz, D., Emsley, L., and Pines, A. (1994) Nmr Measurement Of Resolved Heteronuclear Dipole Couplings In Liquid-Crystals And Lipids. *J. Phys. Chem. 98*, 6668-6670.

(9) Hong, M., Gross, J. D., and Griffin, R. G. (1997) Site-Resolved Determination of Peptide Torsion Angle O from the Relative Orientations of Backbone N-H and C-H Bonds by Solid-State NMR. *J. Phys. Chem. B 101*, 5869-5874.

(10) Wu, C. H., Ramamoorthy, A., and Opella, S. J. (1994) High-Resolution Heteronuclear Dipolar Solid-State Nmr- Spectroscopy. *J. Magn. Reson. Ser. A 109*, 270-272.

(11) Sanders, C. R., and Schwonek, J. P. (1992) Characterization Of Magnetically Orientable Bilayers In Mixtures Of Dihexanoylphosphatidylcholine And Dimyristoylphosphatidylcholine By Solid-State Nmr. *Biochemistry 31*, 8898-8905.

(12) Forbes, J., Bowers, J., Shan, X., Moran, L., Oldfield, E., and Moscarello, M. A. (1988) Some New Developments In Solid-State Nuclear Magnetic-Resonance Spectroscopic Studies Of Lipids And Biological-Membranes, Including The Effects Of Cholesterol In Model And Natural Systems. *J. Chem. Soc., Faraday Trans. 1 84*, 3821-3849.

(13) Sanders, C. R. (1993) Solid state ^{13}C NMR of unlabeled phosphatidylcholine bilayers: Spectral assignments anfd measurement of carbon-phosphorus dipolar couplings and ^{13}C chemical shift anisotropies. *Biophys. J. 64*, 171-181.

(14) Vold, R. R., and Prosser, R. S. (1996) Magnetically oriented phospholipid bilayered micelles for structural studies of polypeptides. Does the idea bicelle exist? *J. Magn. Reson. 113*, 267-271.

(15) Dave, P. C., Tiburu, E. K., Damodaran, K., and Lorigan, G. A. (2004) Investigating structural changes in the lipid bilayer upon insertion of the transmembrane domain of the membrane-bound protein phospholamban utilizing P-31 and H-2 solid-state NMR spectroscopy. *Biophys. J. 86*, 1564-1573.

(16) Jin, Y., Mozsolits, H., Hammer, J., Zmuda, E., Zhu, F., Zhang, Y., Aguilar, M. I., and Blazyk, J. (2003) Influence of tryptophan on lipid binding of linear amphipathic cationic antimicrobial peptides. *Biochemistry 42*, 9395-9405.

(17) Lu, J. X., Caporini, M. A., and Lorigan, G. A. (2004) The effects of cholesterol on magnetically aligned phospholipid bilayers: a solid-state NMR and EPR spectroscopy study. *J. Magn. Reson. 168*, 18-30.

(18) Lu, J. X., Damodaran, K., Blazyk, J., and Lorigan, G. A. (2005) Solid-State NMR Relaxation Studies of the Interaction Mechanism of Antimicrobial Peptides with Phospholipid Bilayer Membranes. *Biochemistry 44*, 10208-10217.

(19) Villalain, J. (1996) Location of cholesterol in model membranes by magic-angle-sample-spinning NMR. *Eur. J. Biochem. 241*, 586-593.

Chapter 3

The Effects of Cholesterol on Magnetically Aligned Phospholipid Bilayers: A Solid-State NMR and EPR Spectroscopy Study

Lu, J.X., Caporini, M. A., and Lorigan, G. A. "The Effects of Cholesterol on Magnetically Aligned Phospholipid Bilayers: A Solid-State NMR and EPR Spectroscopy Study" *J. Magn. Reson.* (2004) 168: 18-30.

3.1 Abstract

This paper presents the first time that both solid-state NMR spectroscopy and EPR spectroscopy were used to study the effects of cholesterol on magnetically aligned phospholipid bilayers (bicelles). Solid-state deuterium NMR spectroscopy was carried out using both chain perdeuterated 1,2-dimyristoyl-*sn*-glycero-3-phosphatidylcholine (DMPC-d_{54}) and a partially deuterated β-[2, 2, 3, 4, 4, 6-$^2H_6$] cholesterol (cholesterol-d_6). Also, EPR spectroscopy was carried out utilizing a 3β-doxyl-5α-cholestane (cholestane) spin probe incorporated into magnetically aligned bilayers to provide a more complete picture about the ordering and dynamics of the phospholipid and cholesterol molecules in the bicelle membrane system. The results demonstrate that cholesterol was successfully incorporated into the phospholipid bilayers. The molecular order parameters extracted directly from the ^2H NMR spectra of both DMPC-d_{54} and cholesterol-d_6 were compared to that from the EPR study of cholestane. The order parameters indicate that the sterol was motionally restricted, and that the DMPC had high order and low motion for the hydrocarbon segments close to the head groups of the phospholipids and less order and more rapid motion toward the terminal methyl groups. Both methods clearly indicate an overall increase in the degree of ordering of the molecules in the presence of cholesterol and a decrease in the degree of ordering at higher temperatures. However, EPR spectroscopy and ^2H-NMR spectroscopy exhibit different degrees of sensitivity in detecting the phospholipid molecular motions in the membrane. Finally, cholesterol increases the minimum alignment temperature necessary to magnetically align the phospholipid bilayers.

3.2 Introduction

Cholesterol is a major constituent of eukaryotic cell membranes. The distribution of cholesterol varies among the membranes depending upon different locations and stages of cell development, suggesting that cholesterol plays an integral role in cell biology and metabolism (*1*). Cholesterol is implicated in many diseases, such as heart disease, stroke, and Alzheimer disease (*2, 3*). The effects of cholesterol on model membranes have been studied extensively by a variety of techniques including molecular dynamics simulations, NMR spectroscopy, EPR spectroscopy, X-ray diffraction, neutron diffraction, differential scanning calorimetric spectroscopy, and Fourier transform infrared spectroscopy (*4-11*). It is believed that cholesterol acts as a regulator by modulating the fluidity of cellular membranes. Cholesterol can enhance the mechanical strength of the membrane, and alter the gel-to-liquid crystalline (L_α) phase transition temperature of the lipid (*12*). Molecular dynamics simulations of phospholipid bilayers as a function of cholesterol concentration indicate a significant increase in ordering of the phospholipid chains, and a reduced fraction of *gauche* conformations as well as a reduction in lateral diffusion of the phospholipids (*13, 14*). Deuterium NMR relaxation studies on phospholipid bilayers containing cholesterol suggest that axial rotations of the phospholipid molecules occur at a higher rate than in pure phospholipid bilayers. Additionally, the rigid cholesterol molecule appears to undergo slower axial rotation than the corresponding phospholipid molecules (*15*). However, the effects of cholesterol on magnetically aligned phospholipid bilayers (bicelle) have never been studied in such detail from both the sides of phospholipids and cholesterol molecules (*16, 17*).

Solid-state ^{2}H-NMR and EPR spectroscopic techniques have been used to study the structural and dynamic properties of phospholipid bilayers (*15, 18-20*). However, the intrinsic difference between NMR and EPR spectroscopy has to be understood in order to correctly apply these techniques to a variety of different systems. Because of the low natural abundance of ^{2}H, no background signals from unlabeled components are observed in ^{2}H NMR studies (*19, 21*). Alternatively, EPR spectroscopy exhibits a high sensitivity to the rate of motion and the degree of organization of the phospholipids, since the characteristic time scale for nitroxide spin-label EPR matches very closely the rates of molecular rotation of the lipids within the membrane (*18*). Both techniques are carried

out and compared in this study in order to better understand the effect of cholesterol on bicelle model membrane systems. The differences between these two magnetic resonance techniques are discussed.

In this work, magnetically aligned phospholipid bilayers have been investigated using solid-state NMR and spin-label EPR spectroscopic techniques in the presence of cholesterol. Previously, most cholesterol studies were based on unoriented or mechanically aligned membrane samples (*9, 22*). The use of multilamellar vesicles in solid-state NMR spectroscopic studies gives rise to broad powder type spectra. To obtain pertinent structural and dynamic information requires deconvoluting the spectra through the so called "dePakeing" process (*23*). Alternatively, uniaxially bilayer membranes aligned in both EPR and solid-state NMR studies reveal high-resolution spectra and pertinent structural and dynamic information. Traditionally, macroscopic uniaxial orientation of membrane bilayers can be accomplished mechanically by stacking phospholipids bilayers between glass plates (*24*). The ^{2}H NMR quadrupolar splittings can yield the dynamic information on deuterium labeled segments of the phospholipid acyl chains. Also the EPR spectra reveal orientational information derived from the hyperfine splitting of the aligned spectra. The anisotropic hyperfine splitting of an aligned spin probe can provide a more detailed structural picture of the probe with respect to the membrane, when compared to randomly dispersed phospholipid bilayer samples (*25*).

The magnetically aligned bicelles are a promising technique that is well suited for a wide variety of spectroscopic studies, such as, NMR spectroscopy and EPR spectroscopy (*24, 26, 27*). Bicelles are formed upon mixing long-chain phospholipid molecules, such as 1,2-dimyristoyl-*sn*-glycero-3-phosphocholine (DMPC) with short lipid molecules, such as 1,2 dihexanoyl-*sn*-glycero-3-phosphocholine (DHPC). The magnetic alignment of bicelles depends on the magnetic susceptibility anisotropy tensor ($\Delta\chi$) of the phospholipid bilayers. The negative sign of $\Delta\chi$ for bicelles dictates that they align with their bilayer normal oriented perpendicular to the direction of the static magnetic field (B_0) (*28-30*). The degree of ordering of bicelles depends upon several factors, including the strength of the magnetic field, the sign and magnitude of the

phospholipid bilayers magnetic susceptibility anisotropy tensor, the viscosity of the sample, the types of lanthanide ions used, and the temperature (*3, 31-33*).

In NMR experiments at high magnetic fields, the bicelles can spontaneously align above the gel-to-liquid crystalline phase transition temperature, T_m (*29*). When placed into weak magnetic fields typically used in an X-band EPR spectrometer, the bilayers cannot spontaneously align at either the perpendicular or the parallel alignment (*27, 30*). Paramagnetic lanthanide ions (i.e. Dy^{3+}, Tm^{3+}) can be used as alignment reagents to help the bilayers align either in the perpendicular or parallel orientations (*24, 33*). The association of paramagnetic lanthanide ions with the bicelles changes the sign and the value of the magnetic susceptibility anisotropy tensor $\Delta\chi$ of the bicelles (*30*). The negative value of $\Delta\chi$ is increased by the addition of Dy^{3+} to the sample. Tm^{3+} with a large positive magnetic susceptibility anisotropy $\Delta\chi$, can cause the bicelles to flip 90° and align with their bilayer normal (n) oriented parallel to the direction of the static magnetic field. For solid-state ^2H NMR studies on bicelles, the spectral resolution is increased in the parallel orientation because the quadrupolar splittings are doubled. The parallel alignment offers advantages in studying membrane-associated peptides with rapid reorientations about the long molecular axis (*26*). In this paper, both orientations are studied by adding either Dy^{3+} or Tm^{3+} to the bicelle membrane system.

In order to understand the interaction between the cholesterol and the phospholipids, molecular order parameters (S_{mol}) are used to define the structural and dynamical properties of the corresponding molecules in the membrane. An ensemble of molecules give rise to $S_{mol} = 0$ for unrestricted motions of every individual molecule. A S_{mol} value of 1 indicates that all the molecules are perfectly aligned and motionally restricted in one direction (*16, 29, 34, 35*). The order parameter (S_{mol}) calculations concerning the analysis of the EPR spectra of the cholestane spin probe and NMR spectra of deuterium-labeled cholesterol or deuterium-labeled phospholipid molecules are presented in this paper. The results indicate that magnetically aligned DMPC/DHPC bicelles are an excellent model membrane system for both EPR and solid-state NMR studies. Also, the bicelle samples are easy to prepare and avoid using dePakeing, altogether making it easier to calculate the molecular order parameters directly from the quadrupolar splittings of each deuteron from NMR spectra.

3.3 Materials and Method:

3.3.1 Materials

1,2-dimyristoyl-*sn*-glycero-3-phosphatidylcholine (DMPC), 1,2-dihexanoyl-*sn*-glycero-3-phosphatidylcholine (DHPC), deuterated 1,2-dimyristoyl-*sn*-glycero-3-phosphatidylcholine (DMPC-d_{54}) and 1,2-dimyristoyl-*sn*-glycero-3-phosphoethanolamine-N-[methoxy-(polyethylene glycol)-2000] (PEG 2000-PE) were purchased from Avanti Polar Lipids (Alabaster, AL). Thulium (III) chloride hexahydrate, Dysprosium (III) chloride hexahydrate, 3β-doxyl-5α cholestane (cholestane), and N-[2-hydroxyethyl] piperazine-N'-[2-ethanesulfonic acid] (HEPES) were obtained from Sigma/Aldrich (St. Louis, MO). The cholesterol was purchased from Avocado Research Chemicals Ltd. (Heysham, England). β-[2,2,3,4,4,6-$2H_6$] cholesterol was purchased from Cambridge Isotope Laboratories (Andover, MA). Deuterium-depleted water was obtained from Isotec (Miamisburg, OH). All phospholipids were dissolved in chloroform and stored at -20°C prior to use. Aqueous solutions of lanthanide ions were prepared fresh each day. All aqueous solutions were prepared with nanopure water.

3.3.2 Sample preparation

The standard DMPC/DHPC bicelle samples, consisting of 25% (w/w) phospholipids to solution with a q ratio of 3.5, were made in 25 mL pear-shaped flasks. Cholesterol concentrations were used from 0 mol% to 20 mol% in 5 mol% increments (molar ratio to DMPC). For EPR samples, DMPC, PEG2000-PE, DHPC, and spin-label cholestane were mixed in molar ratio of 3.5:0.035:1:0.0196, respectively. Different amounts of nondeuterated cholesterol were also added. For the ^2H NMR deuterated cholesterol samples, DMPC, PEG2000-PE and DHPC were mixed in the molar ratio of 3.5:0.035:1. Deuterated cholesterol was added from 0 mol%, 5 mol%, 10 mol%, 15 mol% to 20 mol% with respect to DMPC. For deuterated DMPC-d_{54} samples, DMPC, PEG2000-PE, DHPC, DMPC-d_{54} were mixed in ratios of 3.22:0.035:1:0.22. Nondeuterated cholesterol was then added to the mixture. The lipids were rotoevaporated down at room temperature and placed in a vacuum desiccator overnight to dry.

The following day 100 mM HEPES buffer of pH 7.0 was added to the pear-shaped flask so the amount of lipid in the sample was 25% (wt%). The samples were

chilled in an ice bath and vortexed until all of the lipids were solubilized. Then the samples were sonicated in a Fisher Scientific FS 30 bath sonicator (Florence, KY) for 30 min with the heater turned off and ice added to the bath. The sample was subjected to several freeze/thaw cycles at room temperature. Finally, Tm^{3+} or Dy^{3+} (aq) was added so that the amount of Tm^{3+} (Dy^{3+}) was 20 mol% (molar ratio to DMPC). The sample was gently tilted and slowly rotated for a few minutes until the sample looked homogenous.

3.3.3 EPR Spectroscopy

The bicelle samples were drawn into 1mm ID capillary tubes via a syringe. Both ends of the tube were sealed off with Critoseal purchased from Fisher scientific (Florence, KY). The capillary tube was placed into the standard quartz EPR tube (707-SQ-250M) purchased from Wilmad Glass (Buena, NJ) and filled with light mineral oil.

All EPR experiments were carried out on a Bruker EMX X-band CW-EPR spectrometer consisting of an ER 041XG microwave bridge and a TE_{102} cavity coupled with a BVT 3000 nitrogen gas temperature controller (temperature stability of ±0.2 K). Each cholestane spin-labeled EPR spectrum was acquired by taking a 42-s field swept scan with the center field set to 3350 G, a sweep width of 100 G, a microwave frequency of 9.39 GHz, the modulation frequency was set to 100 kHz, a modulation amplitude of 1.0 G, and the microwave power was set to 2.0 mW. All oriented samples were aligned by warming the sample from 298 K to 318 K at a maximum magnetic field strength of 0.64 T (6400 G) (*30*).

3.3.4 Solid-State ^{2}H NMR spectroscopy

All solid-state NMR experiments were carried out on a Bruker AVANCE 11.4 T wide bore solid-state NMR spectrometer. The solid-state NMR spectra were gathered with a static double-resonance 5 mm round-coil solid-state NMR probe purchased from Bruker. ^{2}H NMR spectra were recorder at 76.77 MHz using a standard quad-echo pulse sequence (*36*). The following spectrometer conditions were used: 2.6 μs 90°pulses for deuterium-labeled cholesterol, 3.1 μs 90°pulse for deuterium-labeled DMPC, 20 μs innerpulse delay, 10 ms acquisition time, 0.4 s recycle delay, and a 170 KHz spectral width for deuterium-labeled cholesterol, and a 150 kHz spectral width for deuterium-labeled DMPC. Typically 10 K scans were accumulated for the deuterium-labeled DMPC samples, and 16 K to 32 K scans were accumulated for the deuterium-labeled

cholesterol in the quadrature detection mode. An exponential line broadening of 300 Hz was applied to the free induction decay before Fourier transformation. The experiments were carried out over the temperature range from 308 K to 348 K in 5 K increments. For deuterium-labeled cholesterol bicelle samples, only Tm^{3+}-doped bicelles were studied. Both Tm^{3+}-doped and Dy^{3+}-doped bicelles were studied for deuterium-labeled DMPC-d_{54} bicelles.

3.3.5 Theory

(1) Spin-label EPR spectroscopy

The EPR spectrum of magnetically aligned phospholipid bilayers with cholestane consists of three peaks (Figures 3.1 and 3.2) as a result of the coupling of the unpaired electron of the nitroxide spin label to a ^{14}N nucleus. A Cartesian coordinate system containing the x, y, and z nitroxide moiety is used with the x-axis extending along the direction of the N-O bond and the z-axis in the direction of the nitrogen 2pπ orbital (*34*). For the co-aligned cholestane in the bicelles, the y-axis represents the long molecular axis (m). The cholestane is assumed to rotate rapidly about the long axis (*25*).

From single-crystal studies, it is known that $A_{xx} \approx A_{yy}$, and the following equation can be used to calculate the S_{33} order parameter (*37*):

$$S_{33} = \frac{\left(A_{//} - A_{\perp}\right)a_N}{\left(A_{zz} - A_{xx}\right)a_N^{'}} \qquad [1]$$

where $A_{//}$ and $A_{\perp}$ are the observed hyperfine splittings measured between the $m_I = +1$ and 0 spectral lines of oriented samples when the long molecular axis of cholestane is respectively perpendicular and parallel to the static magnetic field. A_{xx}, A_{yy}, A_{zz} are the static hyperfine splitting tensor values obtained from the single-crystal data. The values A_{xx} = 5.8G, A_{yy} = 5.8G and A_{zz} = 30.8G are used in the calculations (*34*). a_N represents the isotropic hyperfine splitting constant $a_N = \frac{A_{xx} + A_{yy} + A_{zz}}{3}$. This hyperfine splitting constant is sensitive to changes in the solvent polarity, the polarity of the spin label environment, and can be determined according to $a_N^{'} = \frac{A_{//} + 2A_{\perp}}{3}$.

In general, we are most interested in the molecular order parameter S_{mol} of the long molecular axis.

$$S_{mol} = \left| \frac{S_{33}}{\frac{1}{2}\left(3\cos^2\theta - 1\right)} \right| \qquad [2]$$

where θ denotes the angle between the long molecular axis (m) and the corresponding N-O axis (x). In this case, θ = 90°, $S_{mol} = \left|2S_{33}\right|$.

(2) Deuterium-labeled solid-state NMR spectroscopy

^{2}H NMR spectra of aligned DMPC/DHPC phospholipids bilayers normally consist of a collection of symmetrical doublets (Figure 5), characteristic of molecules undergoing fast, axially symmetrical motion. We can relate the residual quadrupolar splittings, $\Delta\nu_i$ to order parameters S_{CD}^i, of the C-^{2}H bond vector according to (*29*):

$$\Delta\nu_i = \tfrac{1}{2}\Delta p_i S_{CD}^i\left(3\cos^2\theta - 1\right) \qquad [3]$$

where Δp_i is the splitting for a stationary deuteron in a C-^{2}H bond pointing along the external magnetic field and $\Delta p_i = \frac{3}{2}\frac{e^2qQ}{h}$. The quadrupole coupling constant $\frac{e^2qQ}{h}$ of 168 kHz is used here for deuterons bound to an sp^3-hybridized carbon. θ is the angle between the average bicelle normal (n) and the magnetic field in the laboratory frame. When the bicelles are perfectly aligned relative to the magnetic field, θ is equal to 90° for the perpendicular alignment, whereas θ is equal to 0° for the parallel alignment. S_{CD}^i represents the degree of ordering of the *ith* C-^{2}H bond with respect to the average bilayer normal. If *gauche* conformations about C-C bonds are allowed, a wide variety of orientations of the C-^{2}H moieties are possible. The order parameter S_{CD}^i represents the average of all allowed orientations of the C-^{2}H moieties. S_{mol}^i, the molecular order parameter represents the angular fluctuations of the axis of motion of the molecules with respect to the bilayer normal.

$$S_{mol}^i = \left| \frac{S_{CD}^i}{\frac{1}{2}\left(3\cos^2\theta_i - 1\right)} \right| \qquad [4]$$

θ_i is the angle between the C-^{2}H bond and the principal axis of the interaction tensor (m) at the *ith* C-^{2}H bond. For deuterium-labeled phospholipids molecules, we choose the "molecular axis (m)" the normal to the plane containing the three atoms in a methylene group. Therefore, for all C-^{2}H bonds of the methylene groups, θ_i is equal to 90°.

$$S_{mol}^i = \left|2S_{CD}^i\right| \qquad [5]$$

The terminal methyl groups make equal angles (109.5°) with respect to the last C-C bond of the deuterated acyl chain. However, the C-C bond is not parallel to the long molecular axis (m). 35.25° accounts for the segment orientation of the terminal methyl group along the C-C bond with respect to the long molecular axis (*19, 37*):

$$S_{mol} = \left| \frac{S_{CD}}{\frac{1}{2}\left(3\cos^2 109.5^\circ - 1\right) \times \frac{1}{2}\left(3\cos^2 32.25 - 1\right)} \right| \qquad [6]$$

For deuterium-labeled cholesterol, we assume that the sterol ring is rigid. The angle θ_i given by Dufourc et. al is (*9*):

$$\cos\theta_i = \frac{\left(l_i \cos\gamma \sin\beta + m_i \sin\gamma \sin\beta + n_i \cos\beta\right)}{\sqrt{\left(l_i^2 + m_i^2 + n_i^2\right)}} \qquad [7]$$

The axis system is defined such that the x-axis is co-linear with the C_3-axial bond and the z-axis corresponds to the OH-C_3-^{2}H plane. l_i, m_i, and n_i are the direction cosines of the C-^{2}H bond vector in the C_3 reference frame taken from the neutron scattering structure (*38*). The original coordinates are transformed into the C_3 reference system by one translation and three successive rotations. $\beta = 11°$, $\gamma = 9°$ are the polar coordinates of the symmetry axis of motion (m) in the reference frame given by the neutron diffraction structure (*22*). β-[2, 2, 3, 4, 4, 6-$^2H_6$] cholesterol has six different C-^{2}H bonds, which will give six different values of S_{CD}. Individual quadrupolar splittings were obtained by simulation using the DMFIT program (*39*). S_{mol} is calculated using Eq. [4].

3.4 Results

3.4.1. EPR study of magnetically aligned phospholipid bilayers using the cholestane spin probe.

The EPR spectra of cholestane inserted into DMPC/DHPC bicelles of varying cholesterol concentrations are displayed in Figure 3.1 at 318 K (solid line, unaligned bicelles; dotted line, parallel-aligned bicelles; and dashed line, perpendicular-aligned bicelles). The addition of small amounts of lanthanide ions Tm3+ and Dy3+ enables the DMPC/DHPC bicelles to align at the two different orientations in the magnetic field (25, 29). The lineshapes and hyperfine splittings indicate that the phospholipid bilayers are

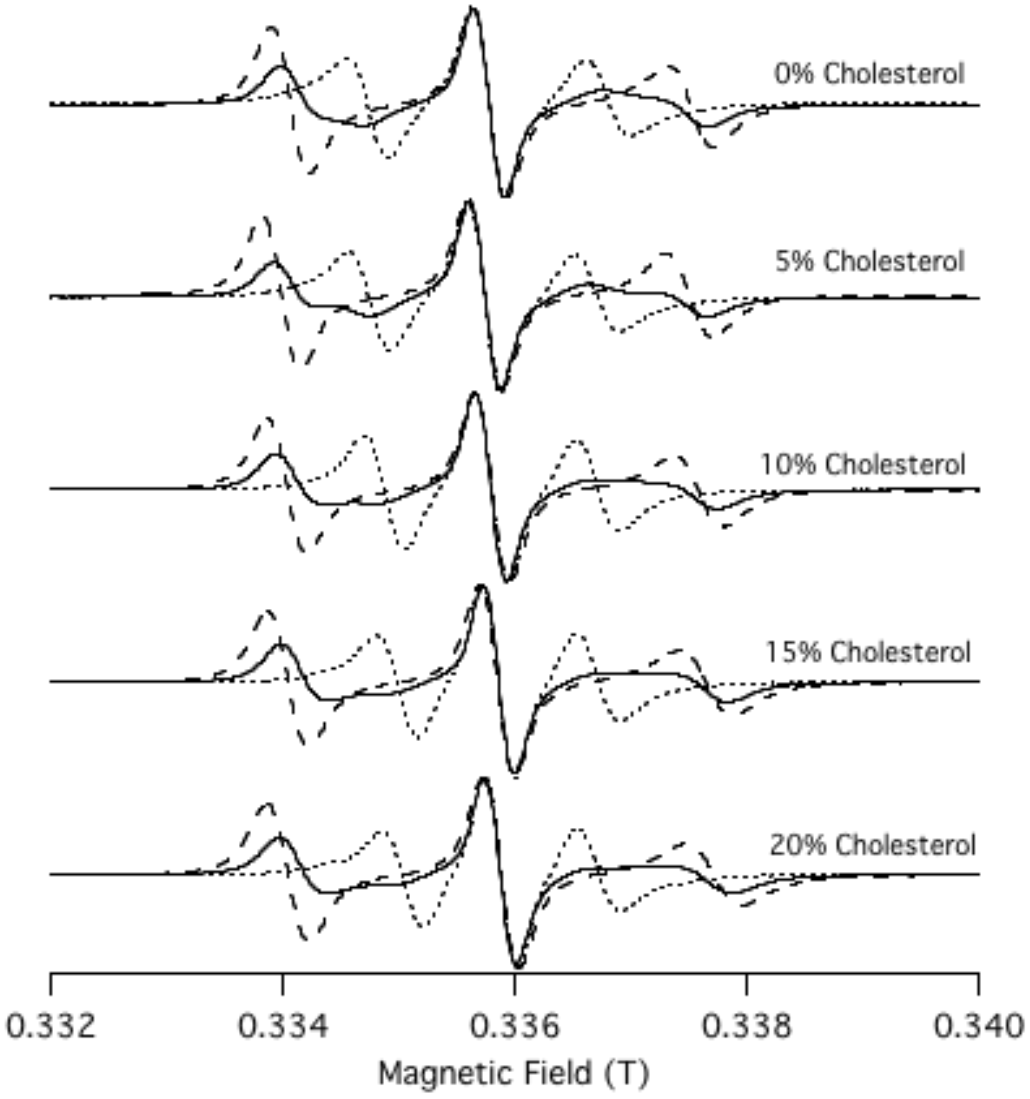

Figure 3.1 EPR spectra taken at 318K of the cholestane spin probe incorporated into oriented and randomly dispersed DMPC/DHPC/cholesterol bicelles at cholesterol concentrations of 0 mol%, 5 mol%, 10 mol%, 15 mol% and 20 mol% with respect to DMPC. The *solid-line* spectra represent the randomly dispersed bicelles without added lanthanide ions. The *dashed-line* spectra represent the Dy^{3+}-doped bicelle sample with the normal of the bilayers being perpendicular to the static magnetic field. The *dotted-line* spectra represent the Tm^{3+}-doped bicelle sample with the normal of the bilayers being parallel to the static magnetic field.

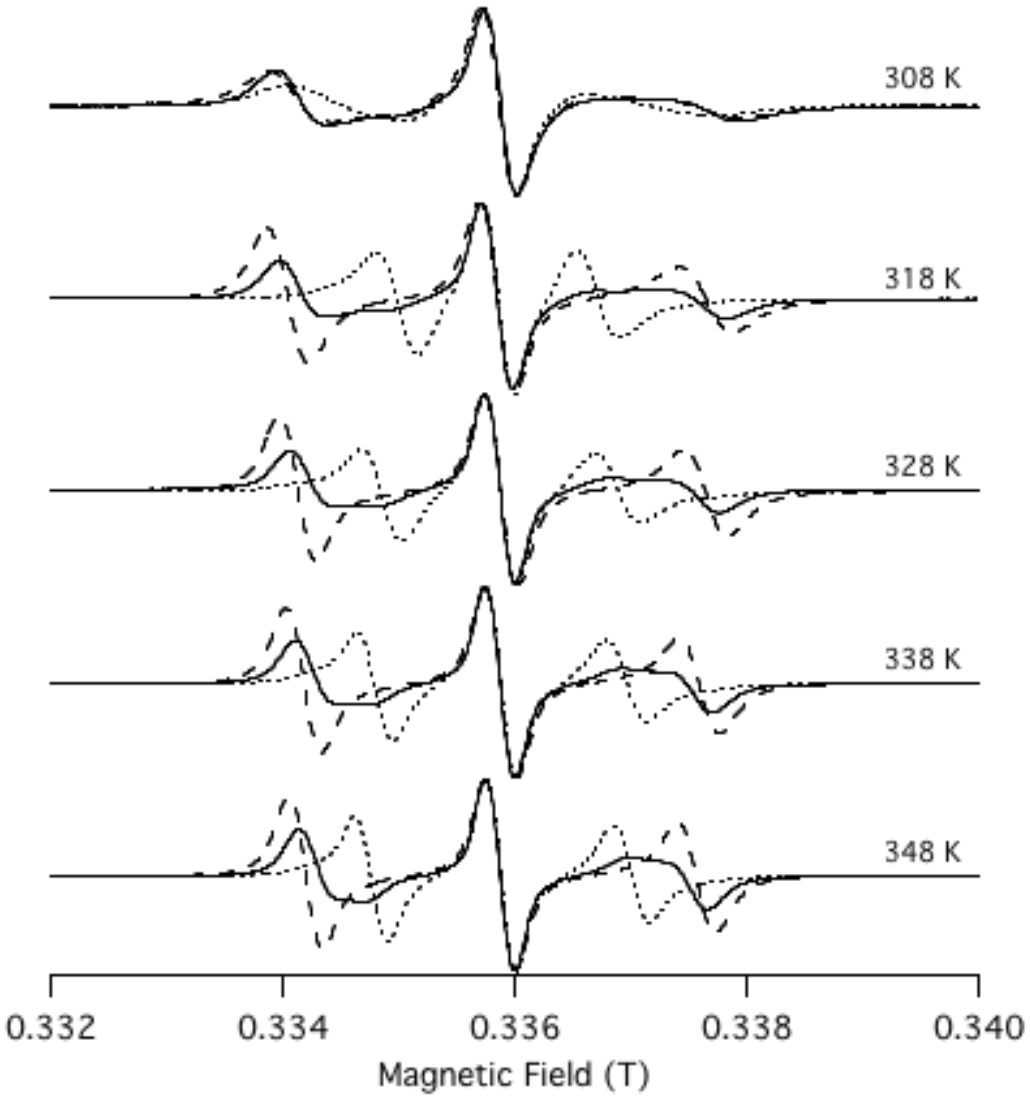

Figure 3.2 EPR spectra of the cholestane spin probe incorporated into oriented and randomly dispersed DMPC/DHPC/cholesterol bicelles at 15 mol% cholesterol with respect to DMPC over the temperature range from 308 K to 348 K. The *solid-line* spectra represent the randomly dispersed bicelles without added lanthanide ions. The *dashed-line* spectra represent the Dy^{3+}-doped bicelle sample with the normal of the bilayers being perpendicular to the static magnetic field. The *dotted-line* spectra represent the Tm^{3+}-doped bicelle sample with the normal of the bilayers being parallel to the static magnetic field.

well aligned. The hyperfine splittings (measured between the m_I = +1 and 0 peaks) for parallel-aligned bicelles decrease from 10.6 G to 8.6 G as the cholesterol concentration increases, while the hyperfine splittings for the perpendicular-aligned bicelles increase from 17.2 G to 18.4 G.

Figure 3.2 shows the EPR spectra of cholestane inserted into DMPC/DHPC bicelle samples with 15 mol% cholesterol with respect to DMPC as a function of temperature. The spectra taken at 308 K indicate that the phospholipid bilayers are not well aligned in the magnetic field, because the hyperfine splitting and lineshape of the spectra with either Tm^{3+} or with Dy^{3+} are nearly the same as the randomly aligned spectrum. At 313 K, the spectra indicate that the bicelles with 15 mol% cholesterol with respect to DMPC are aligned (data not shown) and look similar to the spectra taken at higher temperatures (318 K ~ 348 K) shown in Figure 3.2. The hyperfine splitting decreases from 18.0 G to 16.8 G for the bicelles in the perpendicular orientation, and increases from 8.8 G to 11.3 G in the parallel orientation as the temperature increases. At 20 mol% cholesterol with respect to DMPC, the bicelles are not well aligned at 308 K and 313 K, but are aligned from 318 K up to 348 K (data not shown). However, magnetically aligned phospholipid bilayers prepared with 0 mol%, 5 mol%, 10 mol% cholesterol with respect to DMPC are aligned at both the parallel and perpendicular orientations at 308 K. Therefore, the minimum temperature required for alignment of the phospholipid bilayers increases as the cholesterol concentration increases.

The method for calculating the molecular order parameters (S_{mol}) for the 3β-doxyl-5α-cholestane (cholestane) is described in Section 3.3. Figure 3.3 shows the changes in S_{mol} in the presence of cholesterol as a function of temperature. The concentration of cholesterol ranges from 0 mol% to 20 mol% with respect to DMPC. The ordering of the cholestane in the membrane decreases as the temperature increases. The degree of ordering decreases gradually in the low temperature region. At higher temperatures (above 323 K~333 K), the ordering shows a slower decrease.

For comparison, Figure 3.4 displays the ordering profile of cholestane as a function of cholesterol concentration at different temperatures. At a given temperature,

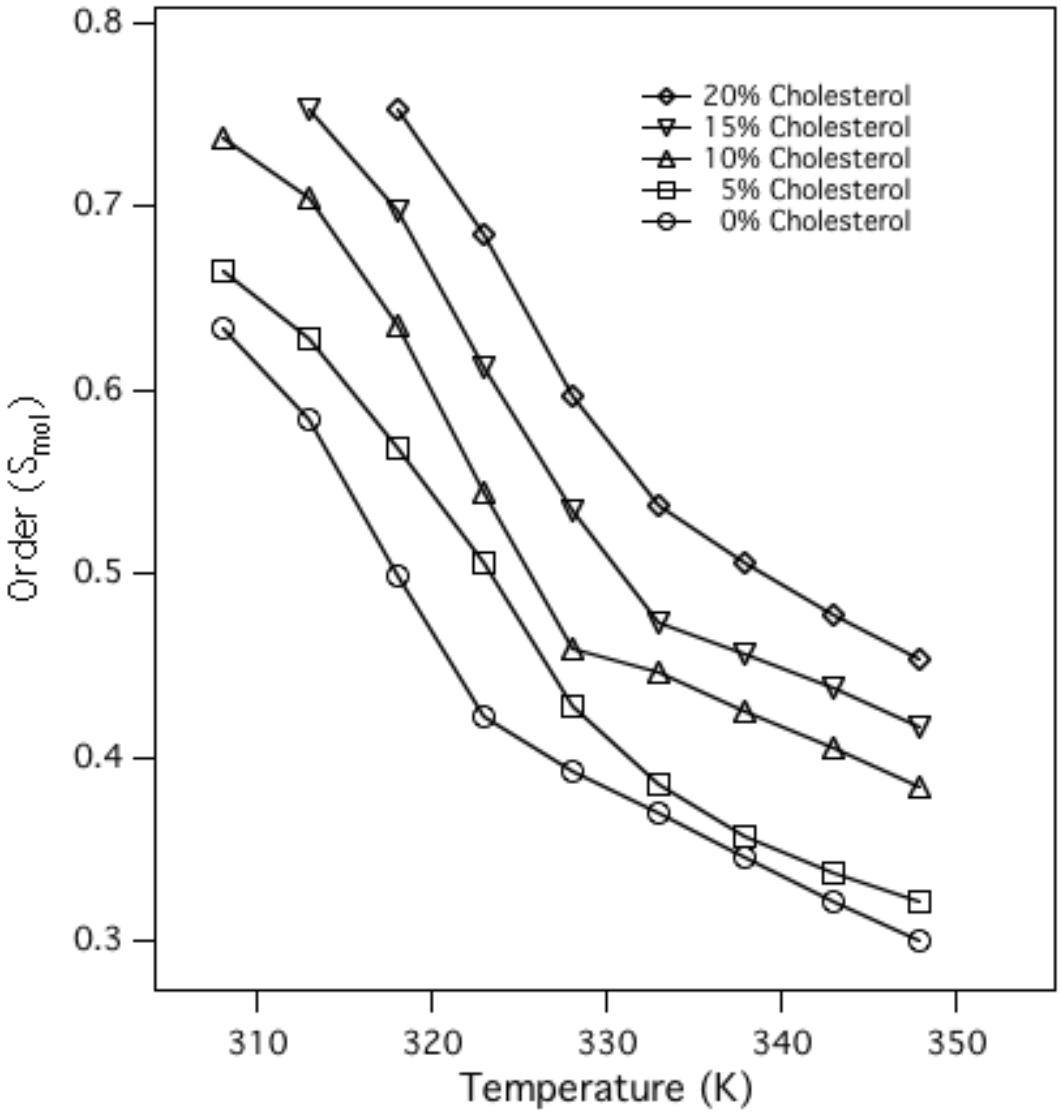

Figure 3.3 The molecular order parameters (S_{mol}) calculated from the spin-labeled cholestane EPR spectra as a function of temperature in magnetically aligned DMPC/DHPC/cholesterol bicelles at cholesterol concentrations of 0 mol%, 5 mol%, 10 mol%, 15 mol% and 20 mol% with respect to DMPC.

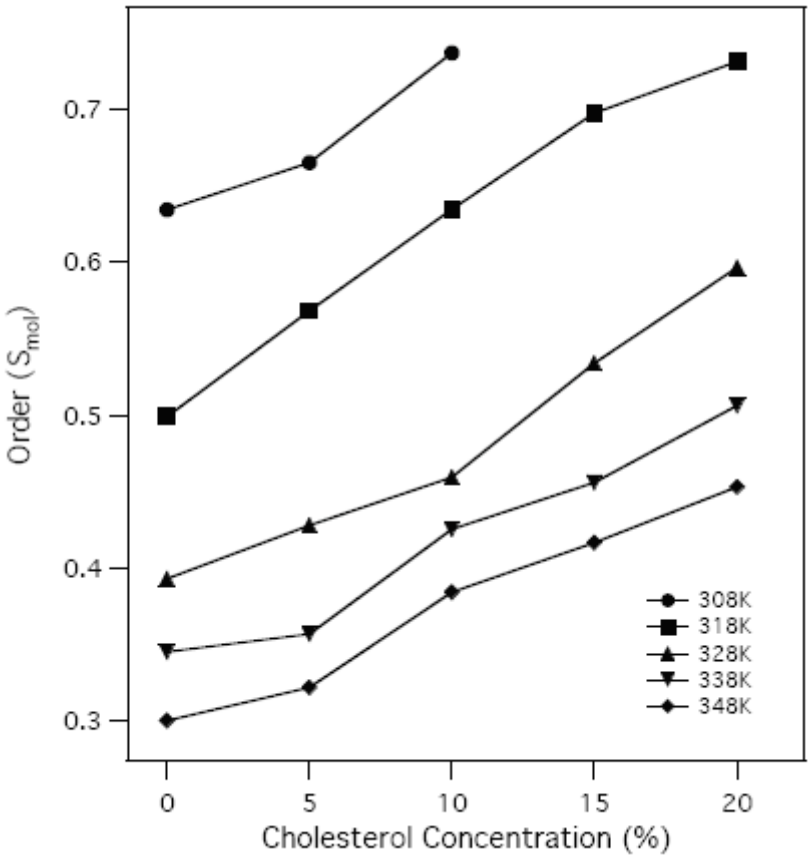

Figure 3.4 The molecular order parameters calculated from the cholestane spin probe EPR spectra as a function of cholesterol concentration in magnetically aligned DMPC/DHPC/cholesterol bicelles. The sample temperature of the spectra ranges from 308 K to 348 K.

the ordering of the membrane increases as the cholesterol concentration increases, and the slope of the increase of ordering is higher for the bicelle samples at lower temperatures. At 318 K, the ordering increases from 0.5 to more than 0.7. In contrast, the ordering changes from 0.3 to about 0.4 at 348 K. The spin-labeled cholestane is used to probe the motions and the dynamics of the phospholipid membranes. The increase in ordering shows that the rigid sterol ring of cholesterol limits the motion of lipid membrane, and the restriction effect is more pronounced at low temperatures (308 K, 318 K).

3.4.2. Solid-state NMR study of magnetically aligned phospholipid bilayers using deuterium-labeled cholesterol

Deuterium-labeled cholesterol-d_6 NMR studies have also been carried out on the same compositions of DMPC/DHPC/cholesterol bicelle samples. Cholesterol has been shown to orient in phospholipids bilayers with its polar hydroxyl group in close vicinity to the head groups of phospholipid molecules and its alkyl side-chain extending towards the bilayer center (*40*). The amount of cholesterol-d_6 in the bicelle samples is titrated from 5 mol% to 20 mol% with respect to DMPC. The ^{2}H NMR spectra of 10 mol% cholesterol-d_6 at 318 K is displayed in Figure 3.5(A). The resolved peaks are simulated using the DMFIT simulation program and are displayed as dotted lines in Figure 3.5 (B) (*39*). The peak assignments are based upon previous work (*22*). The inner doublets with the smallest quadrupolar splitting (4.2 kHz) represent the 6-^{2}H deuteron. The second smallest quadrupolar splittings (48.1 kHz and 50.9 kHz) represent the 4-$^2H_{eq}$ and 2-$^2H_{eq}$ deuterons on the fused ring of cholesterol, and the last set of doublets (73.4 kHz, 76.1 kHz, 79.2 kHz) correspond to the quadrupolar splitting of the 4,2 -$^2H_{ax}$ deuterons and the deuteron at the C_3-^{2}H position, respectively. The molecular order parameters are calculated as described in the Material and Methods section and the results are shown in Figure 3.9. The six quadrupolar splittings from the different C-^{2}H bonds give almost the same molecular order parameter (S_{mol}) values within a small standard deviation. The final result is the average of the six values of S_{mol}. The quadrupolar splittings and S_{mol} values confirm that the cholesterol ring is rather rigid in the phospholipid bilayer under these conditions.

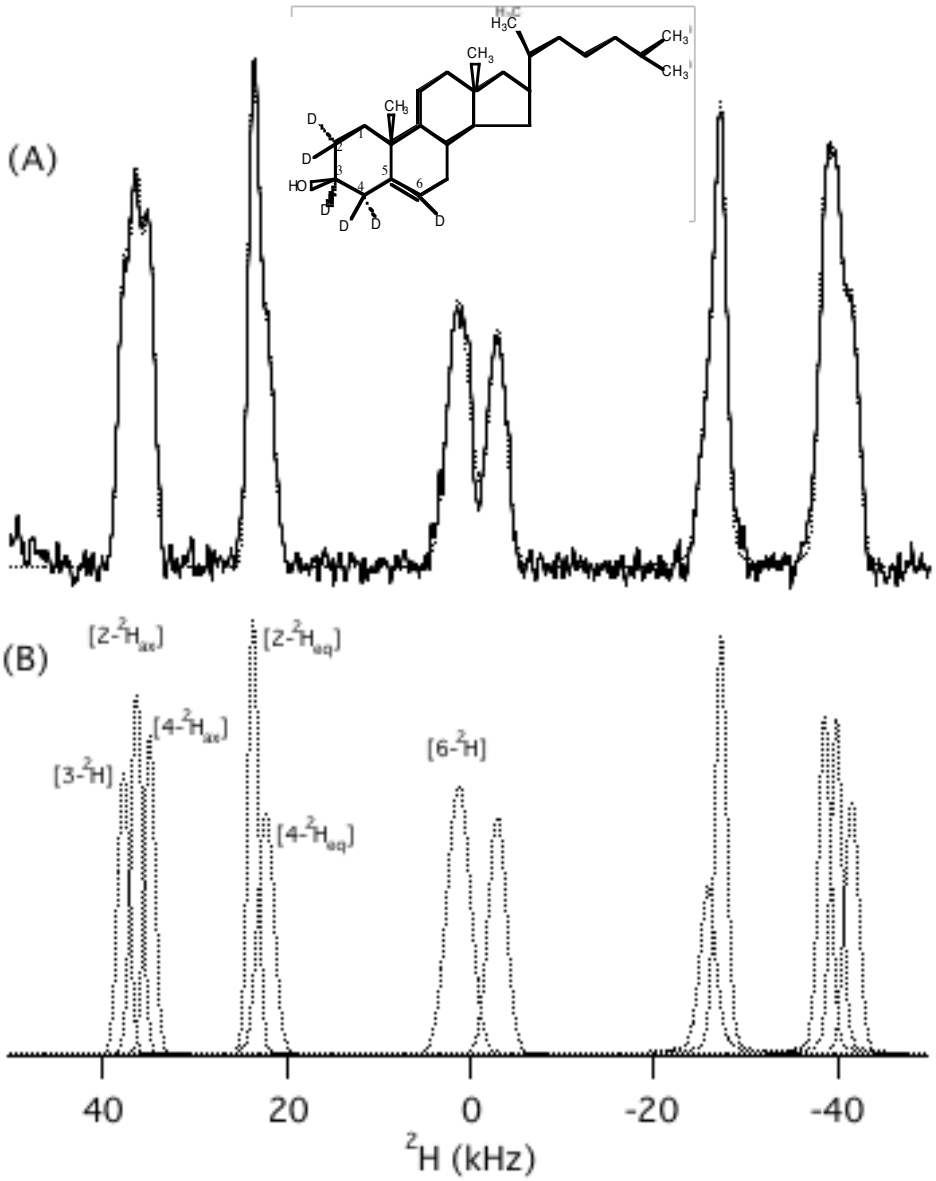

Figure 3.5 ^2H NMR spectra of Tm^{3+}-oped magnetically aligned DMPC/DHPC/ cholesterol-d_6 phospholipids bilayers at 318 K. Cholesterol-d_6 is incorporated into the magnetically aligned bilayers as the deuterium label. The concentration of cholesterol-d_6 is 10 mol% with respect to DMPC. The structure of cholesterol-d_6 is shown in the inset. The simulations were carried out using the DMFIT simulation program. (A) The *solid-line* spectrum represents the ^2H NMR spectrum. The *dotted-line* spectrum is the summed simulated NMR spectrum. (B) The dotted line in the spectrum represents individual peaks that are simulated. The peaks are labeled according to the assignment by Marsan *et.al* (19).

3.4.3. Solid-state NMR study of magnetically aligned phospholipids bilayers using deuterium-labeled DMPC-d_{54}.

The molecular order parameters of ^{2}H-labeled cholesterol will only give information about the flexibility of the lipid chains indirectly. However, by incorporating DMPC-d_{54} into the bicelle samples, the lipid chain dynamics can be directly investigated with ^{2}H solid-state NMR studies. The bicelle samples are analyzed in both the parallel and perpendicular orientations. The molecular order parameters calculated from both bicelle samples are similar. However, only the parallel-aligned phospholipid bilayer data will be presented due to the increased resolution. Figure 3.6 shows a series of ^{2}H NMR spectra of parallel-aligned DMPC/DHPC phospholipid bilayer samples doped with DMPC-d_{54} investigated as a function of cholesterol concentration at 318 K. The ^{2}H NMR spectrum of the bicelle sample with 0 mol% cholesterol with respect to DMPC is well resolved. The good resolution is clearly indicative of well-aligned phospholipid bilayers. As the cholesterol concentration increases, the spectra become broader and start to lose resolution. The bicelle samples prepared in the absence of cholesterol yield well-resolved spectra at 308 K and at a slightly lower temperature. The bicelle samples prepared with 10 mol% cholesterol with respect to DMPC yield well-resolved spectra at a temperature of 318 K or higher. However, for the bicelle samples with 20 mol% cholesterol, well-resolved spectra were obtained only at temperature above 318 K. Thus, the minimum temperature required for alignment of DMPC/DHPC phospholipid bilayers increases as the cholesterol concentration increases from 0 mol% to 20 mol%. This result is consistent with the EPR results.

Figure 3.7 displays the molecular order parameter S_{mol} profile versus the carbon atom position along the acyl chains of DMPC-d_{54} placed into magnetically aligned phospholipid bilayers. The S_{mol} for the individual C-^{2}H bonds of the methylene groups and the terminal methyl groups of the acyl chains is directly evaluated from the corresponding quadrupolar splittings of each group. The quadrupolar splittings for the deuterons in the plateau region are estimated by integration of the last broad peak according to the literature (*41*). Figure 3.7(A) shows the molecular order parameter S_{mol} profile of varying cholesterol concentrations as a function of the carbon number. The

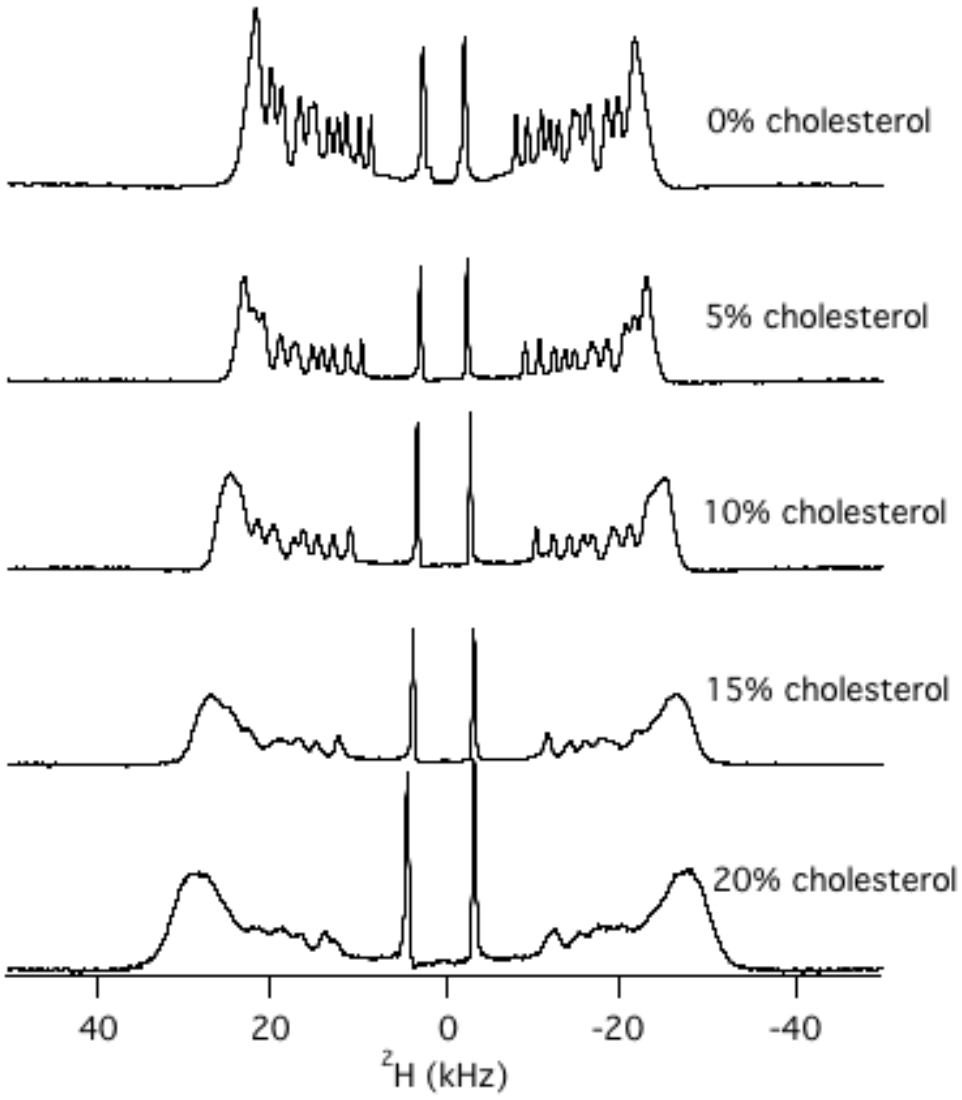

Figure 3.6 ^{2}H-NMR spectra of Tm^{3+}-doped magnetically aligned DMPC/DHPC/DMPC-d_{54}/cholesterol phospholipids bilayers at 318 K. DMPC-d_{54} is incorporated into the magnetically aligned bicelles as the deuterium label. The cholesterol concentration is 0 mol%, 5 mol%, 10 mol%, 15 mol% and 20 mol% with respect to DMPC.

molecular order parameters decrease gradually towards the end of the hydrocarbon chain. Cholesterol enhances the ordering of the entire acyl chain within the phospholipid bilayers as the amount of cholesterol in the bicelle sample increases from 0 to 20 mol% with respect to DMPC. The increase in ordering of the methylene groups near the top of the hydrocarbon chain is almost the same as the increase in ordering of the methyl groups at the end of the hydrocarbon chain as the cholesterol concentration increases. These results indicate that the ordering effect of cholesterol to the phospholipid molecules is uniform along the entire acyl chains of the phospholipid molecules. Figure 3.7(B) shows the temperature effect on the molecular order parameter of DMPC-d_{54} at 15 mol% cholesterol with respect to DMPC. The molecular order parameters decrease as the temperature increases. The decrease in ordering of the methylene groups and methyl groups at different positions along the acyl chain of the phospholipid molecules are almost identical.

The normalized order parameter over the 13 quadrupolar splittings, calculated using $\langle S_{mol} \rangle = \frac{1}{13} \sum_{i=2}^{14} S_{mol}^{i}$, can be used to characterize the ordering of the entire myristoyl chain (*29*). Figure 3.8(A) displays the cholesterol concentration dependence of the normalized order parameter profile as a function of temperature. In Figure 3.8(B), the normalized order parameter is plotted versus cholesterol concentration at various temperatures. $\langle S_{mol} \rangle$ decreases with increasing temperature, but increases with increasing cholesterol concentration. Both graphs indicate that the ordering effect of cholesterol on the membranes is more significant at low temperatures. In contrast, the disordering effect on the membrane caused by increasing the temperature is more significant at high cholesterol concentrations. These results agree well with the corresponding EPR results (Figure 3.3 and 3.4).

Figure 3.9(A) compares the cholestane EPR data from Figure 3.3 with the deuterium-labeled cholesterol-d_6 NMR data. The data show an overall decrease in the S_{mol} order parameters of cholesterol-d_6/cholestane incorporated into the DMPC/DHPC phospholipid bilayers as the sample temperature increases. The cholesterol-d_6/cholestane gives high molecular order parameter values while the phospholipids yield lower

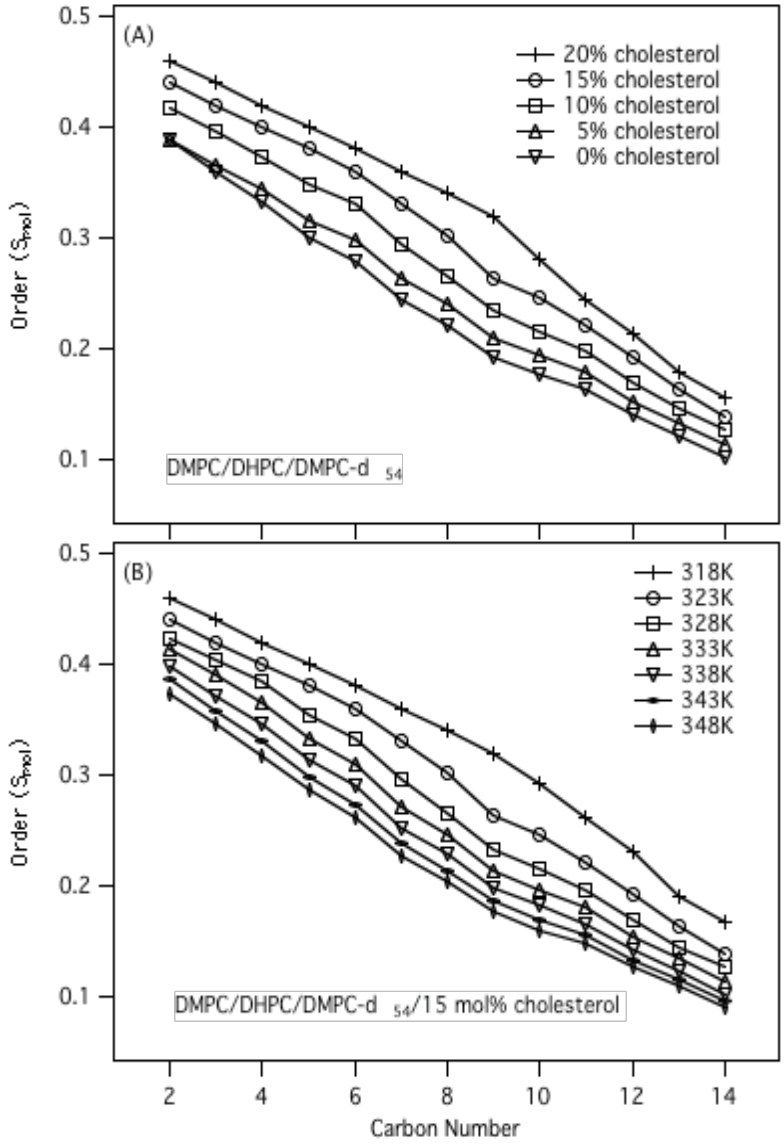

Figure 3.7 Molecular order parameter profiles with respect to the position along the acyl chain of deuterium labeled DMPC-d_{54} incorporated into Tm^{3+}-doped DMPC/DHPC/cholesterol bicelle samples. (A) The cholesterol concentrations are 0 mol%, 5 mol%, 10 mol%, 15 mol% and 20 mol% with respect to DMPC. The sample temperature is 323 K. (B) The cholesterol concentration is 15 mol% with respect to DMPC. The temperature range is from 318 K to 348 K. The DMPC/DHPC/cholesterol bicelles with 15 mol% cholesterol at 308 K and 313 K are not aligned.

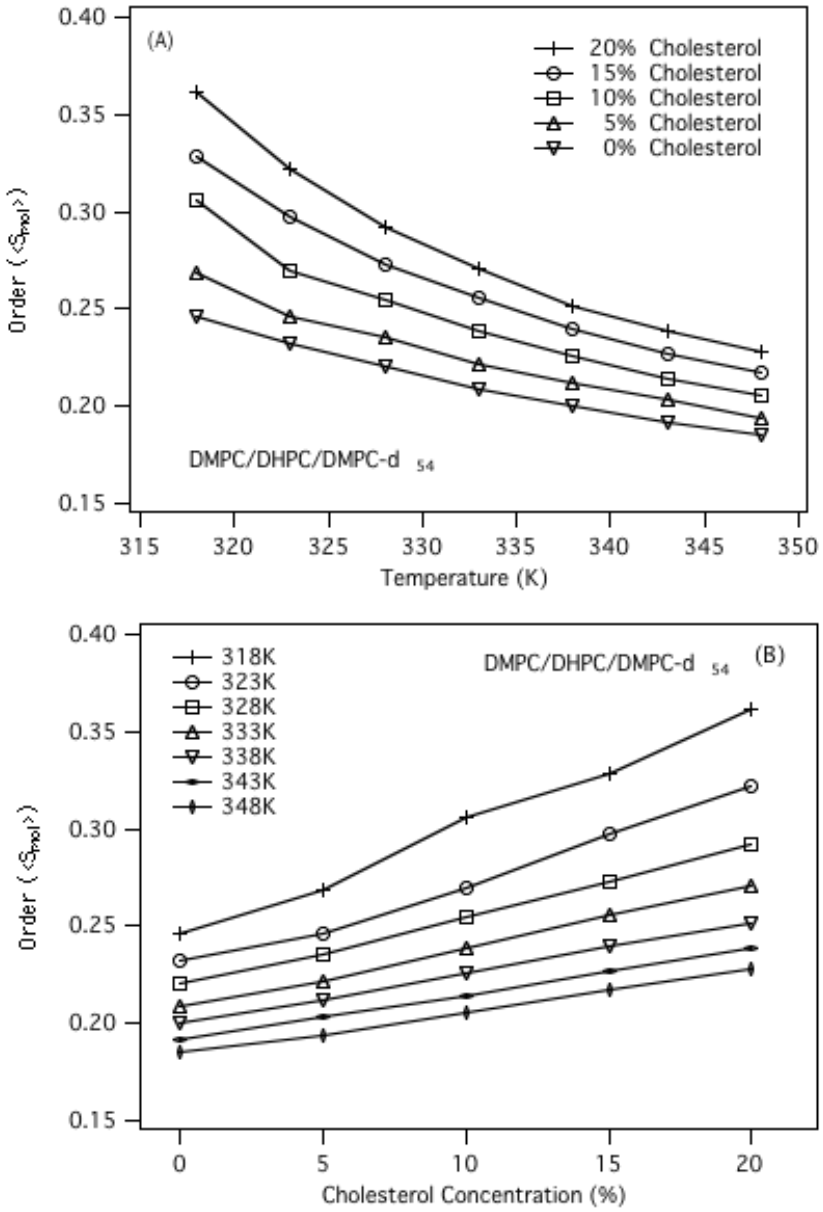

Figure 3.8 (A) The average molecular order parameter profiles over the entire length of the acyl chain of DMPC-d_{54} as a function of temperature in magnetically aligned DMPC/DHPC/cholesterol bicelles at cholesterol concentrations of 0 mol%, 5 mol%, 10 mol%, 15 mol% and 20 mol% with respect to DMPC. (B) The average molecular order parameter profiles over the entire length of the acyl chain of DMPC-d_{54} as a function of cholesterol concentration in magnetically aligned DMPC/DHPC/cholesterol bicelles at different temperatures. Both graphs are from bicelle samples that are aligned with their normal being parallel to the static magnetic field.

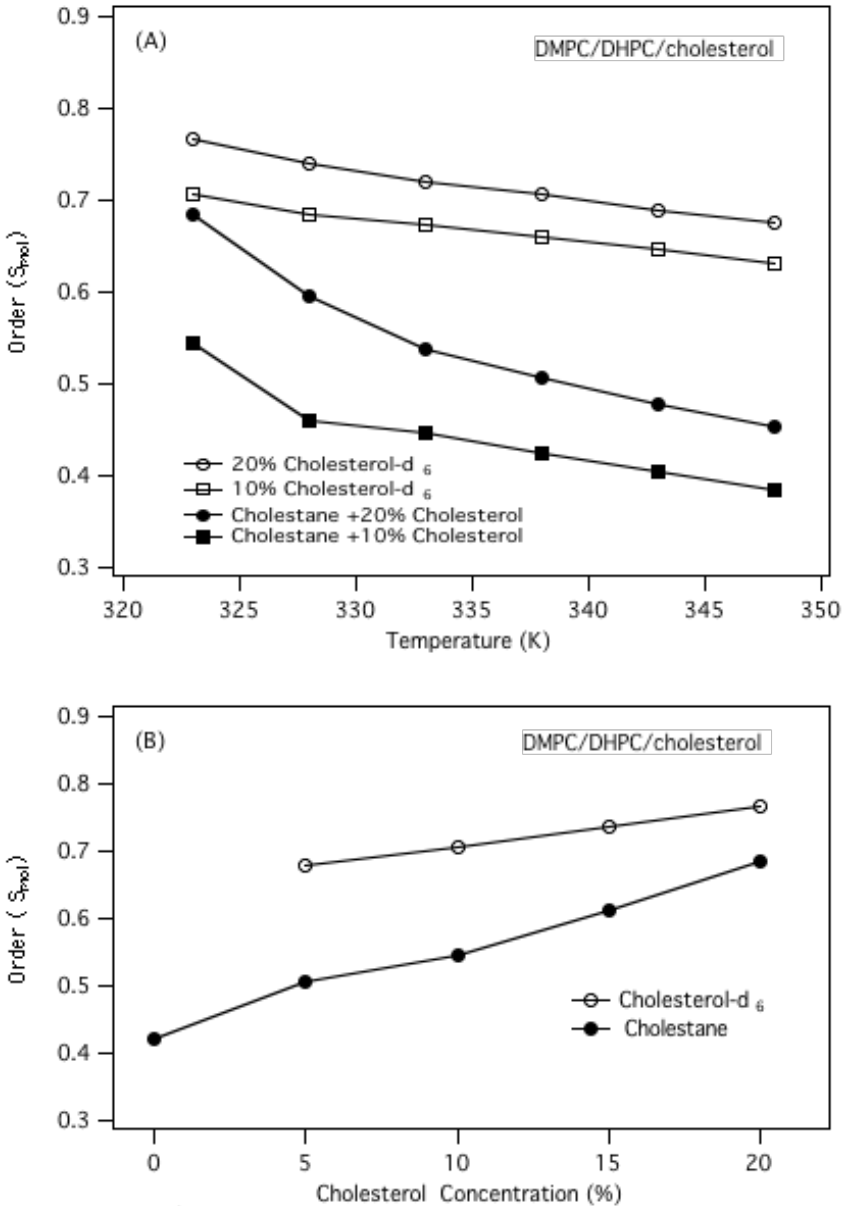

Figure 3.9 A comparison of the molecular order parameters (S_{mol}) obtained by spin-labeled cholestane (open symbols) with S_{mol} obtained by ^{2}H-labeled cholesterol-d_6 (closed symbols) incorporated into DMPC/DHPC/cholesterol bicelles as a function of temperature. (A) S_{mol} is displayed and as a function of the cholesterol concentration. (B) S_{mol} at a temperature of 323K. Tm^{3+}-doped bicelle samples were used to obtain the molecular order parameters from the ^{2}H NMR spectra. Tm^{3+}- and Dy^{3+}- doped bicelle samples were used to obtain the order parameters from cholestane spin probe EPR spectra.

molecular order parameter values (Figure 3.7 and 3.8). These results indicate that phospholipid molecules undergo faster motions than the corresponding cholesterol molecules. ^{2}H-labeled cholesterol and spin-labeled cholestane give slightly different information with deuterium-labeled cholesterol having larger molecular order parameter values and less dependence upon the temperature. Figure 3.9(B) displays the molecular order parameters as a function of cholesterol concentration at 323 K. The cholesterol-d_6/cholestane molecular order parameters increase as the cholesterol concentration increases. ^{2}H NMR spectra of cholesterol-d_6 incorporated into DMPC/DHPC magnetically aligned bilayers show less dependence on the degree of ordering on cholesterol concentration than the corresponding EPR spectra of cholestane incorporated into magnetically aligned phospholipid bilayers.

3.5 Discussion

The EPR lineshapes and hyperfine splittings shown in Figure 3.1 for magnetically aligned phospholipid bilayers are consistent with previously published spectra of aligned bicelles containing cholestane (*30*). The bicelle samples incorporated with cholesterol-d_6 or DMPC-d_{54} yield well-resolved NMR peaks (Figure 3.5 and 3.6). The magnetically aligned spectra demonstrate that cholesterol/cholestane molecules have been successfully incorporated into the bicelle membranes and that the phospholipid bilayers can be well aligned in both EPR and NMR magnetic fields at certain temperatures.

In this paper, we present for the first time the molecular order parameters obtained from both deuterium-labeled cholesterol and deuterium-labeled phospholipid molecules inserted into magnetically aligned phospholipid bilayers. The deuterium-labeled cholesterol-d_6 NMR spectrum yields six different quadrupolar splittings corresponding to C-^{2}H bonds at six different positions of the sterol ring. However, the molecular order parameters calculated from the six quadrupolar splittings are similar to each other in magnitude. The result confirms that cholesterol molecules are fairly rigid inside the DMPC/DHPC phospholipid bilayers. The molecular order parameter profiles of the acyl chains of DMPC-d_{54} incorporated into the bilayers as a function of temperature and cholesterol concentration are also compared in Figure 3.7. The magnitude of change of ordering is uniform along the entire acyl chains from carbon 2 to 14. The phospholipid

acyl chain carbons at position 2-10 have been estimated to lie close to the sterol ring structure of cholesterol (*40*) and the carbons at positions 11 through 14 are close to the side chain tail of cholesterol. Analysis of the data indicates that the cholesterol side chain located at the end of the sterol ring is also rigid and has a similar ordering effect on the phospholipid molecules. The effective length of cholesterol has been estimated to correspond to a 17-carbon all-trans hydrocarbon chain (*40*), while DMPC has 14 carbons on one of its acyl chains. Therefore, the side chain of cholesterol is probably highly packed and tangled in the middle of the phospholipid bilayers, which induces ordering of the membrane in that region.

Three sets of S_{mol} order parameters on cholestane, cholesterol, and phospholipid molecules from both spin-label EPR and ^{2}H NMR spectroscopic studies are presented in this work for the first time on bicelles and are consistent with each other. The degree of ordering increases as the amount of cholesterol in the DMPC/DHPC bilayer samples increases. Actually cholesterol molecules have a higher degree of ordering and slower motion than the corresponding phospholipids molecules in the same sample. The dynamics of the phospholipid membrane can be characterized by three correlation times corresponding to the rotation about the principal diffusion axis of the molecule (chain rotation), rotation about this axis (chain fluctuation or wobbling), and a *trans-gauche* isomerization of the acyl chain. The flat cholesterol molecule with cylindrical symmetry probably has the relatively higher activation energy for molecular rotation about its molecular axis than the corresponding phospholipid molecules. The molecular rotation of phospholipid molecules will slow down because of the close contact of cholesterol molecules with slower motions. At the same time, the rigidity of the cholesterol molecules can also restrict the *trans-gauche* isomerization of the acyl chains of the phospholipid molecules next to it. As the temperature increases, the molecules gain more energy; thus, both the intermolecular motion (chain rotation and fluctuation) and intramolecular motion will increase. Therefore, the molecular ordering decreases when the temperature increases.

A detailed analysis of the EPR spectra of phospholipid bilayers with the nitroxide spin label cholestane revealed that the hyperfine anisotropy tensor has the following values A_{xx}=5.8G, A_{yy}=5.8G and A_{zz}=30.8G (*34*). The observed hyperfine splittings depend

upon the orientation of the spin probe with respect to the magnetic field and the motion of the molecules about its three tensor-axes. The long molecular axis of the cholestane molecule and y-axis of the nitroxide spin label are reported to lie approximately parallel to the membrane normal of the phospholipid bilayers when cholestane is inserted into the membranes. If the phospholipid bilayers are aligned with their bilayer normal perpendicular to the magnetic field, the hyperfine splitting should equal the average value of A_{zz} and A_{xx} ((A_{xx}+A_{zz})/2=18.3 G). The measured hyperfine splitting ranges from 17~18 G, slightly less than the theoretical value of 18.3 G. This variation is attributed to the fluctuation of the long molecular axis of cholestane or the slight difference in the orientation between the long molecule axis and y-axis of the nitroxide spin probe. As the cholesterol concentration reaches 20 mol% in the phospholipid bilayers, the hyperfine splitting increases to 18.4 G at 318K. These results indicate that the addition of cholesterol to the DMPC/DHPC membrane reduces the fluctuation of the molecular axis. Conversely, the hyperfine splitting of cholestane inserted into DMPC/DHPC bilayers in the perpendicular orientation decreases from 18.0 G to 16.8 G when the temperature increases. The decrease in the hyperfine splitting is due to the faster molecular axis fluctuations at higher temperatures. The fast molecular motion makes A_{yy} a nonnegligible factor in determining the hyperfine splittings. An ideal motionally averaged isotropic sample yields an isotropic hyperfine value of 14.5 G ((A_{xx}+A_{yy}+A_{zz})/2=14.5 G).

In Figure 3, the EPR studies indicate that the decrease of ordering displays a steep slope in the low temperature range (308 K to 323 K). At higher temperatures, the decrease of ordering is slower with a smaller slope. There is a noticeable turning point from the steep decrease to the slow decrease around 323 K to 333 K, depending on the cholesterol concentration. This may indicate a morphological change corresponding to the liquid crystalline nematic phase changing to a smectic phase at a temperature around 323 K to 333 K (*30*). When the cholesterol concentration is raised, the presumed nematic-to-smetic phase transition temperature is also raised. At this temperature range, the ^{2}H NMR spectra show higher resolution. These results agree with work in the literature and indicates that a conversion from a positively aligned nematic to a positive aligned smectic phase coexists with an isotropic phase between about 313 K to 328 K (*3*). Previously, we have characterized the nematic to smectic phase change of DMPC/DHPC

bicelle samples with ^{2}H NMR spectroscopy in the absence of cholesterol and cholestane (*30*). However, the changes in the molecular order parameters of DMPC-d_{54} and cholesterol-d_6 given by ^{2}H NMR in Figure 8 and 9 show a gradually decrease as the temperature increases. As mentioned before, EPR spectroscopy is sensitive to molecular motions of phospholipids within the membrane. EPR spectra of nitroxide radicals are particularly sensitive to motions with correlation times between 10^{-10} and 10^{-8} s, which is in the range of correlation times for molecular "long-axis" rotations and wobbling (*18*). In this sense, EPR spectroscopy can provide more detailed information about the membrane than NMR spectroscopy.

In the present paper, both deuterium-labeled cholesterol and spin-labeled cholestane are used to study the DMPC/DHPC bicelle membrane system. The data indicates that the behavior of the two probes is similar. The degree of ordering of the membrane increases as the amount of cholesterol increases in the sample and the ordering decreases as the temperature increases. However, the degree of ordering of cholesterol in the membranes is lower for the EPR data than for the corresponding NMR data (Figure 3.9). This result can be explained by the different properties of the two probes. The cholesterol OH group is replaced by a bulky nitroxide spin label in cholestane, which will probably slightly distort the close packing of the headgroups of the phospholipids bilayers. For the molecular order parameter calculations, different rotational axes are used for the deuterium-labeled cholesterol and the spin-labeled cholestane. The rotation axis of cholesterol is defined in the OH-C_3-^{2}H reference systems (*22*), whereas the motion of the cholestane is believed to be about the nitroxide y-axis (*34*). The small deviation of the rotation axis would also result in the difference observed in the molecular order parameter values.

Inspection of Figure 3.9 indicates that the cholesterol-d_6 NMR data yield larger molecular order parameter values with less dependence upon temperature than the cholestane EPR data. The order parameters given by cholestane show a larger dependence upon temperature and cholesterol concentration. The correspondence between the magnitudes of the molecular order parameters for the two probes is best in situations of high inherent order (high cholesterol and low temperature). The S_{mol} values from EPR and NMR data diverge as the membrane becomes more flexible and the degree

of ordering decreases. The degree of ordering in the membrane with cholestane is more sensitive to changes in membrane composition and environment probably duo to the existence of the nitroxide radicals. In a comparison study of phospholipid bilayer systems that contain the cholestane spin probe or a cholesterol-3α–*d* deuterium probe, the NMR results show less dependence upon temperature and cholesterol concentration, which agrees with our results (*8*). The discrepancy between the EPR and NMR data observed in this paper is also caused by the difference in sensitivity of the two techniques over the various molecular motion time scales. ^{2}H NMR spectra are sensitive to motions with correlation times between 10^{-3} and 10^{-9} s (*42*), whereas EPR spectra of nitroxide spin probes are particularly sensitive to faster motions with correlation times between 10^{-10} and 10^{-8} s (*21*). The phospholipids molecular chain rotation and wobbling will be at the fast-motional limit of NMR time scale. When the temperature increases or the amount of cholesterol in the bilayers decreases, the membrane will be more fluid and the molecules will undergo faster motions. Under these conditions, the correlation time fits better on the EPR time scale. Thus, spin-label EPR spectroscopy is more sensitive for probing faster motions, when compared to solid-state ^{2}H NMR spectroscopy. This explains why the molecular order parameter values obtained by EPR spectroscopy and NMR spectroscopy studies are more consistent under conditions of higher ordering in the membrane.

In both the EPR and NMR spectroscopic studies, the minimum alignment temperature of the bicelles increases as the cholesterol concentration increases. The DMPC/DHPC phospholipid bilayers in the absence of cholesterol are aligned at a minimum temperature of 308 K. The DMPC/DHPC phospholipid bilayers with 20 mol% cholesterol with respect to DMPC are aligned at a minimum temperature of 318 K (10 K higher). The alignment of the bicelles is a cooperative phenomenon. The alignment of bicelles only occurs when the sample temperature is raised above the lipid gel-to-liquid crystalline phase transition temperature. In the gel phase, the ^{2}H NMR spectrum exhibits only an isotropic peak, which suggests the formation of small rapidly tumbling bicelles in an isotropic phase (*20, 30*). Above the gel-to-liquid crystalline phase transition temperature, the bicelles become aligned in the magnetic field. The phase of the phospholipid bilayers is sensitive to membrane compositions, membrane hydration,

temperature and other factors (*31, 42*). The incorporation of cholesterol alters the physical and phase properties of the phospholipid bilayers. Cholesterol increases the molecular ordering of the phospholipid molecules at the temperature above the gel-to-liquid crystalline phase transition temperature, most likely by restricting the motions of the neighboring acyl chains, reducing the fraction of *gauche* bonds of the acyl chains, making the acyl chains pack tighter together. As discussed above, the membrane nematic-to-smectic phase transition temperature also increases as the cholesterol concentration is raised in the DMPC/DHPC phospholipid bilayer samples. The data suggests that the lipid gel-to-liquid phase transition temperature is raised by increasing the cholesterol concentration, and the minimum bicelle alignment temperature increases as well.

3.6 Conclusion

We present here for the first time a comparison of both spin-labeled EPR and ^{2}H-labeled NMR techniques to study the cholesterol effect on DMPC/DHPC magnetically aligned phospholipid bilayer membranes. Both techniques are ideal ways to study the unique phospholipid membrane system. Our study provides a relatively complete picture of the cholesterol effect on bicelles by both EPR and solid-state NMR techniques with different sensitivity. Cholesterol molecules are rather rigid. Cholesterol incorporated into the phospholipid bilayers increases the molecular ordering of the phospholipid acyl chains, stabilizes the liquid crystalline phase of the phospholipids, increases the minimum alignment temperature of the DMPC/DHPC phospholipid bilayers, and increases the liquid crystalline nematic-to-smectic phase transition temperature. The S_{mol} values obtained in this paper for DMPC/DHPC bilayers are consistent with previous EPR and solid-state NMR studies on other phospholipid bilayer systems (*8, 9, 18, 22, 43, 44*). Thus, magnetically aligned phospholipid bilayers represent an excellent model membrane system for both spin-labeled EPR and solid-state NMR studies.

ACKNOWLEDGEMENTS

The X-band EPR spectrometer was obtained from National Science Foundation Grant CHE-97, 24192. This work was supported by a National Science Foundation

CAREER Award (CDE-0133433) Award and an American Heart Association Scientist Development Grant (0130396). We would like to acknowledge Krishnan Damodaran and Dr. Hongcai Zhou for their help in the spectral simulations and the order parameter calculations.

3.7 References

(1) Yeagle, P. L. (1985) Cholesterol and the cell membrane. *Biochim. Biophys. Acta 822*, 267-287.

(2) Borroni, B., Pettenati, C., Bordonali, T., Akkawi, N., Luca, M. D., and Padovani, A. (2003) Serum cholesterol levels modulate long-term efficacy of cholinesterase inhibitors in Alzherimer disease. *Neuroscience Lett. 343*, 213-215.

(3) Mironov, V. S., Galyametdinov, Y. G., Ceulemans, A., and Binnemans, K. (2000) On the magnetic anisotropy of lanthanide-containing metallomesogens. *J. Chem. Phys. 113*, 10293-10303.

(4) Chiu, S. W., Jakobsson, E., Mashl, J., and Scott, H. L. (2002) Cholesterol-induced modifications in lipid bilayers: a simulation study. *Biophys. J. 83*, 1842-1853.

(5) Kessel, A., Ben-Tal, N., and May, S. (2001) Interactions of cholesterol with lipid bilayers: the preferred configuration and fluctuations. *Biophys. J. 81*, 643-658.

(6) Jedlovszky, P., and Mezei, M. (2003) Effect of cholestrol on the properties of phospholipid membranes. 1. structural features. *J. Phys. Chem. B 107*, 5311-5321.

(7) Epand, R. M., Bain, A. D., Sayer, B. G., Bach, D., and Wachtel, E. (2002) Properties of mixtures of cholesterol with phosphatidylcholine or with phosphatidylserine studied by ^{13}C magic angle spinning nuclear magnetic resonance. *Biophys. J. 83*, 2053-2063.

(8) Taylor, M. G., and Smith, I. C. P. (1981) Reliability of nitroxide spin probes in reporting membrane properties: a comparison of nitroxide- and deuterium-labeled steroids. *Biochemistry 20*, 5252-5255.

(9) Dufourc, E. J., Parish, E. J., Chitrakorn, S., and Smith, I. C. P. (1984) Structural and dynamical details of cholesterol-lipid interaction as revealed by deuterium NMR. *Biochemistry 23*, 6062-6071.

(10) Lemmich, J., Mortensen, K., Ipsen, J. H., Honger, T., Bauer, R., and Mouritsen, O. G. (1997) The effect of cholesterol in small amounts on lipid-bilayer softness in the region of the main phase transition. *Eur. Biophys. J. 25*, 293-304.

(11) Rappolt, M., Vidal, M. F., Kriechbaum, M., Steinhart, M., Amenitsch, H., Bernstorff, S., and Laggner, P. (2003) Structural, dynamic and mechanical properties of POPC at low cholesterol concentration studied in pressure/temperature space. *Euro. Biophys. J. Biophys. Lett. 31*, 575-585.

(12) McMullan, R. K., and McElhaney, R. N. (1996) Physical studies of cholesterol-phospholipid interactions. *Curr. Opin. Colloid Interface Sci. 1*, 83-90.

(13) Hofsäb, C., Lindahl, E., and Edholm, O. (2003) Molecular dynamics simulations of phospholipid bilayer with cholesterol. *Biophys. J. 84*, 2192-2206.

(14) Smondyrev, A. M., and Berkowits, M. L. (1999) Structure of dipalmitoylphosphatidylcholine/cholesterol bilayer at low and high cholesterol concentrations: molecular dynamics simulation. *Biophys. J. 77*, 2075-2089.

(15) Trouard, T. P., Nevzorov, A. A., Alam, T. M., Job, C., Zajicek, J., and Brown, M. F. (1999) Influence of cholesterol on dynamics of dimyristoylphosphatidylcholine bilayers as studied by deuterium NMR relaxation. *J. Chem. Phys. 110*, 8802-8818.

(16) Dave, P. C., Tiburu, E. K., Nusair, N. A., and Lorigan, G. A. (2003) Calculating order parameter profiles utilizing magnetically aligned phospholipid bilayers for ^{2}H solid-state NMR studies. *Solid State Nucl. Magn. Reson. 24*, 137-149.

(17) Tiburu, E. K., Dave, P. C., and Lorigan, G. A. (2004) Solid-state ^{2}H NMR studies of the effects of cholesterol on the acyl chain dynamics of magnetically aligned phospholipid bilayers. *Magn. Reson. in Chem. 42*, 132-138.

(18) Moser, M., Marsh, D., Meier, P., Wassmer, K. H., and Kothe, G. (1989) Chain configuration and flexibility gradient in phospholipid membranes. Comparison between spin-label electron spin resonancee and deuteron nuclear magnetic resonance, and identification of new conformations. *Biophys. J. 55*, 111-123.

(19) Seelig, J., and Niederberger, W. (1974) Two pictures of a lipid bilayer. A comparison between deuterium label and spin-label experiments. *Biochemistry 13*, 1585-1588.

(20) Tiburu, E. K., Moton, D. M., and Lorigan, G. A. (2001) Development of magnetically aligned phospholipid bilayers in mixtures of palmitoylsteroylphosphatidylcholine and dihexanoylphosphatidylcholine by solid-state NMR spectroscopy. *Biochim. Biophys. Acta 1512*, 206-214.

(21) Blume, A. (1993) Dynamic Properties, in *Phospholipids handbook* (Cevc, G., Ed.) pp 988, Marcel Dekker, INC., New York.

(22) Marsan, M. P., Muller, I., Ramos, C., Rodriguez, F., Dufourc, E. J., Czaplicki, J., and Milon, A. (1999) Cholesterol orientation and dynamics in dimyristoylphosphatidylcholine bilayers: a solid state deuterium NMR analysis. *Biophys. J. 76*, 351-359.

(23) Schäfer, H., Mädler, B., and Sternin, E. (1998) Determination of orientational order parameters from ^{2}H NMR spectra of magnetically partially oriented lipid bilayers. *Biophys. J. 74*, 1007-1014.

(24) Prosser, R. S., Hunt, S. A., DiNatale, J. A., and Vold, R. R. (1996) Magnetically aligned membrane model systems with positive order parameter: switching the sign of S_{zz} with paramagnetic ions. *J. Am. Chem. Soc. 118*, 269-270.

(25) Cardon, T. B., Tiburu, E. K., Padmanabhan, A., Howard, K. P., and Lorigan, G. A. (2001) Magnetically aligned phospholipid bilayers at the parallel and perpendicular orientations for X-band spin-label EPR studies. *J. Am. Chem. Soc. 123*, 2913-2914.

(26) Howard, K. P., and Opella, S. J. (1996) High-resolution solid-state NMR spectra of integral membrane proteins reconstituted into magnetically oriented phospholipid bilayers. *J. Magn. Reson. B. 112*, 91-94.

(27) Mangels, M. L., Cardon, T. B., Harper, A. C., Howard, K. P., and Lorigan, G. A. (2000) Spectroscopic characterization of spin-labeled magnetically oriented phospholipid bilayers by EPR spectroscopy. *J. Am. Chem. Soc. 122*, 7052-7058.

(28) Sanders, C. R., Hare, B. J., Howard, K. P., and Prestegard, J. H. (1994) Magnetically-oriented phospholipid micelles as a tool for the study of membrane-associated molecules. *Prog. in NMR Spectrosc. 26*, 421-444.

(29) Prosser, R. S., Hwang, J. S., and Vold, R. R. (1998) Magnetically aligned phospholipid bilayers with positive ordering: a new model membrane system. *Biophys. J. 74*, 2405-2418.

(30) Cardon, T. B., Tiburu, E. K., and Lorigan, G. A. (2003) Magnetically aligned phospholipid bilayers in weak magnetic fields: optimization, mechanism, and advantages for X-band EPR studies. *J. Magn. Reson. 161*, 77-90.

(31) Faure, C., Bonakdar, L., and Dufourc, E. J. (1997) Determination of DMPC hydration in the La and Lb' phases by ^{2}H solid state NMR of D_2O. *FEBS Lett. 405*, 263-266.

(32) Raffard, G., Steinbruckner, S., Arnold, A., Davis, J. H., and Dufourc, E. J. (2000) Temperature-composition diagram of dimyristoylphosphatidylcholine-dicaproylphosphatidylcholine "bicelles" self-orienting in the magnetic field. A solid state ^{2}H and ^{31}P NMR study. *Langmuir 16*, 7655-7662.

(33) Caporini, M. A., Padmanabhan, A., Cardon, T. B., and Lorigan, G. A. (2003) Investigating magnetically aligned phospholipid bilayers with various lanthanide ions for X-band spin-label EPR studies. *Biochim. Biophys. Acta 1612*, 52-58.

(34) Smith, I. C. P., and Butler, K. W. (1976) Oriented lipid systems as model membranes, in *Spin labeling, theory and application* (Berliner, J. B., Ed.) pp 592, Academic Press, INC, New York.

(35) Aussenac, F., Tavares, M., and Dufourc, E. J. (2003) Cholesterol dynamics in membranes of raft composition: a molecular point of view from ^{2}H and ^{31}P solid-state NMR. *Biochemistry 42*, 1383-1390.

(36) Powels, J. G., and Strange, J. H. (1963) Zero time resolution nuclear magnetic resonance (N. M. R.) transients in solids. *Proc. Phys. Soc. 82*, 6-15.

(37) Seelig, J. (1976) Anisotropic motion in liquid crystalline structure, in *Spin labeling, theory and applications* (Berliner, J. B., Ed.) pp 592, Academic Press, INC., New York.

(38) McMullan, R. K., and Koetzle, T. F. (1992) Structure of [20-CH_3], [20-CD_3]-Methylpregnene-3,20-diol Methanolate from neutron diffraction at 123K. *Acta. Cryst. C48*, 1509-1512.

(39) Massiot, D., Fayon, F., Capron, M., King, I., Le Calvé, S., Alonso, B., Durand, J.-O., Bujoli, B., Gan, Z., and Hoatson, G. (2002) Modelling one- and two-dimensional solid state NMR spectra. *Magn. Reson. in Chem. 40*, 70-76.

(40) Ohvo-Rekilä, H., Ramstedt, B., Leppimäki, P., and Slotte, J. P. (2002) Cholesterol interactions with phospholipids in membranes. *Prog. in Lipid Res. 41*, 66-97.

(41) Huster, D., Arnold, K., and Garisch, K. (1998) Influence of docosahexaenoic acid and cholesterol on lateral lipid organization in phospholipid mixtures. *Biochemistry 37*, 17299-17308.

(42) Meier, P., Ohmes, E., Kothe, G., Blume, A., Weldner, J., and Elbl, H. (1983) Molecular order and dynamics of phospholipid membranes. a deuteron magnetic resonance study employing a comprehensive line-shape model. *J. Phys. Chem. 87*, 4904-4912.

(43) Lange, A., Marsh, D., Wassmer, K. H., Meier, P., and Kothe, G. (1985) Electron spin resonance study of phospholipid membranes employing a comprehensive line-shape model. *Biochemistry 24*, 4383-4392.

(44) Meier, P., Ohmes, E., and Kothe, G. (1986) Multipulse dynamic nuclear magnetic resonance of phospholipid membranes. *J. Chem. Phys. 85*, 3598-3614.

Chapter 4

Solid-State NMR Relaxation Studies of the Interaction Mechanism of Antimicrobial Peptides with Phospholipid Bilayer Membranes

Lu, J.X., Damodaran, K., Blazyk, J., and Lorigan, G. A. "Solid-State NMR Relaxation Studies of the Interaction Mechanism of Antimicrobial Peptides with Phospholipid Bilayer Membranes" *Biochemistry* (2005) 44, 10208-10217.

Abbreviations: KIGAKI, KWGAKIKIGAKIKIGAKI-NH_2; POPC, 1-Palmitoyl-2-oleoyl-3-*sn*-glycero-3-phospholcholine; POPG, 1-Palmitoyl-2-oleoyl-3-*sn*-glycero-3-[phospho-rac-1-glycerol]; POPC-d_{31}1-Palmitoyl-d_{31}-2-oleoyl-3-*sn*-glycero-3-phospholcholine; POPG-d_{31}, 1-Palmitoyl-d_{31}-2-oleoyl-3-*sn*-glycero-3-[phospho-rac-1-glycerol]; HEPES, N-[2-hydroxyethyl] piperazine-N'-[2-ethanesulfonic acid], TFE, 2,2,2, trifluoroethanol; EDTA, ethylenediamine tetraacetic acid; Fmoc, N-(9-fluorenyl)methoxycarbonyl; HPLC, high performance liquid chromatography; CPMAS, cross-polarization magic angle spinning; MLVs, multilamellar vesicles; LUVs, large unilamellar vesicles.

4.1 Abstract

An 18-residue peptide, KWGAKIKIGAKIKIGAKI-NH_2 was designed to form amphiphilic β-sheet structures when bound to lipid bilayers. The peptide possesses high antimicrobial activity when compared to naturally occurring linear antimicrobial peptides, most of which adopt an amphipathic α-helical conformation upon binding to the lipids. The perturbation of the bilayer by the peptide was studied by static ^{31}P and ^{2}H solid-state NMR spectroscopy using POPC and POPG/POPC (3/1) bilayer membranes with *sn-1* chain perdeuterated POPC and POPG as the isotopic labels. ^{31}P NMR powder spectra exhibited two components for POPG/POPC bilayers upon addition of the peptide, but only a slight change in the lineshape for POPC bilayers, indicating that the peptide selectively disrupted the membrane structure consisting of POPG lipids. ^{2}H NMR powder spectra indicated a reduction in the lipid chain order for POPC bilayers and no significant change in the ordering for POPG/POPC bilayers upon the peptide association with the bilayers, suggesting the peptide acts as a surface peptide in POPG/POPC bilayers. Relaxation rates are more sensitive to the motions of the membranes over a large range of time scales. Longer ^{31}P longitudinal relaxation times for both POPG and POPC in the presence of the peptide indicated a direct interaction between the peptide and the POPG/POPC bilayer membranes. ^{31}P longitudinal relaxation studies also suggested that the peptide prefers to interact with the POPG phospholipids. However, inversion-recovery ^{2}H NMR spectroscopic experiments demonstrated a change in the relaxation rate of the lipid acyl chains for both the POPC membranes and the POPG/POPC membranes upon interaction with the peptide. Transverse relaxation studies indicated an increase in the spectral density of the collective membrane motion caused by the interaction between the peptide and the POPG/POPC membrane. The experimental results demonstrate significant dynamic changes in the membrane in the presence of the antimicrobial peptide, and support a carpet mechanism for the disruption of the membranes by the antimicrobial peptide.

4.2 Introduction

A large number of antimicrobial peptides have been studied recently because of their potential to serve as medical alternatives to antibiotics (*1, 2*). These defense peptides usually possess a net positive charge and are able to form an amphipathic structure when bound to phospholipid bilayers. Many of these antimicrobial peptides, such as PGLa (*3, 4*) and magainins (*5, 6*), adopt an amphipathic α-helical conformation when interacting with the membrane. Conversely, some antimicrobial peptides form an amphipathic β-sheet structure because of their intrinsic intra-molecular disulfide bonds (*6*). In this paper, a novel linear amphiphilic β-sheet cationic antimicrobial peptide KIGAKI was used. This peptide was designed to have a high hydrophobic moment value (0.63) for a β-sheet structure and low hydrophobic moment value (0) for an α-helical structure (*7*). The absence of cysteine residues precludes the formation of either inter- or intra-molecular disulfide bonds to stabilize the secondary structure. In a previous paper, CD and FTIR spectroscopy results showed that this peptide does indeed adopt a β-sheet conformation when bound to anionic lipids (*7*). One important factor in determining the potential application of these antimicrobial peptides is the ability of the peptides to disrupt prokaryotic membranes at concentrations that are not harmful to host membranes. The antimicrobial and hemolytic activity of KIGAKI showed higher antimicrobial activity than PGLa and magainins and an increased selectivity between bacterial and mammalian cells (*7, 8*).

While these functional properties appear promising, no studies on KIGAKI have been reported to address the origin of the selectivity at the molecular level. In order to obtain a better understanding of the mechanism of the antimicrobial activity and selectivity of this peptide, solid-state NMR longitudinal (T_1) and transverse relaxation (T_2) experiments are reported here that examine the effects of KIGAKI on membrane structure and lipid mobility.

Recently, solid-state NMR spectroscopy has been widely applied to studying short membrane active peptides, such as human LL-37, HIV intracellular domain gp41, magainin, protegrin-1, colicin Ia (*3-6, 9-15*), using uniformly labeled or site-specifically labeled peptides while details of the dynamic and conformational information were obtained. Little useful information about the dynamics of the phospholipid bilayer

membranes could be determined from these results. Static ^{31}P and ^{2}H solid-state NMR spectroscopy are the most common techniques used in studying the perturbation of the phospholipid bilayers by peptides. In fact, the bilayer membranes possess a variety of motions with a hierarchy of correlation times, including the fast *trans-gauche* isomerization of acyl chains (10^{-10}-10^{-9} s), the long axis rotation of the lipids (10^{-9}-10^{-8} s), the lipid lateral diffusion (10^{-8}-10^{-7} s), and the whole membrane slow-order director fluctuations whose correlation times depend upon membrane size and thickness (16). Depending upon the nature of the interaction, the peptide can modify these motions in different time scales (17). It is very important to choose the appropriate technique to detect these motions. One type of interaction may appear fast (averaged) and featureless when viewed by one technique, but slow (discrete) with the other techniques. Solid-state NMR spectroscopy is a powerful method that can determine molecular motions over a wide range of time scales (*16*). The averaging deuterium quadrupolar interaction can detect molecular motions of ~10-100 kHz, and the averaging ^{31}P chemical shift anisotropy is effective for probing rates of ~4-6 kHz (*16*). Moreover, NMR relaxation time measurements are more appropriate to probe the dynamics of the phospholipid bilayers (18). The longitudinal relaxation time (T_1) is sensitive to the lipid molecular motions in the ns-μs time scale, which includes rapid conformational changes of lipid acyl chains and polar head groups and long axis rotations and diffusion of the lipids (fast molecular motion) (19-21). The transverse relaxation time (T_2) is sensitive to motions in the ms range which is effective for measuring collective lipid motions in the bilayer (slow molecular motion) (22-24).

Two biologically relevant membrane systems were studied here. Multilamellar vesicles (MLVs) contain either POPC or a mixture of POPG and POPC at 3/1 molar ratio. POPC is a neutral zwitterionic phospholipid that is abundant in mammalian cell membranes. POPG is an anionic lipid that is commonly found in bacterial plasma membranes (*7*). ^{2}H-labeled POPC and POPG acyl chains were used in order to localize the influence of the peptide on each lipid class in the bilayer. The static powder spectra of ^{31}P from the lipid headgroups and ^{2}H from the acyl chains showed significant difference between POPC bilayers and POPG/POPC bilayers, indicating that KIGAKI interacts with these membrane systems in a selective manner. We propose that this short

cationic peptide aggregates into β-sheet structures and disrupts the membrane through an electrostatic interaction at the surface of the bilayers when it binds to the membrane containing anionic lipids, such as POPG. The relaxation studies carried out in this work reveal unique dynamic information over a large time scale range that further supports this mechanism. A significant change occurs in the ^{31}P T_1 and T_2 relaxation times at the surface of the bilayers as well as the ^{2}H relaxation times in the hydrophobic interior of the bilayers upon addition of the KIGAKI peptide. A complete picture of the membrane dynamics in the presence of the antimicrobial peptide is discussed.

4.3 Material and Methods

4.3.1 Material

POPC, POPG, POPC-d_{31} and POPG-d_{31} were purchased from Avanti Polar Lipids (Alabaster, AL) and used without further purification. All phospholipids were dissolved in chloroform and stored at -20°C prior to use. Deuterium-depleted water was obtained from Isotec (Miamisburg, OH). HEPES, TFE and EDTA were obtained from Sigma/Aldrich (St. Louis, MO). The antimicrobial peptide KIGAKI was synthesized using Fmoc chemistry by ResGen (Huntsville, AL). The crude peptides were purified by reverse-phase HPLC. The purity of the peptide (>95%) was checked by reverse-phase HPLC and electrospray mass spectrometry.

4.3.2 NMR sample preparation

MLV samples containing either POPC MLV or POPG/POPC (3/1) MLV were prepared according to the following procedure (25). The phospholipid mixture (0.1 mmol) was first dried under a steady stream of N_2 gas for ~ 30 mins to remove the organic solvent. The deuterated lipids represented 15 mol% of the total phospholipids. The sample was then left under a high vacuum dessicator overnight. MLVs were formed by resuspension of the dry lipids in 190μL HEPES buffer (5mM EDTA, 20mM NaCl, and 30mM HEPES, pH 7.0) with frequent vortexing to homogenize the sample. Samples were then allowed to sit in a warm water bath (50 °C) for 20 mins. The peptides were dissolved in 100μL TFE and sonicated for 10 mins. Bilayer samples with peptides were prepared by mixing the peptides in TFE solvent with phospholipids in chloroform followed with the same drying down procedure described above. Next, the samples were

hydrated using 190μL HEPES buffer (5mM EDTA, 20mM NaCl, and 30mM HEPES, pH 7.0). After vortexing, the samples were put in a water bath (50 °C) for 20 mins.

4.3.3 NMR spectroscopy

All experiments were recorded on a Bruker Avance 500 MHz WB solid-state NMR spectrometer using a 4mm triple resonance CPMAS probe. ^{31}P static NMR spectra were acquired at 202.4 MHz using a spin-echo pulse sequence with proton decoupling. ^{2}H static NMR experiments were performed at 76.77 MHz using a quadrupolar echo pulse sequence. The 90° pulses used for ^{31}P and ^{2}H were 4.0 μsec, 3.0 μsec respectively.

^{31}P T_{1z} longitudinal relaxation experiments were conducted using an inversion-recovery pulse sequence 180°-T-90°-acq. The delay time (T) was varied from 10.0 msec to 6.0 sec. ^{31}P T_2 transverse relaxation experiments were studied using a spinecho sequence 90°-τ-180°-τ-acq. The innerpulse delay time (τ) was varied over a range from 243.7 μsec to 99.994 msec. The ^{31}P solid-state NMR relaxation study was conducted when the sample was spun at 4 kHz at the magic angle. For the ^{31}P transverse relaxation experiments, rotor synchronization was used (26, 27). ^{2}H T_{1z} longitudinal relaxation experiments were recorded using the inversion-recovery quadrupolar echo sequence 180°-T-90°-τ-90°-τ-acq. The delay time (T) was varied from 2.0 msec to 1.5 sec. ^{2}H T_2 transverse relaxation experiments were carried out using a standard quadrupolar echo pulse sequence: 90°-τ-90°-τ-acq. The innerpulse delay time (τ) was varied between 10.0 μsec to 6.0 msec (28).

4.3.4 NMR data analysis

Powder-type ^{2}H NMR spectra of multilamellar dispersions of POPC-d_{31} or POPG-d_{31} were deconvoluted (dePaked) using the algorithm of McCabe and Wassall (29). The spectra were deconvoluted such that the bilayer normal was parallel with respect to the direction of the static magnetic field. The ^{2}H order parameters S_{CD} were calculated according to the equation: $S^{i}_{CD} = \Delta\nu_i / (3/2(e^2qQ/h))$, where $\Delta\nu_i$ is the quadrupolar splitting for a deuteron attached to the *ith* carbon of the POPC or POPG acyl chain, and e^2qQ/h is the quadrupole coupling constant (168 kHz for deuteron in C-D bonds) (30, 31). The order parameters of the methyl groups at the end of the acyl chain were 3 times of the calculated S_{CD} (30). Powder-type ^{31}P NMR spectra of POPG/POPC MLVs

associated with 4 mol% peptide with respect to the total lipids concentration were fitted using two components with the DMFIT program (32).

For the ^{31}P and ^{2}H longitudinal relaxation study, the change in the area under a particular peak was fitted to a single exponential function: $I(t) = I(0)-Aexp(-t/T_1)$, where I(0) is close to 1 and A is about 2 (28). The standard deviation of each ^{31}P T_1 value is within ± 0.005 ms. The ^{2}H longitudinal relaxation rate $R_{1z} = 1/T_1$. The standard deviation of each R_{1z} value is within ± 0.02 s^{-1}. A double exponential decay $I(t) = A_s exp(-2t/T_{2S}) + A_f exp(-2t/T_{2F})$ was used to fit the ^{31}P transverse relaxation data. The standard deviation of T_{2S} value (the slow component with longer ^{31}P transverse relaxation time) is within ± 0.5 ms, whereas the standard deviation of T_{2F} value (the fast component with shorter ^{31}P transverse relaxation time) is within ± 0.1 ms. For the ^{2}H transverse relaxation study, the decay of the peak area was fitted to the equation: $I(t) = Aexp(-2t/T_2)$, where A is about 1 (28). The standard deviation of each T_2 value is within ± 0.1 μs. The fitting was performed using Igor Pro Carbon version 4.05A (WaveMetrics Inc.) on a G5 Mac computer.

4.4 Results

The effect of the antimicrobial peptide KIGAKI on the dynamic properties of phospholipid bilayers was examined using ^{31}P and ^{2}H NMR longitudinal and transverse relaxation studies. Three MLV samples consisting of POPC/POPC-d_{31}, POPG/POPC/POPC-d_{31} and POPG/POPC/POPG-d_{31} were studied with and without peptide. First, the static ^{31}P and ^{2}H NMR powder spectra were compared for the POPC and POPG/POPC (3/1) MLVs. Then the ^{31}P and ^{2}H NMR longitudinal relaxation times were measured. ^{31}P and ^{2}H NMR transverse relaxation were then performed only for POPG/POPC (3/1) MLVs.

4.4.1 ^{31}P and ^{2}H Solid-State NMR spectroscopy of POPC and POPG/POPC MLVs interacting with KIGAKI

Static ^{31}P solid-state NMR spectra were collected for POPC lipid dispersions with different peptide concentrations (from 0 mol% to 8 mol% with respect to the total lipids

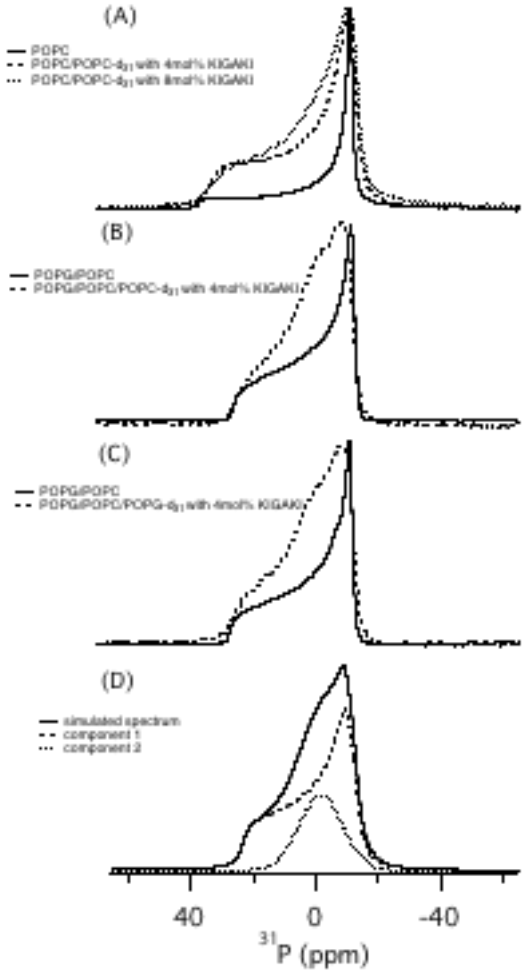

Figure 4.1 (A) ^{31}P NMR powder spectra of POPC MLVs at 25 °C. The *solid line* represents the spectrum of the control POPC MLVs. The *dash line* represents the spectrum of the POPC MLVs with 4 mol% antimicrobial peptide. The *dotted line* represents the spectrum of the POPC MLVs with 8 mol% antimicrobial peptide. (B) and (C) ^{31}P NMR powder spectra of POPG/POPC/POPC-d_{31} MLVs and POPG/POPC/POPG-d_{31} MLVs respectively at 25 °C. The *solid line* represents the spectra of the control sample, while the *dash line* represents the spectra of MLVs with 4 mol% peptide. (D) The best fitting of ^{31}P NMR spectrum of POPG/POPC/POPC-d_{31} MLVs at 25 °C using the DMFIT program (32). Two spectral components are used to simulate the spectrum. One anisotropic component (*dash line*) and one isotropic component (*dotted line*), contributing approximately 72% and 28% respectively to the total peak area. The sum of the two components is shown in *solid line*.

concentration) as a function of temperature (spectra not shown). The ^{31}P NMR spectra indicate the formation of MLVs in the L_α phase. The ^{31}P NMR spectrum for POPC MLVs at 25°C revealed an axial symmetric lineshape with a CSA of approximately 50 ppm (Figure 4.1(A)). The spectral lineshape retained axial symmetry with no change in the CSA in the presence of 4 mol% and 8 mol% KIGAKI. The ^{31}P NMR powder spectra with 4 mol% and 8 mol% KIGAKI were easily simulated with one spectral component. The phosphocholine headgroup has a large dipole moment, and behaves like a sensitive "molecular electrometer" (33). An increase in the surface positive electric charge should change both the orientation of the $^{-}$P-N^{+} dipole and the corresponding ^{31}P CSA. The lack of a significant CSA change suggests little or no electrostatic interaction between the cationic peptide and the POPC headgroups. The intensity ratio between the $\sigma_{\parallel}$ edge and the $\sigma_{\perp}$ edge, however, changes upon addition of the peptides. The slight change in the lineshape indicates that the peptide perturbs the fast motion of the lipid headgroup (34, 35).

The static ^{31}P NMR spectra of POPG/POPC MLVs are shown in Figures 4.1 (B) and 4.1(C). The single CSA of ~40 ppm observed for POPG/POPC MLVs is much smaller than the CSA of pure POPC MLVs (~50 ppm). ^{31}P CSA values of ~37 ppm for pure POPG bilayers (36) and ~48 ppm for pure POPC bilayers (33) have been reported. The single CSA value for POPG/POPC MLVs supports a direct interaction between the headgroups of POPC and POPG and no lateral phase separation of the lipids in this binary lipid mixture over the NMR time scale. However, the powder pattern spectra of mixed POPG/POPC MLVs at 4 mol% peptide concentration were able to be deconvoluted into two different components using the DMFIT simulation program. The isotropic component contributes about 28% to the whole peak area, and the anisotropic component with a CSA of approximate 40 ppm contributes about 72% (Figure 4.1(D)). The two components correspond to two different phospholipid species. These results clearly indicate that the antimicrobial peptide selectively perturbs and alters the POPG membranes.

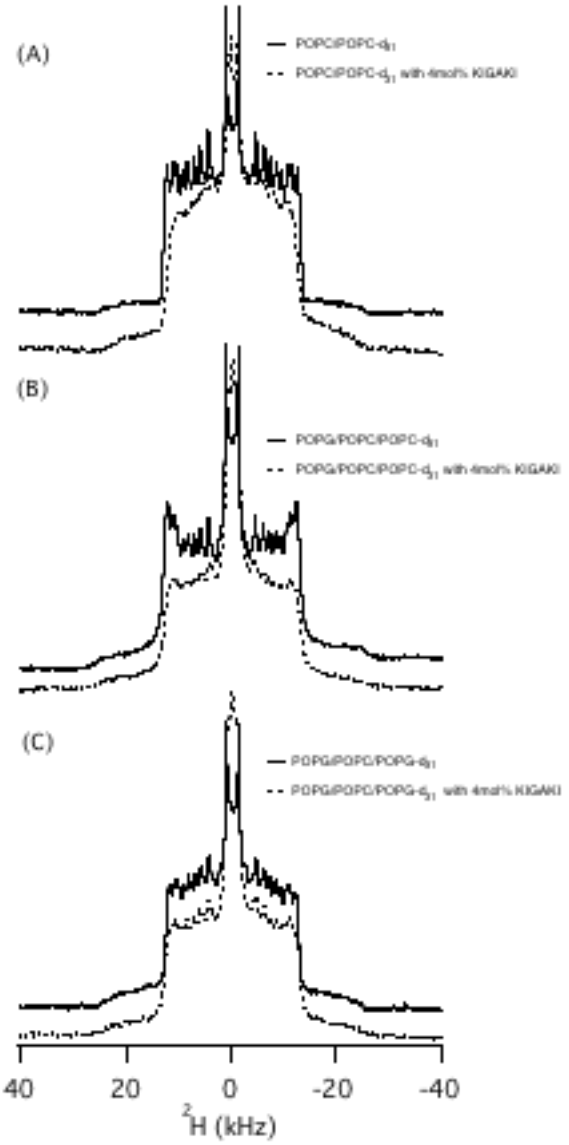

Figure 4.2 ^{2}H NMR powder spectra of POPC MLVs with and without the antimicrobial peptide, using POPC-d_{31} as the isotopic label at 30 °C (A). ^{2}H NMR powder spectra of POPG/POPC MLVs with and without the antimicrobial peptide, using POPC-d_{31} as the isotopic label (B) or using POPG-d_{31} as the isotopic label (C) at 25 °C. The *solid line* represents the spectra of the control sample, while the *dash line* represents the spectra of the MLVs with 4 mol% peptide. The deuterium quadrupolar splittings decrease along the lipids acyl chain toward the center of the bilayer with the smallest deuterium quadrupolar splitting corresponding to the methyl groups (CD_3) at the end of lipids acyl chain (*37, 38*).

Solid-state ^2H NMR spectra were obtained for POPC and POPG/POPC phospholipid bilayers with peptide concentrations of 0 mol% and 4 mol% with respect to the phospholipids. The ^2H NMR spectra for POPC MLVs with peptide concentrations of 0 mol% and 4 mol% at 30°C are shown in Figure 4.2(A). The ^2H NMR spectra for POPG/POPC MLVs with either POPC-d_{31} or POPG-d_{31} as the deuterium labels at 25°C are shown in Figures 4.2(B) and (C), respectively. The resolution decreased significantly at a peptide concentration of 4 mol%. The phospholipid molecule in the bilayer is characterized by an axial-symmetric motion with fast rotation around the long molecular axis and a slower reorientation rate perpendicular to the axis (*39*). The fast rotation gives a sharp peak at the $\sigma_\perp$ edge. The decrease in resolution indicates that interactions with the peptide have changed the motion of the lipids. An isotropic peak also appears at the higher peptide concentration, indicative of an isotropic reorientation, which is in slow exchange with the remaining lipids in the bilayers on the solid-state deuterium NMR time scale (~10^{-6} s) (*16*). The results clearly show that the antimicrobial peptide perturbs the membranes for all of the samples.

The order parameters for each individual C-^2H were calculated after dePakeing the ^2H NMR spectra. The order parameter profiles for ^2H at different carbon positions along the *sn-1* POPC or *sn-1* POPG phospholipids acyl chain are shown in Figures 4.3(A), (B), and (C) for each MLV sample. The degree of ordering slightly decreased along the whole acyl chains for POPC MLVs in the presence of KIGAKI. Conversely, for the mixed POPG/POPC MLVs, the degree of ordering of each C-^2H did not change in the presence of the peptide using either POPC or POPG as the deuterium label (Figures 4.3(B) and (C)). The difference in the order parameter changes between Figure 4.3(A) and Figures 4.3(B), (C) indicates that the mechanism by which the lipids and peptides interact is slightly different for the POPC MLVs and the POPG/POPC MLVs.

4.4.2 ^{31}P and ^2H longitudinal relaxation study

^{31}P longitudinal relaxation solid-state NMR studies were carried out for both POPC and POPG/POPC phospholipid bilayers with and without KIGAKI. Magic angle spinning was employed for this section of the relaxation study to give high-resolution

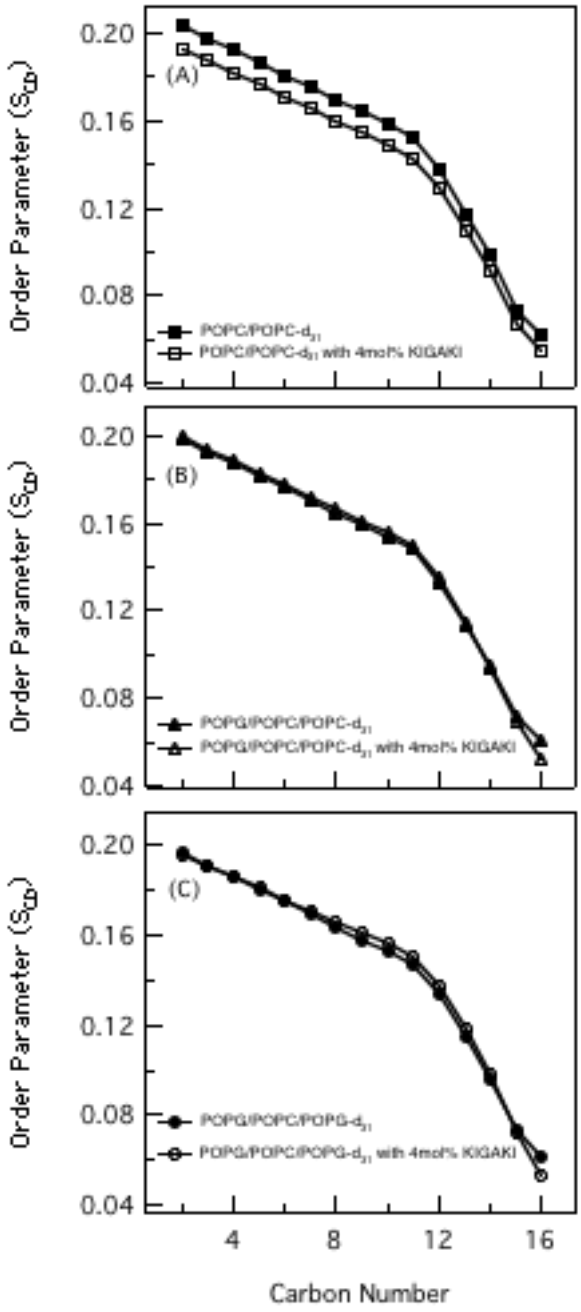

Figure 4.3 Molecular order parameter profiles with respect to the carbon positions along the acyl chain of deuterium labeled phospholipids with and without 4 mol% peptide, calculated from the dePaked ^{2}H NMR powder spectra. (A) POPC/POPC-d_{31} MLVs at 30 °C, (B) POPG/POPC/POPC-d_{31} MLVs at 25 °C, (C) POPG/POPC/POPG-d_{31} MLVs 25 °C. The solid symbols represent the data from control MLVs. The open symbols represent the MLVs with 4 mol% peptide.

solid-state NMR spectra. The isotropic peak position of POPC doesn't change upon addition of the peptide into pure POPC bilayers. For POPG/POPC mixed bilayers, POPG and POPC exhibit ^{31}P isotropic peaks at 0.68 ppm and –0.41 ppm, respectively (see inset in Figure 4.4). In the presence of KIGAKI both ^{31}P peaks position shift upfield by about 0.05 ppm with a slight line broadening (spectrum not shown). The ^{31}P chemical shift of the lipids headgroup is sensitive to the surface charge density (*40*). The binding of the cationic peptides to the anionic bilayers will shift the ^{31}P peak of the phospholipids headgroup upfield slightly (*40*). These results demonstrate that the peptide interacts with the POPG/POPC membrane surface and the surface charge of the membrane is reduced.

The ^{31}P longitudinal relaxation time (T_1) changes upon addition of the peptide into the membrane at 25 °C shown in Table 4.1. The ^{31}P relaxation time T_1 of POPC MLVs decreases slightly from 763 ms to 755 ms within the experimental error when the peptide is added into the bilayers. The error was calculated by the average ^{31}P T_1 obtained from three individual samples with the same composition. Conversely, the ^{31}P T_1 values increase significantly for both POPG lipids and POPC lipids once the peptide is integrated into the POPG/POPC MLVs at 25 °C (Figure 4.4). The increase in the spin-lattice relaxation time upon addition of the peptide indicates a less efficient longitudinal relaxation mechanism, probably caused by the interaction between the peptide and lipids and therefore a reduction in the fast axis rotational motion of the lipids.

Figure 4.4(A) exhibits the ^{31}P T_1 value changes as a function of temperature before and after addition of the peptide into the POPG/POPC MLVs. The ^{31}P T_1 value of POPG/POPC MLVs decreases with increasing temperature from 5 °C to around 15 °C, and then increases at temperatures above 15 °C. The ^{31}P longitudinal relaxation time T_1 is related to the correlation time (τ_c) of fast molecular motion according to $1/T_1 \propto \tau_c/(1+ \omega_0{}^2\tau_c{}^2)$, where ω_0 is the Larmor frequency. If the molecular correlation time fits the equation $\omega_0\tau_c \cong 1$, the relaxation mechanism is the most efficient, and the T_1 relaxation time is at the minimum (26, 27). The molecular correlation time changes as the corresponding molecular motion increases at higher temperature. The relaxation process is most efficient around 15 °C for both POPC and POPG, where the molecular correlation time τ_c is approximately equal to $1/\omega_0$. A significant difference between POPC and POPG lipids

Table 4.1 The comparison of ^{31}P longitudinal relaxation times T_1 between control MLV samples and MLVs with 4 mol% KIGAKI for both POPC MLVs and POPG/POPC MLVs at 25 °C.

		^{31}P T_1 (ms) MLVs control	^{31}P T_1 (ms) MLVs with 4% peptide	^{31}P ΔT_1 (ms)*
POPC MLVs	POPC	763±3	755±5	-8
POPG/POPC MLVs	POPG	764±3	805±5	+41
	POPC	768±2	800±6	+32

* ^{31}P ΔT_1 (ms)= ^{31}P T_1 (MLVs with 4 mol% peptide)-^{31}P T_1 (MLVs control)

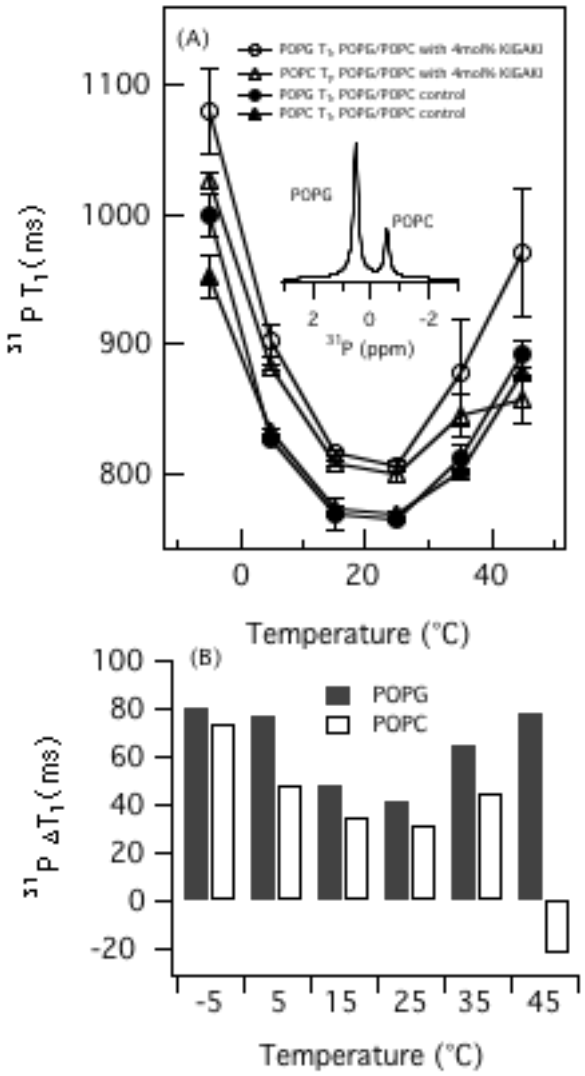

Figure 4.4 (A) ^{31}P longitudinal relaxation times (T_1) as a function of temperature for POPG/POPC MLVs. The solid symbols represent the control MLVs. The open symbols represent the samples with 4 mol% peptide. The circles represent POPG phospholipids. The triangle represents POPC phospholipids. The error bar was obtained by averaging ^{31}P T_1 values obtained from three samples with the same sample components. The inset is the NMR spectrum of control POPG/POPC bilayers spun at 4K at the magic angle. (B) The ^{31}P T_1 values difference (Δ T_1) was calculated by subtracting the control T_1 value from the T_1 value of MLVs in the presence of KIGAKI for both POPG (black bars) and POPC (white bars) phospholipids at variable temperatures.

is found at 35 °C and 45°C for POPG/POPC membranes with the addition of 4 mol% peptide. POPG lipids experience a large increase in their corresponding ^{31}P T_1 values, while the ^{31}P T_1 values of POPC lipids only increase slightly at high temperatures.

Figure 4.4(B) shows the difference in the ^{31}P relaxation time T_1 values (^{31}P ΔT_1) between the control sample and POPG/POPC MLVs with 4 mol% KIGAKI at variable temperatures for both POPG and POPC phospholipids. Generally, the ^{31}P T_1 value increases upon association of KIGAKI with the bilayers. Over a wide temperature range (-5 °C to 45 °C), the increase in the value of the POPG ^{31}P relaxation time T_1 is greater than the corresponding increase in the POPC ^{31}P relaxation time T_1. However, at 45 °C, the POPG ^{31}P relaxation time T_1 increases in the presence of KIGAKI, whereas the POPC ^{31}P T_1 decreases in the presence of the antimicrobial peptide.

Additionally, a ^2H longitudinal relaxation study for POPC bilayers with POPC-d_{31} utilizing an inversion-recovery pulse sequence was carried out at 30°C. The longitudinal relaxation rate (R_{1z}) profiles for ^2H at different carbon positions along the POPC phospholipids acyl chain are shown in Figure 4.5(A). The relaxation rates ^2H R_{1z} decrease monotonically with C-^2H group position going from the interfacial segments of the membrane to the terminal methyl group of the lipid acyl chain. In the presence of KIGAKI, the ^2H relaxation rates R_{1z} decrease. This is consistent with the results obtained from the ^2H order parameter studies, which show a slight decrease in the ordering of the C-^2H groups along the whole acyl chain of POPC in the presence of the peptide (Figure 4.3(A)). Figures 4.5(B) and (C) exhibit the ^2H longitudinal relaxation rates R_{1z} of POPC-d_{31} and POPG-d_{31} respectively in the POPG/POPC (3/1) phospholipid bilayers with and without 4 mol% KIGAKI at 25°C. The ^2H R_{1z} rates of both lipids decrease upon association of the antimicrobial peptide with the bilayer.

4.4.3 ^{31}P and ^2H transverse relaxation NMR study

^{31}P solid-state NMR transverse relaxation times (T_2) were investigated on POPG/POPC lipid mixtures as a function of temperature from -5 °C to 45 °C (Figure 4.6). Since a single exponential fit of the data was not adequate, a bi-exponential fit for both POPG and POPC phospholipids was used. For the POPG/POPC control sample, the

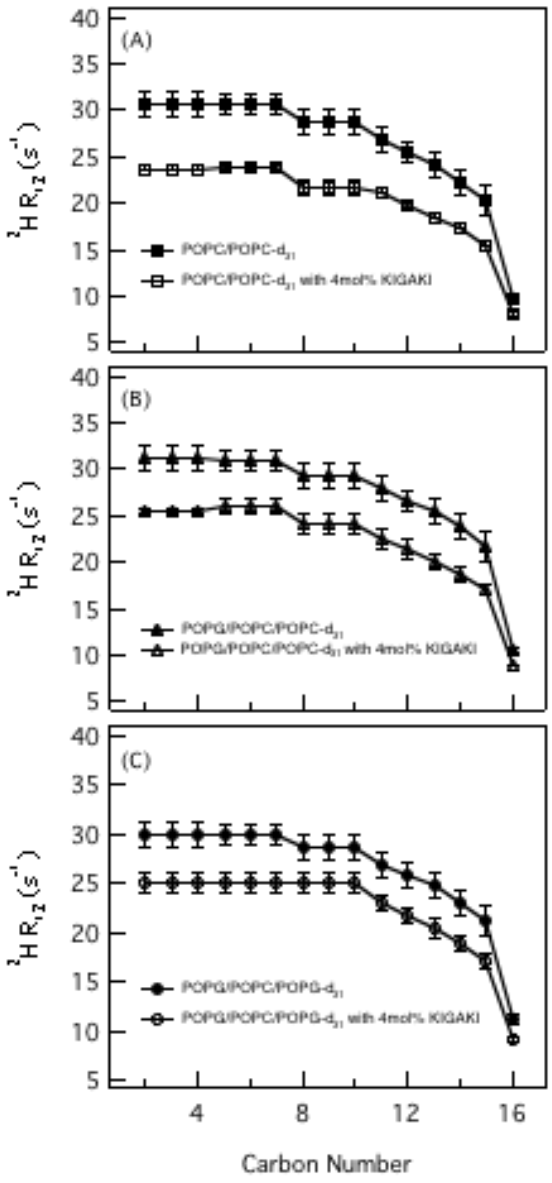

Figure 4.5 ^2H NMR longitudinal relaxation rate R_{1z} profiles with respect to the carbon positions along the acyl chain of deuterium labeled phospholipids with and without 4 mol% peptide. (A) POPC/POPC-d_{31} MLVs at 30 °C, (B) POPG/POPC/POPC-d_{31} MLVs at 25 °C, (C) POPG/POPC/POPG-d_{31} MLVs at 25 °C. The solid symbols represent the control MLVs data. The open symbols represent the data with 4 mol% peptide. The error of each individual ^2H R_{1Z} value is obtained by averaging ^2H R_{1z} values from two samples with the same sample components.

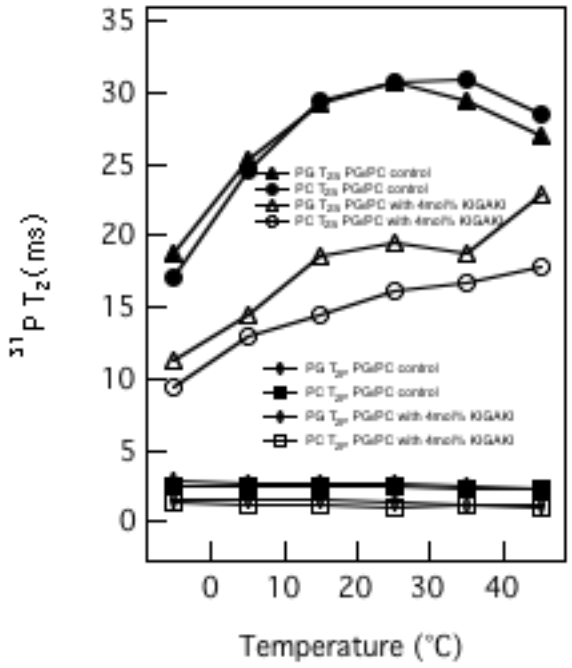

Figure 4.6 ^{31}P transverse relaxation time T_2 as a function of temperature for POPG/POPC MLVs. The solid symbols represent the control POPG/POPC MLVs. The open symbols represent the POPG/POPC MLVs with 4 mol% peptide. The triangles represent the POPG slow relaxation component. The circles represent the POPC slow relaxation component. The diamonds represent the POPG fast relaxation component. The squares represent the POPC fast relaxation component.

^{31}P transverse relaxation time T_2 of the fast relaxation component is about 2~3 ms for both POPG and POPC over the temperature range studied. The T_2 value of the slow relaxation component varies over the range of 20~30 ms. Upon addition of 4 mol% peptide into the membrane, the relaxation times of both the slow component and the fast component decrease. The transverse relaxation rate is sensitive to changes in slow collective membrane motions (23). The reduction in the slow component T_2 relaxation time in the presence of the peptide indicates a more efficient relaxation mechanism caused by the interaction of the antimicrobial peptide with the lipids.

^{2}H NMR transverse relaxation experiments were used to examine the overall slow collective membrane motion for POPG/POPC membranes with POPC-d_{31} or POPG-d_{31}. The transverse relaxation rates at different carbon positions along the acyl chain of POPC-d_{31} or POPG-d_{31} were calculated using the dePaked ^{2}H NMR spectra, and did not for POPG/POPC bilayers with and without KIGAKI using POPG-d_{31} as the deuterium show any significant changes between the different C-^{2}H groups. These results confirm that only the collective phospholipid motion dominates the relaxation mechanism. Fast molecular motions, such as *trans-gauche* isomerizations, which are different for each C-^{2}H group, is not the dominant transverse relaxation mechanism. Therefore, the final transverse relaxation rates were calculated by fitting the total area of all the ^{2}H NMR peaks. Figure 4.7 shows the ^{2}H transverse relaxation time T_2 at four different temperatures for POPG/POPC bilayers with and without KIGAKI using POPG-d_{31} as the deuterium labels. The relaxation time T_2 decreases by a factor of 2 when the peptide is added into the mixed membrane. Similar results were obtained for POPG/POPC bilayers with POPC-d_{31} (data not shown). These results also indicate that the transverse relaxation is more efficient in the presence of the antimicrobial peptide, which agrees with the result obtained from the ^{31}P transverse relaxation experiments. The ^{2}H transverse relaxation time is not very sensitive to temperature changes. Over the experimental temperature range (15 °C to 45 °C), the ^{2}H T_2 relaxation time does not change significantly.

4.5 Discussion

KIGAKI is known to form a β-sheet structure when bound to anionic POPG lipids (*7*). The minimum inhibitory concentration of the peptide against E. *coli*, S. *aureus* and

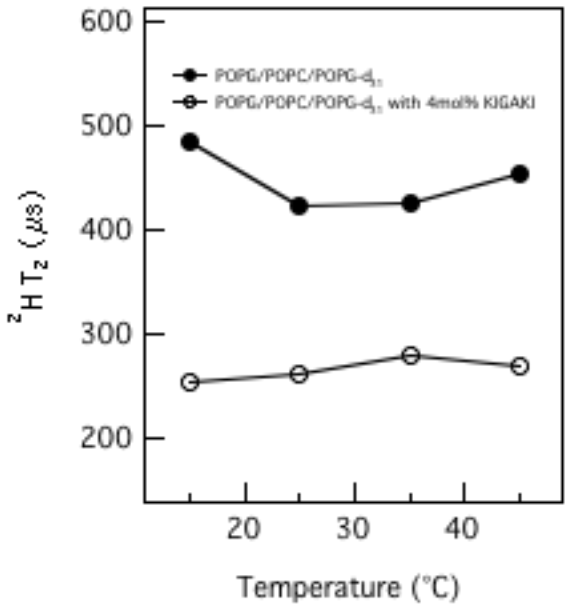

Figure 4.7 ^{2}H transverse relaxation times (T_2) as a function of temperature for POPG/POPC MLVs with POPG-d_{31} as the isotopic label. The solid symbols represent the control MLVs data. The open symbols represent the sample with 4 mol% antimicrobial peptide.

P. *aeruginosa* is much lower than the naturally occurring peptides magainin2 and PGLa peptides (*7, 8*). It is believed that the high percentage of anionic lipids in the bacterial membrane plays a crucial role in the function of antimicrobial peptides. POPC MLVs and POPG/POPC MLVs were used in this study to mimic the mammalian membrane and bacterial membrane, respectively, to test this hypothesis.

4.5.1 The phospholipid selectivity of the antimicrobial peptide KIGAKI

Static ^{31}P powder pattern NMR spectra clearly indicate that KIGAKI disrupts POPG/POPC bilayers into two major species at 4 mol% concentration, whereas the peptide only slightly perturbs POPC bilayers at twice (8 mol%) this peptide concentration (Figure 4.1). The ^{31}P NMR powder pattern spectrum of POPC MLVs at 4 mol% peptide concentration only revealed one axial symmetric component. This result supports that KIGAKI has a greater ability to perturb the membrane structure that mimics bacterial membranes (*7*).

The ^{31}P longitudinal relaxation study exhibits a significant increase in the values of both POPG and POPC T_1 upon association of KIGAKI with POPG/POPC MLVs. However, the ^{31}P T_1 values do not change significantly upon association of KIGAKI with POPC MLVs (Table 4.1). The ^{31}P longitudinal relaxation time T_1 is sensitive to fast rotational phospholipid headgroup motions (*16*). The increase in the longitudinal relaxation time T_1 indicates a less efficient relaxation mechanism caused by a reduction in the molecular motion of the lipids. The decrease in motion of the lipid head groups, clearly indicates that a strong interaction exists between the peptide and the POPG/POPC phospholipid bilayers. Conversely, there is no significant interaction between KIGAKI and POPC phospholipid bilayers. The slight decrease in the ^{31}P T_1 value upon addition of the peptide to the POPC bilayers indicates a small increase in lipid motion. A subtle increase in the lipid motion would result in a slight decrease in ordering for both the lipid headgroups and the acyl chains. This agrees well with the static ^{31}P and ^{2}H solid-state NMR data (Figure 4.3(A)).

4.5.2 The KIGAKI-phospholipid interaction mechanism

The interaction mechanism between KIGAKI and the membrane was analyzed by ^{2}H solid-state NMR spectroscopy. ^{2}H order parameters along the lipid acyl chains were calculated for both POPC MLVs and POPG/POPC MLVs. Both POPG-d_{31} and POPC-d_{31}

deuterium labels were used in the POPG/POPC bilayers to distinguish between the different motional properties of POPG and POPC in the presence of KIGAKI. The ordering along the POPC and POPG acyl chains (Figure 4.3(B) and (C)) does not change upon association of the peptide into POPG/POPC MLVs. This result suggests that no significant influence on the packing of the lipid acyl chain upon peptide binding to the POPG/POPC membranes, indicating that the peptide binds to the POPG/POPC membranes near the membrane surface.

The ^{2}H order parameter reveals information about the amplitudes of the acyl chain fluctuations at different carbon positions, while the longitudinal relaxation rates depend upon both the amplitude of the motion and the corresponding rate of the motion (*41*). ^{2}H longitudinal relaxation rate R_{1z} profiles exhibit a decrease in the relaxation rate along the POPC acyl chains as well as the POPG acyl chains upon association of the peptide with POPG/POPC MLVs (Figures 4.5(B) and (C)). Considering the ordering of the lipids acyl chains doesn't show much change in the presence of the peptide, this result clearly indicates that only the rates of the lipids motion are disturbed upon peptide binding to the lipid bilayers.

The ^{31}P MAS spectra of POPG/POPC MLVs show an upfield shift in both POPG and POPC isotropic peaks upon addition of the antimicrobial peptide. The ^{31}P chemical shift of the lipid headgroup is sensitive to the surface charge density (*40*). A decrease in the surface charge density will cause an upfield shift in the ^{31}P isotropic peak (*34, 40*). Our result indicates that the binding of the cationic antimicrobial peptide to the anionic membrane surface decreases the membrane surface charge density. Conversely, the ^{31}P isotropic peak position of POPC MLVs does not show any shift when the peptide is added. The ^{31}P CSA value of the POPC bilayers is also very sensitive to the changes in membrane surface charge because of its phosphocholine headgroup with a large dipole moment (*33, 40*). The ^{31}P CSA value of pure POPC bilayer remains unchanged upon addition of the peptide (Figure 1(A)). These results suggest that the electrostatic interaction plays an important role in the peptide binding to the POPG/POPC phospholipid bilayers, but not with pure POPC phospholipid bilayers.

Since the electrostatic interaction is important to the binding between KIGAKI and the mixed POPG/POPC phospholipid bilayers, one would expect that the cationic

peptide would prefer to interact with anionic phospholipid POPG. ^{31}P and ^{2}H longitudinal relaxation experiments on POPG/POPC MLVs would show a big difference in the change of T_1 value between POPG and POPC lipids upon addition of the peptide. However, the ^{31}P longitudinal relaxation experiments indicate that both the POPC and POPG lipid T_1 values increase upon association of the peptide with the mixed POPG/POPC phospholipid bilayers at 25 °C. Similarly, the ^{2}H longitudinal relaxation study displays a similar relaxation rate R_{1Z} reduction for both POPG and POPC samples in the presence of the KIGAKI peptide. In order to further elucidate the molecular mechanism of the interaction between the antimicrobial peptide and the POPG/POPC lipid bilayers, ^{31}P longitudinal relaxation studies on POPG/POPC MLVs as a function of temperature were carried out. It is very interesting to observe that the change in the ^{31}P T_1 value for POPG phospholipids is larger than POPC lipids over a wide temperature range (Figure 4.4(B)). This result supports the peptide's preference to interact with the POPG lipids and indicates that the interaction between the peptide and the POPG headgroup is greater than that between the peptide and the POPC headgroup.

At 45 °C, the POPC and the POPG phospholipids ^{31}P longitudinal relaxation T_1 exhibit totally different changes upon association of the antimicrobial peptide with the POPG/POPC bilayers (Figure 4.4(B)). The POPC ^{31}P longitudinal relaxation T_1 value decreases, while the POPG ^{31}P longitudinal relaxation T_1 value increases significantly. The increase in T_1 value indicates an interaction between the peptide and lipids and a more restricted phospholipid headgroup motion, while a decrease in T_1 value suggests a relatively less-restricted lipid headgroup motion than the lipids in the control POPG/POPC MLVs. This result can be explained by the changes in peptide-lipid and lipid-lipid interactions upon association of KIGAKI with POPG/POPC bilayers. For the binary mixed bilayer POPG/POPC system, only one ^{31}P CSA value was obtained (Figures 1(B) and (C)) in the ^{31}P powder pattern spectra. Since the ^{31}P CSA of pure POPG and pure POPC bilayers are significantly different, the result indicates a strong interaction between the POPG and POPC headgroups (36). Once the peptide is associated with bilayer, the ^{31}P relaxation time T_1 of both of the phospholipids increases at low temperature, suggesting there are probable interactions between the peptide and both of the lipids. The intensity of all these interactions changes as the temperature increases. At

high temperatures (45 °C), if the interaction between the POPC headgroup and the peptide becomes very weak and finally broken and the interaction between the POPG headgroup and the peptide is retained, the POPC ^{31}P relaxation time T_1 value would be close to the POPC ^{31}P T_1 value of the control. However, the result demonstrates a decrease in the POPC ^{31}P T_1 value when compared to the control, suggesting that it is important to consider the interaction between the POPC and POPG phospholipid molecules together. It is more possible that the peptide interacts with POPG directly and restricts the POPG headgroup motion. The POPC headgroup motion is only affected indirectly by the interaction between the POPC and POPG headgroups. At 45 °C, the interaction between the POPC and POPG headgroups decreases in the presence of the peptide, causing the POPC headgroup motion to be faster than the POPC headgroup motion in the control POPG/POPC MLVs. These results suggest that the interaction between the phospholipids is strongly affected upon the peptide binding to the POPG/POPC membranes.

Magainin is a surface peptide and disrupts the membrane via a carpet mechanism (*42*). The antimicrobial peptide first binds at the membrane surface at low concentrations like a carpet spreading on the floor (*42*). When the peptide concentration reaches a threshold value, the membrane will be disintegrated into small vesicles. It has been reported that magainin associates with the lipid headgroups without significantly disturbing the lipid acyl chain packing even at very high peptide concentrations (*43*). In this paper, the ^{2}H order parameter shows that the acyl chain packing of both POPG and POPC is unperturbed in the presence of the peptide, and supports that the peptide binds the POPG/POPC membranes near the membrane surface. ^{31}P NMR chemical shift and CSA analysis indicates that the electrostatic interaction is important in the binding of the antimicrobial peptide KIGAKI to the POPG/POPC membranes. At 4 mol% peptide concentration, the peptide is able to disrupt the POPG/POPC membranes into two species with one isotropic component, which possesses a faster vesicle tumbling motion than the normal MLVs (*44*). The ^{31}P longitudinal relaxation data suggest that the interaction between the POPG and POPC molecules decreases upon association of the peptide, providing the probable mechanism of the disruption of the POPG/POPC membranes. All

of these results suggest that a carpet mechanism may also apply to the KIGAKI peptide perturbing the POPG/POPC membranes.

As to the pure POPC MLVs, ^{31}P NMR powder type spectra and longitudinal relaxation data indicate that there is no strong interaction between KIGAKI and the POPC membranes, although the lipids headgroup motion is slightly perturbed. ^{2}H order parameters show a decrease in the ordering of each C-^{2}H group along the POPC-d_{31} acyl chain upon association of the antimicrobial peptide with the POPC MLVs (Figure 4.3(A)). Additionally, the longitudinal relaxation rate ^{2}H R_{1Z} of POPC acyl chains also decrease in the presence of the peptide (Figure 4.5(A)). The ^{2}H NMR data suggest that the acyl chain packing of the POPC bilayers is disturbed. Considering the amphipathic characteristics of the peptide, the peptide may randomly aggregate in the phospholipid headgroup region and create space between different phospholipid molecules. The loose packing phospholipid molecules, therefore, are able to move more freely and exhibit a decrease in the ordering of the acyl chain. The similar effects on ^{31}P and ^{2}H NMR spectra were also observed on DMPC membranes by some antimicriobial peptides from Australian frogs (*45*). A previous study on KIGAKI using high sensitivity fluorescence spectroscopy indicates that no tryptophan emission intensity changes at 330 nm upon peptide binding to pure POPC large unilamellar vesicles (LUVs), suggesting that the peptide remains in a very hydrophilic environment upon peptide binding (*8*). LUVs have a significant high hydration level (lipids concentration ~1 mg/ml in buffer) when compared to MLVs (lipids concentration ~76 mg/190 μl in buffer). The peptide may prefer to stay closer to the membrane aqueous surface when a bulk aqueous solution exists in LUVs. In MLVs, however, it is more likely that KIGAKI is inserted in the lipid headgroup region since the perturbation of the lipids motion is clearly observed in both lipids headgroup region and acyl chain region.

In conclusion, the cationic antimicrobial peptide acts differently in POPC and POPG/POPC bilayers. For POPC bilayers, the antimicrobial peptide has a weak interaction with the membranes although it does perturb the lipids motion slightly in this research. For POPG/POPC mixed bilayer membranes, the peptide has a strong ability to disrupt the membrane. The electrostatic interaction between the peptide and the membrane surface is very critical in the initiation of the binding. The binding of the

antimicrobial peptide KIGAKI to the membrane surface disturbs the interaction between the phospholipids, changes the dynamics of the lipid motion and thereby makes the membrane more fragile. The results suggest a carpet mechanism for bilayer disruption (*42, 46, 47*).

This research obtains information purely from the perspective of the phospholipid membranes and demonstrates that solid-state NMR relaxation experiments, specially designed to probe molecular motions, can be extremely powerful in probing membrane-peptide interactions.

ACKNOWLEDGEMENTS:

This work was supported by an American Heart Association Scientist Development grant 0130396N and a National Institutes of Health grant GM60259-01 to GAL and AI047165-02 to JB. The 500MHz wide-bore NMR spectrometer was obtained from a National Science Foundation grant 10116333.

4.6 References

(1) Hancock, R. E. W., and Diamond, G. (2000) The role of cationic antimicrobial peptides in innate host defences. *Trends Microbiol. 8*, 402-410.

(2) Chen, J., Falla, T. J., Liu, H. J., Hurst, M. A., Fujii, C. A., Mosca, D. A., Embree, J. R., Loury, D. J., Radel, P. A., Chang, C. C., Gu, L., and Fiddes, J. C. (2000) Development of protegrins for the treatment and prevention of oral mucositis: Structure-activity relationships of synthetic protegrin analogues. *Biopolymers 55*, 88-98.

(3) Glaser, R. W., Sachse, C., Durr, U. H. N., Wadhwani, P., and Ulrich, A. S. (2004) Orientation of the antimicrobial peptide PGLa in lipid membranes determined from F-19-NMR dipolar couplings of 4-CF3- phenylglycine labels. *J. Magn. Reson. 168*, 153-163.

(4) Bechinger, B., Zasloff, M., and Opella, S. J. (1998) Structure and dynamics of the antibiotic peptide PGLa in membranes by solution and solid-state nuclear magnetic resonance spectroscopy. *Biophys. J. 74*, 981-987.

(5) Hallock, K. J., Lee, D. K., and Ramamoorthy, A. (2003) MSI-78, an analogue of the magainin antimicrobial peptides, disrupts lipid bilayer structure via positive curvature strain. *Biophys. J. 84*, 3052-3060.

(6) Buffy, J. J., Waring, A. J., Lehrer, R. I., and Hong, M. (2003) Immobilization and aggregation of the antimicrobial peptide protegrin-1 in lipid bilayers investigated by solid-state NMR. *Biochemistry 42*, 13725-13734.

(7) Blazyk, J., Wiegand, R., Klein, J., Hammer, J., Epand, R. M., Epand, R. F., Maloy, W. L., and Kari, U. P. (2001) A novel linear amphipathic beta-sheet cationic antimicrobial peptide with enhanced selectivity for bacterial lipids. *J. Biol. Chem. 276*, 27899-27906.

(8) Jin, Y., Mozsolits, H., Hammer, J., Zmuda, E., Zhu, F., Zhang, Y., Aguilar, M. I., and Blazyk, J. (2003) Influence of tryptophan on lipid binding of linear amphipathic cationic antimicrobial peptides. *Biochemistry 42*, 9395-9405.

(9) Hallock, K. J., Lee, D. K., Omnaas, J., Mosberg, H. I., and Ramamoorthy, A. (2002) Membrane composition determines pardaxin's mechanism of lipid bilayer disruption. *Biophys. J. 83*, 1004-1013.

(10) Harzer, U., and Bechinger, B. (2000) Alignment of lysine-anchored membrane peptides under conditions of hydrophobic mismatch: A CD,N-15 and P-31 solid-state NMR spectroscopy investigation. *Biochemistry 39*, 13106-13114.

(11) Koenig, B. W., Ferretti, J. A., and Gawrisch, K. (1999) Site-specific deuterium order parameters and membrane-bound behavior of a peptide fragment from the intracellular domain of HIV-1 gp41. *Biochemistry 38*, 6327-6334.

(12) Wildman, K. A. H., Lee, D. K., and Ramamoorthy, A. (2003) Mechanism of lipid bilayer disruption by the human antimicrobial peptide, LL-37. *Biochemistry 42*, 6545-6558.

(13) Hirsh, D. J., Hammer, J., Maloy, W. L., Blazyk, J., and Schaefer, J. (1996) Secondary structure and location of a magainin analogue in synthetic phospholipid bilayers. *Biochemistry 35*, 12733-12741.

(14) Afonin, S., Dur, U. H. N., Glaser, R. W., and Ulrich, A. S. (2004) 'Boomerang'-like insertion of a fusogenic peptide in a lipid membrane revealed by solid-state F-19 NMR. *Magn. Reson. Chem. 42*, 195-203.

(15) Huster, D., Yao, Y. L., Jakes, K., and Hong, M. (2002) Conformational changes of colicin Ia channel-forming domain upon membrane binding: a solid-state NMR study. *Biochim. Biophys. Acta-Biomembranes 1561*, 159-170.

(16) Watts, A. (1998) Solid-state NMR approaches for studying the interaction of peptides and proteins with membranes. *Biochim. Biophys. Acta-Rev. on Biomem. 1376*, 297-318.

(17) Cornell, B. A., Davenport, J. B., and Separovic, F. (1982) Low-frequency motion in membranes the effect of cholesterol and proteins. *Biochim. Biophys. Acta 689*, 337-345.

(18) Cornell, B. A., Hiller, R. G., Raison, J., Separovic, F., Smith, R., Vary, J. C., and Morris, C. (1983) Biological-Membranes Are Rich In Low-Frequency Motion. *Biochim. Biophys. Acta 732*, 473-478.

(19) Mayer, C., Grobner, G., Muller, K., Weisz, K., and Kothe, G. (1990) Orientation-Dependent Deuteron Spin-Lattice Relaxation-Times in Bilayer-Membranes - Characterization of the Overall Lipid Motion. *Chem. Phys. Lett. 165*, 155-161.

(20) Meier, P., Ohmes, E., and Kothe, G. (1986) Multipulse Dynamic Nuclear-Magnetic-Resonance of Phospholipid- Membranes. *J. Chem. Phys. 85*, 3598-3614.

(21) Mayer, C., Muller, K., Weisz, K., and Kothe, G. (1988) Deuteron Nmr Relaxation Studies of Phospholipid-Membranes. *Liq. Cryst. 3*, 797-806.

(22) Simatos, G. A., Forward, K. B., Morrow, M. R., and Keough, K. M. W. (1990) Interaction between Perdeuterated Dimyristoylphosphatidylcholine and Low-Molecular-Weight Pulmonary Surfactant Protein Sp-C. *Biochemistry 29*, 5807-5814.

(23) Althoff, G., Heaton, N. J., Grobner, G., Prosser, R. S., and Kothe, G. (1996) NMR relaxation study of collective motions and viscoelastic properties in biomembranes. *Colloid Surf. A-Physicochem. Eng. Asp. 115*, 31-37.

(24) Pinheiro, T. J. T., Duer, M. J., and Watts, A. (1997) Phospholipid headgroup dynamics in DOPG-d(5) cytochrome c complexes as revealed by H-2 and P-31 NMR: The effects of a peripheral protein on collective lipid fluctuations. *Solid State Nucl. Magn. Reson. 8*, 55-64.

(25) Dave, P. C., Tiburu, E. K., Damodaran, K., and Lorigan, G. A. (2004) Investigating structural changes in the lipid bilayer upon insertion of the transmembrane domain of the membrane-bound protein phospholamban utilizing P-31 and H-2 solid-state NMR spectroscopy. *Biophys. J. 86*, 1564-1573.

(26) Pinheiro, T. J. T., and Watts, A. (1994) Lipid Specificity in the Interaction of Cytochrome-C with Anionic Phospholipid-Bilayers Revealed by Solid-State P-31 Nmr. *Biochemistry 33*, 2451-2458.

(27) Pinheiro, T. J. T., and Watts, A. (1994) Resolution of Individual Lipids in Mixed Phospholipid-Membranes and Specific Lipid Cytochrome-C Interactions by Magic-Angle- Spinning Solid-State P-31 Nmr. *Biochemistry 33*, 2459-2467.

(28) Aussenac, F., Laguerre, M., Schmitter, J. M., and Dufourc, E. J. (2003) Detailed structure and dynamics of bicelle phospholipids using selectively deuterated and perdeuterated labels. H-2 NMR and molecular mechanics study. *Langmuir 19*, 10468-10479.

(29) McCabe, M. A., and Wassall, S. R. (1995) Fast-Fourier-Transform Depaking. *J. Magn. Reson. Ser. B 106*, 80-82.

(30) Lu, J. X., Caporini, M. A., and Lorigan, G. A. (2004) The effects of cholesterol on magnetically aligned phospholipid bilayers: a solid-state NMR and EPR spectroscopy study. *J. Magn. Reson. 168*, 18-30.

(31) Dave, P. C., Tiburu, E. K., Nusair, N. A., and Lorigan, G. A. (2003) Calculating order parameter profiles utilizing magnetically aligned phospholipid bilayers for H-2 solid-state NMR studies. *Solid State Nucl. Magn. Reson. 24*, 137-149.

(32) Massiot, D., Fayon, F., Capron, M., King, I., Le Calvé, S., Alonso, B., Durand, J.-O., Bujoli, B., Gan, Z., and Hoatson, G. (2002) Modelling one- and two-dimensional solid state NMR spectra. *Magn. Reson. in Chem. 40*, 70-76.

(33) Scherer, P. G., and Seelig, J. (1989) Electric Charge Effects on Phospholipid Headgroups - Phosphatidylcholine in Mixtures with Cationic and Anionic Amphiphiles. *Biochemistry 28*, 7720-7728.

(34) Lindstrom, F., Bokvist, M., Sparrman, T., and Grobner, G. (2002) Association of amyloid-beta peptide with membrane surfaces monitored by solid state NMR. *Phys. Chem. Chem. Phys. 4*, 5524-5530.

(35) Rajan, S., Kang, S. Y., Gutowsky, H. S., and Oldfield, E. (1981) Phosphorus Nuclear Magnetic-Resonance Study of Membrane- Structure - Interactions of Lipids with Protein, Polypeptide, and Cholesterol. *J. Biol. Chem. 256*, 1160-1166.

(36) Santos, J. S., Lee, D. K., and Ramamoorthy, A. (2004) Effects of antidepressants on the conformation of phospholipid headgroups studied by solid-state NMR. *Magn. Reson. Chem. 42*, 105-114.

(37) Sanders, C. R., and Schwonek, J. P. (1992) Characterization Of Magnetically Orientable Bilayers In Mixtures Of Dihexanoylphosphatidylcholine And Dimyristoylphosphatidylcholine By Solid-State Nmr. *Biochemistry 31*, 8898-8905.

(38) Seelig, J., and Seelig, A. (1974) The dynamic structure of fatty acyl chains in a phospholipid bilayer measured by deuterium magnetic resonance. *Biochemistry 13*, 4839-4845.

(39) Smith, I. C. P., and Ekiel, I. H. (1984) Phosphorus-31 NMR of phospholipids in membranes, in *Phosphorus-31 NMR* (Gorenstein, D. G., Ed.) pp 447-475, New York.

(40) Bonev, B., Watts, A., Bokvist, M., and Grobner, G. (2001) Electrostatic peptide-lipid interactions of amyloid-beta peptide and pentalysine with membrane surfaces monitored by P- 31 MAS NMR. *Phys. Chem. Chem. Phys. 3*, 2904-2910.

(41) Brown, M. F., and Nevzorov, A. A. (1999) H-2-NMR in liquid crystals and membranes. *Colloid Surf. A-Physicochem. Eng. Asp. 158*, 281-298.

(42) Oren, Z., and Shai, Y. (1998) Mode of action of linear amphipathic alpha-helical antimicrobial peptides. *Biopolymers 47*, 451-463.

(43) Williams, R. W., Starman, R., Taylor, K. M. P., Gable, K., Beeler, T., Zasloff, M., and Covell, D. (1990) Raman spectroscopy of synthetic antimicrobial frog peptides magainin 2a and PGLa. *Biochemistry 29*, 4490-4496.

(44) Burnell, E. E., Cullis, P. R., and Kruijff, B. D. (1980) Effects of tumbling and lateral diffusion on phosphatidylcholine model membrane ^{31}P-NMR lineshape. *Biochim. Biophys. Acta 603*, 63-69.

(45) Balla, M. S., Bowie, J. H., and Separovic, F. (2004) Solid-state NMR study of antimicrobial peptides from Australian frogs in phospholipid membranes. *Eur. Biophys. J. 33*, 109-116.

(46) Yamaguchi, S., Huster, D., Waring, A., Lehrer, R. I., Kearney, W., Tack, B. F., and Hong, M. (2001) Orientation and dynamics of an antimicrobial peptide in the lipid bilayer by solid-state NMR spectroscopy. *Biophys. J. 81*, 2203-2214.

(47) Shai, Y., and Oren, Z. (2001) From "carpet" mechanism to de-novo designed diastereomeric cell-selective antimicrobial peptides. *Peptides 22*, 1629-1641.

Chapter 5

Exploring membrane selectivity of the antimicrobial peptide KIGAKI using solid-state NMR spectroscopy

Lu, J.X., Blazyk J. and Lorigan, G. A. Exploring membrane selectivity of the antimicrobial peptide KIGAKI using Solid-State NMR spectroscopy *Biochim. Biophys. Acta* (2006) 1758, 1303-1313.

Abbreviations: KIGAKI, KIGAKIKIGAKIKIGAKI-NH_2; POPC, 1-Palmitoyl-2-oleoyl-3-*sn*-glycero-3-phosphocholine; POPG, 1-Palmitoyl-2-oleoyl-3-*sn*-glycero-3-[phospho-rac-1-glycerol]; POPE 1-Palmitoyl-2-oleoyl-*sn*-glycero-3-phosphoethanolamine; POPC-d_{31}1-Palmitoyl-d_{31}-2-oleoyl-3-*sn*-glycero-3-phosphocholine; POPG-d_{31}, 1-Palmitoyl-d_{31}-2-oleoyl-3-*sn*-glycero-3-[phospho-rac-1-glycerol]; HEPES, N-[2-hydroxyethyl] piperazine-N'-[2-ethanesulfonic acid], TFE, 2,2,2, trifluoroethanol; EDTA, ethylenediamine tetraacetic acid; Fmoc, N-(9-fluorenyl)methoxycarbonyl; HPLC, high performance liquid chromatography; CP, cross-polarization; MAS, magic angle spinning; MLVs, multilamellar vesicles; LUVs, large unilamellar vesicles; T_1, longitudinal relaxation time.

5.1 Abstract

The designed antimicrobial peptide KIGAKIKIGAKIKIGAKI possesses enhanced membrane selectivity for bacterial lipids, such as phosphatidylethanolamine and phosphatidylglycerol. The perturbation of the bilayer by the peptide was first monitored using oriented bilayer samples on glass plates. The alignment of POPE/POPG model membranes with respect to the bilayer normal was severely affected at 4 mol% KIGAKI while the alignment of POPC bilayers was retained. The interaction mechanism between the peptide and POPE/POPG bilayers was investigated by carefully comparing three bilayer MLV samples (POPE bilayers, POPG bilayers, and POPE/POPG 4/1 bilayers). KIGAKI induces the formation of an isotropic phase for POPE/POPG bilayers, but only a slight change in the ^{31}P NMR CSA line shape for both POPE and POPG bilayers, indicating the synergistic roles of POPE and POPG lipids in the disruption of the membrane structure by KIGAKI. ^{2}H NMR powder spectra shows no reduction of the lipid chain order for both POPG and POPE/POPG bilayers upon peptide incorporation, supporting the evidence that the peptide acts as a surface peptide. ^{31}P longitudinal relaxation studies confirmed that different dynamic changes occurred upon interaction of the peptide with the three different lipid bilayers, indicating that the strong electrostatic interaction between the cationic peptide KIGAKI and anionic POPG lipids is not the only factor in determining the antimicrobial activity. Furthermore, ^{31}P and ^{2}H NMR powder spectra demonstrated a change in membrane characteristics upon mixing of POPE and POPG lipids. The interaction between different lipids, such as POPE and POPG, in the mixed bilayers may provide the molecular basis for the KIGAKI carpet mechanism in the permeation of the membrane.

5.2 Introduction

Antimicrobial peptides were discovered in a wide range of species as part of organisms offensive or defensive systems (*1, 2*). These membrane-active peptides permeate the cell membrane and cause the death of target cells. Antimicrobial peptides have potential application as antibiotics in the health care and as preservatives in the food industry (*3*). However, the toxicity of these naturally occurring antimicrobial peptides to not only microorganisms but also eukaryotic cells has made it important to design novel antimicrobial peptides with higher efficacy (*3*).

KIGAKI was designed to form a highly amphipathic β-sheet structure when bound to lipids (*4, 5*). The absence of cysteine residues precludes the formation of either inter- or intramolecular disulfide bonds to stabilize the secondary structure. Previous data indicated that the antimicrobial activity of KIGAKI was better than PGLa and $(KLAGLAK)_3$-NH_2 and suggested that KIGAKI had enhanced selectivity between bacterial and mammalian lipids (*4*). A solid-state NMR relaxation study confirmed that the electrostatic interaction between the peptide and the charged POPG lipids in the membrane is very critical for the function of KIGAKI (*6*). Although the electrostatic interaction between the peptide and POPG is one important factor for the peptide to fulfill its activity, the various lipid composition of the membranes is believed to be another modulating factor for antimicrobial activity (*7, 8*). Mammalian and bacterial cell membranes have different membrane compositions. The neutral zwitterionic lipid POPC is a major component of mammalian cell membranes (*9, 10*), while another zwitterionic phospholipid POPE with a smaller headgroup is the main lipid component of bacterial membranes. POPG is an anionic lipid commonly found in bacterial plasma membranes (*10, 11*). The conformation of KIGAKI peptide and its activity are different towards various membranes (*4*). Therefore the functional and structural roles of these lipids (POPC, POPE, and POPG) upon interaction with KIGAKI become very important.

Numerous biophysical studies have been conducted on the interaction between antimicrobial peptides and membranes (*12*). These studies have revealed two major mechanisms: (1) the barrel-stave mechanism in which peptides insert into the hydrophobic core of the membrane and form transmembrane pores (*13, 14*) and (2) the carpet or the detergent-like mechanism in which peptides bind onto the surface of the

membrane and cause membrane leakage when the peptide threshold concentration is reached (*14, 15*). An intermediate step before membrane disruption may include the formation of transmembrane channels, referred as "toroidal pores" (*3, 7, 11, 16*). Previously a carpet mechanism was proposed to describe the interaction between KIGAKI and POPC/POPG membranes. In this paper, solid-state NMR spectroscopy was utilized to decipher the interaction mechanism of the KIGAKI peptide with a variety of different membranes. Four model membrane systems consisting of POPC bilayers, POPC/POPG (4/1) bilayers, POPE bilayers, and POPE/POPG (4/1) bilayers were investigated to mimic mammalian and bacterial membranes and to examine the function of anionic lipids upon interaction between KIGAKI and the membrane. The effects of KIGAKI towards the alignment of the four different model membrane systems were compared. The alignment of POPE/POPG model membranes was severely disrupted upon association of the peptide while the alignment of POPC membranes was barely altered at the same peptide concentration.

The perturbation of POPE/POPG MLV bilayers to KIGAKI was investigated using ^{31}P and ^{2}H solid-state NMR spectroscopy. ^{31}P NMR spectroscopy reveals information on the interaction between KIGAKI and the lipids headgroup. Meanwhile ^{2}H NMR spectroscopy using acyl chain deuterated phospholipids can demonstrate the peptide influence in the bilayer hydrophobic interior. ^{31}P NMR relaxation measurements were used to probe the dynamic characteristics of the lipid headgroup upon interaction with the KIGAKI peptide. The longitudinal relaxation time T_1 is sensitive to lipid motions in the nanosecond-to-microsecond time scale, which includes the polar lipids headgroup fast conformational change and rotational motions (*17*). The experimental results suggest a toroidal pore mechanism upon KIGAKI interaction with POPG MLVs and a carpet mechanism upon KIGAKI interaction with POPE/POPG MLVs. The synergistic role of POPE and POPG lipids upon interaction between KIGAKI and the membrane is discussed.

5.3 Material and Methods

5.3.1 Material

POPC, POPE, POPG, POPC-d_{31} and POPG-d_{31} were purchased from Avanti Polar Lipids (Alabaster, AL) and used without further purification. All phospholipids were dissolved in chloroform and stored at -20°C prior to use. Deuterium-depleted water was obtained from Isotec (Miamisburg, OH). HEPES, TFE and EDTA were obtained from

Sigma/Aldrich (St. Louis, MO). The antimicrobial peptide KIGAKI was synthesized using Fmoc chemistry by ResGen (Huntsville, AL). The crude peptides were purified by reverse-phase HPLC. The purity of the peptide (>95%) was checked by reverse-phase HPLC and electrospray mass spectrometry (data not shown). Microscope cover glasses (8.5 ×14 mm) were purchased from Marienfeld Laboratory Glassware (Germany).

5.3.2 NMR sample preparation

Mechanically aligned membranes were prepared using a procedure described previously (*18*). The peptide was dissolved in a small amount TFE (≈50 μl) and mixed with an appropriate amount of phospholipids in chloroform. If needed, 10 mol% of deuterated lipids with respect to the total phospholipids amount was added. The solution was spread onto glass plates (~1.4 mg lipids/plate) and allowed to air-dry. The glass plates were then placed in a desiccator under vacuum overnight to remove any residual solvents. The dried sample was directly hydrated using deuterium-depleted water 2 μl/plate, stacked and placed in a humidity chamber consisting of saturated ammonium monophosphate at a relative humidity of about 93% at 45°C for one day. The glass plates were wrapped in Parafilm and sealed in polyethylene bags to prevent sample dehydration during data acquisition.

MLV samples were prepared according to a previously reported procedure (*19*). The phospholipids mixture (0.1 mmol) was first dried under a steady stream of N_2 gas for ~ 30 mins to remove the organic solvent. The deuterated lipids represented 20 mol% of the total phospholipids. The sample was then left under a high vacuum desiccators overnight. MLVs were formed by resuspension of the dry lipids in 190 μL HEPES buffer (5mM EDTA, 20mM NaCl, and 30mM HEPES, pH 7.0) with frequent vortexing to homogenize the sample. Samples were then allowed to sit in a warm water bath (50 °C) for 20 mins. Bilayer samples with peptides were prepared by mixing the peptides in a minimal amount of TFE solvent with phospholipids in chloroform followed with the same procedure described above.

5.3.3 NMR spectroscopy

All experiments were recorded on a Bruker Avance 500 MHz WB solid-state NMR spectrometer. A static double-resonance flat-coil probe (Doty) was used for oriented-membrane experiments. Unoriented membrane samples were studied using a

4mm triple resonance CPMAS probe (Bruker). ^{31}P static NMR spectra were acquired at 202.4 MHz using either a single pulse or a spin-echo pulse with proton decoupling. The ^{31}P NMR spectra were referenced by assigning the 85% H_3PO_4 ^{31}P peak to 0 ppm. ^{2}H static NMR experiments were performed at 76.77 MHz using a quadrupolar echo pulse sequence. The 90° pulses used for ^{31}P and ^{2}H were 5.0 μsec, 4.1 μsec for the flat coil probe and 4.0 μsec, 3.0 μsec for the CPMAS probe, respectively. Powder-type ^{31}P NMR spectra of POPE/POPG MLV samples incorporated with 4 mol% peptide were simulated using two components with the DMFIT program (*20*). Each component is defined to have its distinctive ^{31}P line shape and/or CSA width. Here one component is the isotropic component and the other component has an axially symmetric line shape. Powder-type ^{2}H NMR spectra of multilamellar dispersions of POPG-d_{31} were deconvoluted (dePaked) using the algorithm of McCabe and Wassall (*21*). The spectra were deconvoluted such that the bilayer normal was parallel with respect to the direction of the static magnetic field. The ^{2}H order parameters S_{CD} were calculated according to the equation: $S^{i}_{CD} = \Delta\nu_i/(3/2(e^2qQ/h))$, where $\Delta\nu_i$ is the quadrupolar splitting for a deuteron attached to the *ith* carbon of the POPC or POPG acyl chain, and e^2qQ/h is the quadruple coupling constant (168 kHz for deuteron in C-D bonds)(*22, 23*). The order parameters of the methyl groups at the end of the acyl chain were given the value of 3 times as the calculated S_{CD} (*22*). ^{31}P T_{1z} longitudinal relaxation experiments were conducted using an inversion-recovery pulse sequence 180°-T-90°-acquire with 4 kHz sample spinning at the magic angle (*24*). The delay time (T) was varied from 10.0 msec to 6.0 sec, with a recycle delay of 10 s. The change of the isotropic peak area was fitted to a single exponential function: $I(t) = I(0)-Aexp(-t/T_1)$, where I(0) is close to 1 and A is about 2. The error of ^{31}P T_1 value is within ± 10 ms by averaging ^{31}P T_1 values of the samples with same composition but from the different preparations.

5.4 Results

5.4.1 KIGAKI perturbation of the oriented model membranes.

The membrane alignment of four different bilayer systems is displayed in Figure 1 utilizing ^{31}P NMR spectroscopy on mechanically aligned samples. The peptide concentration varied from 0 mol% to 4 mol% with respect to the total phospholipids. The

alignment of the bilayers was studied in both orientations with the alignment axis parallel (left) or perpendicular (right) to the static magnetic field. In the absence of KIGAKI, the ^{31}P NMR spectrum of the four bilayers exhibited a predominant peak at ~30 ppm for the parallel orientation and ~-15 ppm for the perpendicular orientation, indicating that all the lipids are well aligned.

The addition of KIGAKI up to 4 mol% did not significantly disturb the bilayer alignment for the POPC bilayers (Figure 5.1(A)). The linewidth of the peak was only slightly increased in the presence of KIGAKI when compared to the control sample. However, at the same peptide concentration, POPC/POPG bilayers were perturbed (Figure 5.1(B)). A broad peak showed up at the 90° edge for the parallel alignment spectrum, indicating that the orientation of the lipids was distributed. This result was also confirmed by the POPC/POPG ^{31}P spectrum at the perpendicular orientation, where the ^{31}P chemical shift spans from ~28 ppm to ~ -15 ppm at 4 mol% KIGAKI, indicating perturbed bilayers at several orientations. The perturbation of KIGAKI on POPE bilayers was similar to that POPC/POPG on bilayers (Figure 5.1(C)). The addition of KIGAKI caused the ^{31}P 0° edge peak to shift slightly with an increase in the distribution of the ^{31}P chemical shift. POPE/POPG bilayers experienced the most significant disturbance upon association with KIGAKI (Figure 5.1(D)). For the parallel alignment spectrum, the 90° edge peak intensity is even higher than that of 0° edge peak and the high absorption spans the entire chemical shift range at 4% KIGAKI. Since ^{31}P NMR spectra only reflect the perturbation of the peptide to the lipid headgroup, ^{2}H NMR studies on membranes with acyl chain deuterated lipids were also carried out to probe the changes that occur in the hydrophobic part of the membranes. Figure 5.2 shows ^{2}H NMR spectra of (A) POPC/ POPC-d_{31}, (B) POPC/POPC-d_{31}/POPG and (C) POPE/POPG/POPG-d_{31} bilayers. The spectra exhibit multiple splittings that correspond to different methylene groups and methyl group along the lipids sn-2 chains. The largest splittings result from the groups close to the glycerol backbone with a high molecular ordering. The smaller splittings originate from the mobile chain with lower molecular orderings. The ^{2}H NMR spectra of all three control bilayers are well-resolved with the largest quadrupolar splitting about 62 kHz for the parallel alignment spectra and ~31 kHz for the perpendicular aligned spectra.

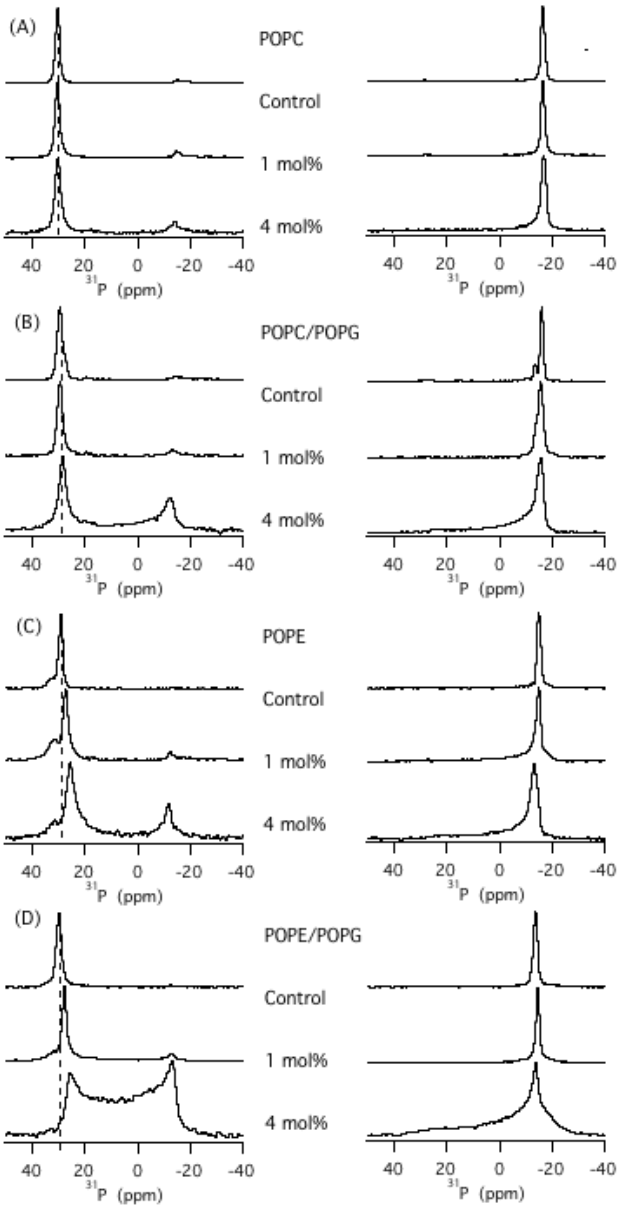

Figure 5.1 ^{31}P NMR spectra of oriented bilayer samples showing the perturbation of KIGAKI on the lipid headgroup as a function of KIGAKI concentration in different bilayers (A) POPC, (B) POPC/POPG (4/1), (C) POPE, (D) POPE/POPG (4/1). The alignment axis was either parallel (left column) or perpendicular (right column) to the magnetic field. The spectra were taken at 30°C for the POPC, POPC/POPG, POPE/POPG bilayers. The spectra of POPE bilayers were taken at 37°C. At these temperatures the spectra were optimally aligned.

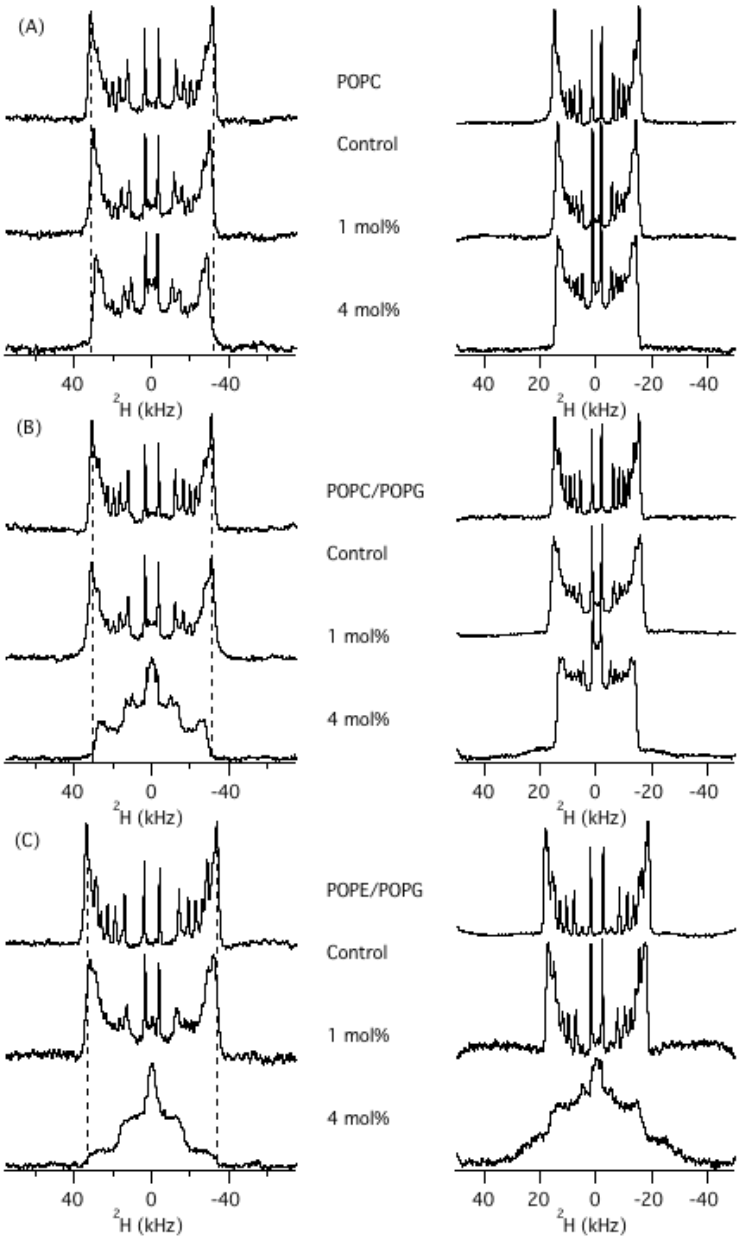

Figure 5.2 ^{2}H NMR spectra of oriented bilayer samples showing the perturbation of KIGAKI on the lipid acyl chain as a function of KIGAKI concentration at 30°C in different bilayers (A) POPC, (B) POPC/POPG (4/1), (C) POPE/POPG (4/1). POPC-d_{31} was used as the chain deuterated lipids to probe the KIGAKI perturbation in the hydrophobic interior of the membranes in POPC and POPC/POPG bilayers while POPG-d_{31} was used in POPE/POPG bilayers. The alignment axis was either parallel (left column) or perpendicular (right column) to the magnetic field.

For the POPC bilayers, the ^{2}H spectral resolution was maintained with only a slight decrease in the quadrupolar splittings at 4 mol% KIGAKI (Figure 5.2(A)). This is consistent with the results obtained from POPC ^{31}P NMR spectra, indicating a minimal perturbation of KIGAKI into POPC bilayers. The orientational disorder effect caused by KIGAKI was further studied using POPC/POPG (Figure 5.2(B)) and POPE/POPG (Figure 5.2(C)) bilayers. Both samples contain anionic POPG lipids. At 1 mol% KIGAKI, the ^{2}H spectral resolution of POPC/POPG sample decreases slightly. At 4 mol% KIGAKI, the spectral resolution decreases significantly. The parallel alignment spectrum displays an increase in the signal intensity of the small splittings. The significant ^{2}H NMR line shape changes for the mixed POPC/POPG bilayer, but not for the POPC bilayers suggests an important role for the charged POPG lipids upon interaction with KIGAKI. For POPE/POPG bilayers, the ^{2}H NMR spectra resolution deteriorates severely upon incorporation of the peptide for both the parallel and perpendicular orientation. Combined with the ^{31}P NMR study results, POPE/POPG is the most vulnerable membrane subject upon interaction with the antimicrobial peptide KIGAKI.

5.4.2 The interaction of KIGAKI with POPE/POPG bilayers.

To understand the individual roles of POPE lipids and POPG lipids upon interaction of KIGAKI with POPE/POPG bilayers, ^{31}P and ^{2}H NMR studies were applied on MLV samples of POPE, POPG and binary POPE/POPG bilayers, respectively. The ^{31}P NMR spectra of POPE MLVs are shown in Figure 5.3(A). The ^{31}P CSA spans from around 32 ppm to -18 ppm. The addition of 4 mol% KIGAKI did not alter the ^{31}P CSA line shape. Only one axially symmetric CSA component was needed to simulate the line shape of the POPE ^{31}P NMR spectrum at 4 mol% KIGAKI (Figure 5.3(D)). Figure 5.3(B) displays the ^{31}P NMR spectrum that probes the interaction between the cationic peptide and the anionic POPG bilayers. The ^{31}P CSA span of POPG (26 ppm to -15 ppm) is much smaller than that of POPE. Surprisingly, the association of KIGAKI to the negative charged bilayer surface did not cause a significant change in the ^{31}P NMR line shape.

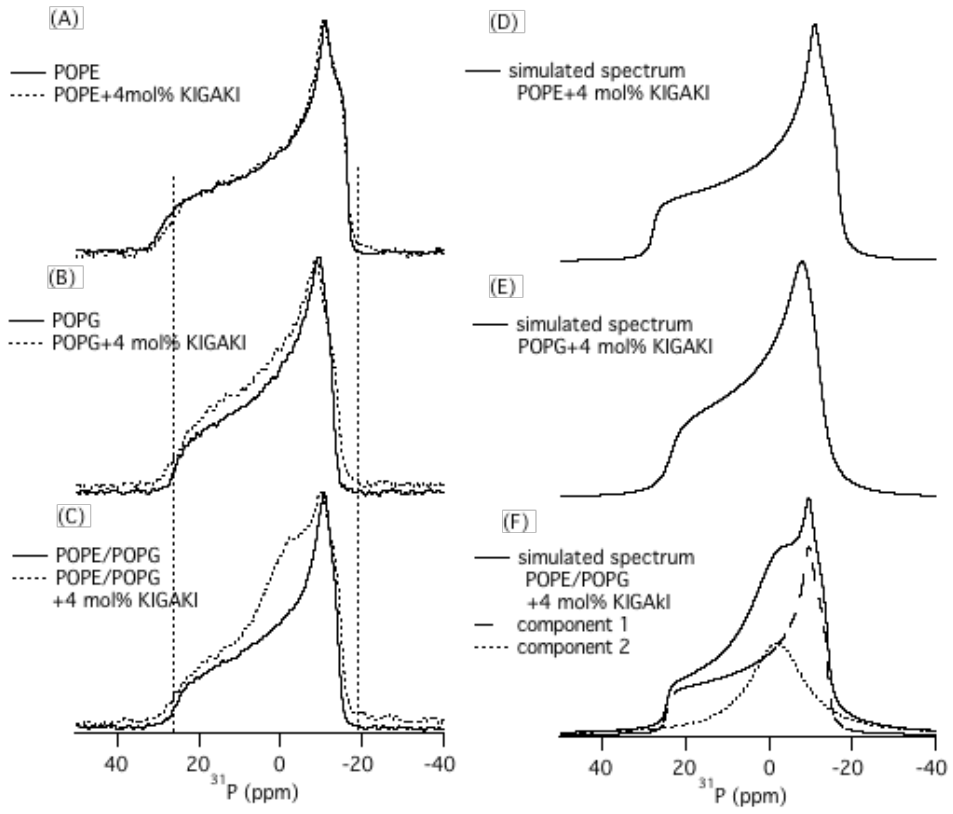

Figure 5.3 ^{31}P NMR powder type spectra of MLV samples exhibiting the effect of KIGAKI on the ^{31}P spectra line shape for three different bilayers (A) POPE, (B) POPG, (C) POPE/POPG at 30°C. The solid line represents the control spectra and the dashed line represents the spectra of bilayers at 4 mol% KIGAKI on the left column. The corresponding simulated data representing ^{31}P NMR spectra of (D) POPE bilayers, (E) POPG bilayers and (F) POPE/POPG bilayers in the presence of KIGAKI are displayed on the right column. Two components were needed to simulate the spectrum of (F) POPE/POPG bilayer with one isotropic component contributing 40%± 1% (dotted line) and another anisotropic component 60%± 1% (dash line) to the total spectrum area. The error range was estimated so that the best fit of the spectra was obtained at these values.

Only one ^{31}P CSA component was needed to simulate the spectrum (Figure 5.3(E)). The effect of KIGAKI on mixed binary POPE/POPG bilayers is displayed in Figure 5.3(C). The mixed bilayers with 80% POPE and only 20% POPG exhibit a CSA span (26 ppm to -16 ppm) much smaller than that of POPE and close to that of POPG. The ^{31}P CSA line shape of the lipids in the liquid-crystalline phase reflects an axially symmetric motion of lipids. The orientation and the additional wobbling motion of the lipid headgroup with respect to the molecular axis determine the ^{31}P CSA span (*25-27*). This result suggests that the minor POPG component plays a pivotal role in the mixed bilayer lipid headgroup orientation and molecular motions. The association of 4 mol% KIGAKI with POPE/POPG bilayers caused a ^{31}P NMR line shape change with an increase of intensity around 0 ppm. The powder pattern spectrum can be deconvoluted into two components with an anisotropic component contributing 60% to the total spectrum area and an isotropic component representing the remainder 40% (Figure 5.3(F)). Considering little change in the ^{31}P NMR line shape for POPE and POPG bilayers upon the association of KIGAKI, this result indicates that the peptide can cause a membrane phase separation only in bilayers consisting of both neutral POPE lipids and anionic POPG lipids.

The interference of KIGAKI with the membrane hydrophobic core was investigated using ^{2}H NMR powder pattern spectra (Figures 5.4(A) and (B)). POPG bilayers have a smaller spectral width than POPE/POPG bilayers, suggesting less molecular ordering and /or faster acyl chain motion when compared to POPE/POPG bilayers. The corresponding lipid's molecular order parameters are shown in Figure5.4(C). The mixing of 80% POPE phospholipids to 20% POPG bilayers significantly increases the ordering of the bilayer lipids. The ^{2}H quadrupolar splittings are also increased upon incorporation of KIGAKI to POPG bilayers, whereas the addition of 4 mol% KIGAKI to POPE/POPG bilayers is not accompanied by any changes in the ^{2}H quadrupolar splittings. A decrease in the lipids ^{2}H quadrupolar splitting upon incorporation of the peptide suggests the disordering of the lipids. No disordering effects for the lipid acyl chains were observed after the peptide was added to both POPG and POPE/POPG bilayers, suggesting that the peptide didn't penetrate inside the bilayers. An

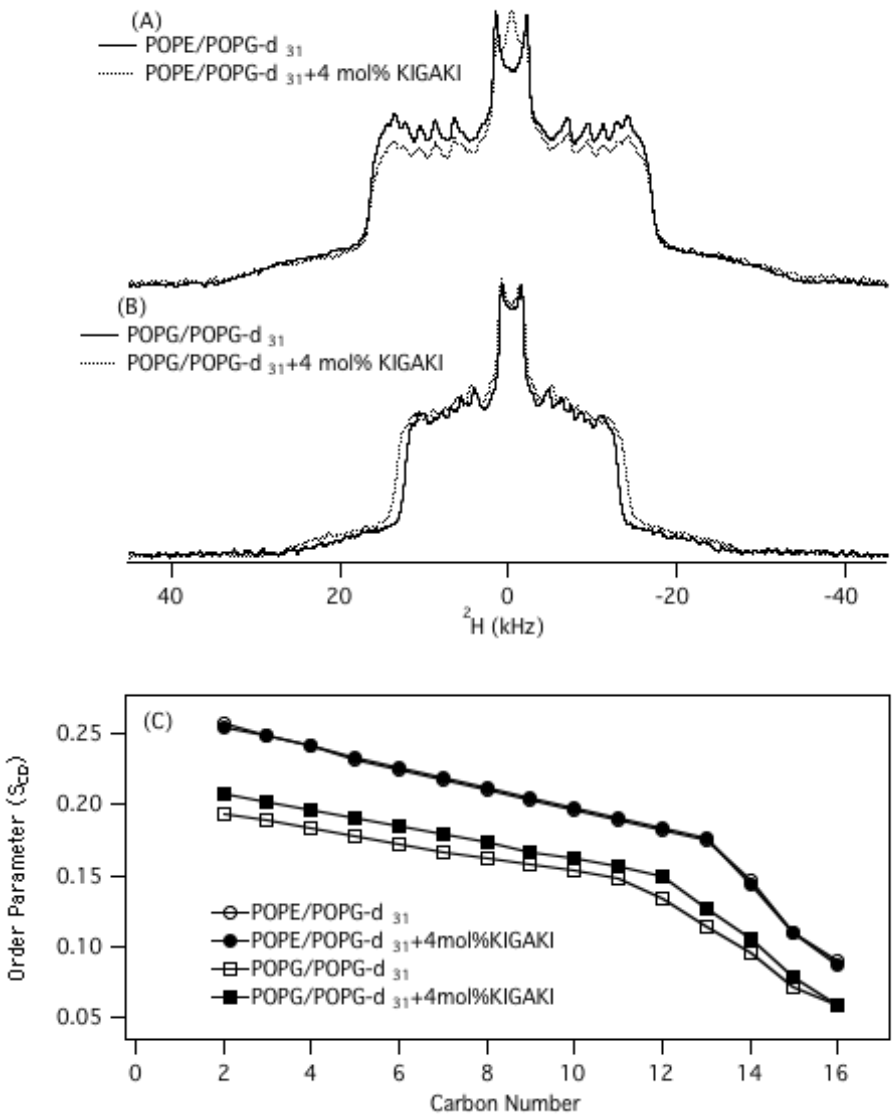

Figure 5.4 ^{2}H NMR powder spectra of MLV samples at 25°C showing the effect of KIGAKI on the membrane hydrophobic interior for two bilayers (A) POPE/POPG (B) POPG bilayers. POPG-d_{31} was used here as the deuterium probe. The corresponding molecular order parameters of the individual groups along the lipid acyl chains were obtained by dePakeing the ^{2}H NMR spectra (C).

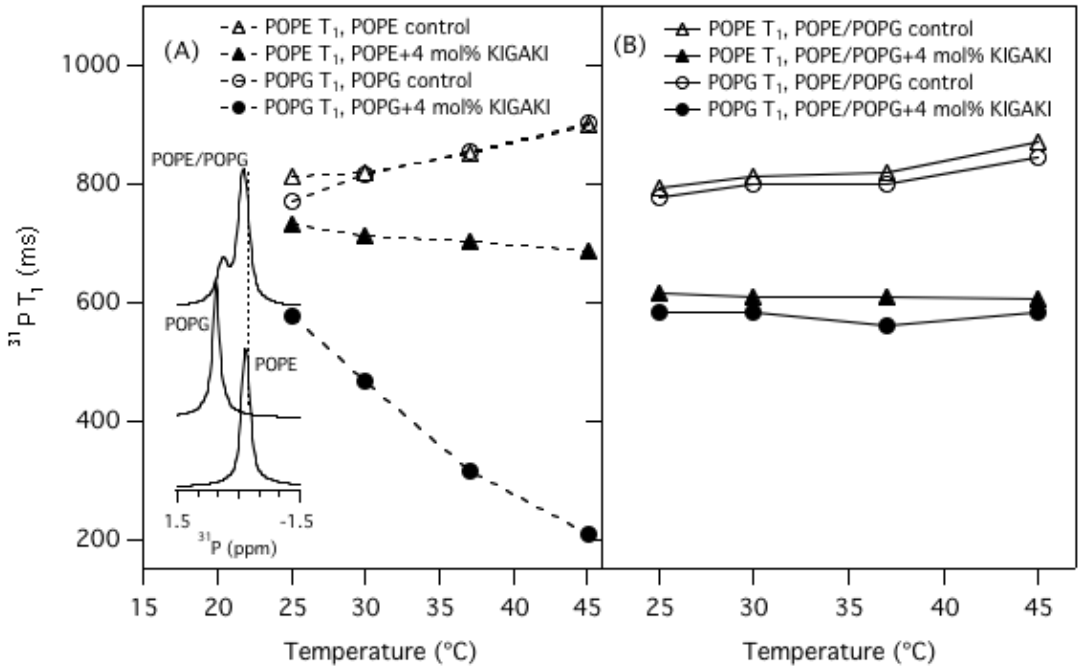

Figure 5.5 ^{31}P longitudinal relaxation time (T_1) as a function of temperature for (A) POPE and POPG bilayers (B) POPE/POPG bilayers. The open symbol represents the ^{31}P T_1 of the control sample while the solid symbol represents the ^{31}P T_1 of the bilayers with 4 mol% KIGAKI. The dotted line represents the bilayers with single lipid component POPE or POPG and the solid line represents the binary mixed POPE/POPG bilayer sample. The experimental error was within ± 10 ms by averaging ^{31}P T_1 values of the samples with same composition but from the different preparations. The isotropic peak positions of the three bilayer samples at 4 kHz MAS are shown in the inset.

isotropic component is exhibited for POPE/POPG bilayers at 4 mol% KIGAKI. This is consistent with the ^{31}P NMR powder pattern spectra studies, where the POPE/POPG bilayer phase is disintegrated into two species by the peptide KIGAKI.

5.4.3 ^{31}P NMR relaxation study of lipids headgroup dynamics.

The ^{31}P longitudinal relaxation time T_1 is sensitive to fast lipid headgroup rotational motions (*17*). Lipid headgroup dynamics for POPE, POPG and binary POPE/POPG bilayers were examined using ^{31}P NMR longitudinal relaxation inversion-recovery pulse scheme at various temperatures. Using magic angle spinning, two resolved resonances were observed around 0 ppm for the binary POPE/POPG bilayers (Figure 5.5 inset). At 25°C, the control POPE/POPG bilayers exhibit two ^{31}P isotropic peaks at -0.12 ppm and 0.38 ppm for POPE and POPG respectively. The addition of 4 mol% KIGAKI shifted the POPE isotropic peak to -0.18 ppm and POPG isotropic peak to 0.23 ppm with a slight increase in line broadening. Similar isotropic peak shifts were also observed for POPE and POPG bilayers with a single lipid component when the peptide was added to the MLVs sample. The isotropic ^{31}P chemical shift of the lipid headgroup is sensitive to the surface charge density. A upfield peak shift is consistent with a decrease in the negative surface charge density of the membrane upon interaction with KIGAKI (*28, 29*). Careful analysis of the spectra indicates that both POPE and POPG lipids experience a slight shift in the isotropic peak of the binary POPE/POPG bilayers. These small shifts are a manifestation of the interaction between POPE and POPG headgroups in the mixed bilayers, which was also indicated by the POPE/POPG ^{31}P powder spectra.

The ^{31}P T_1 values as a function of temperature for different bilayers are summarized in Figure 5. The POPE and POPG lipids ^{31}P T_1 (~800 ms at 25°C) are very close for the three control bilayer samples. The ^{31}P T_1 increases as the temperature increases from 25°C to 45°C. The ^{31}P longitudinal relaxation time T_1 is related to the correlation time (τ_c) of fast molecular motion according to $1/T_1 \propto \tau_c/(1+ \omega_0{}^2\tau_c{}^2)$, where ω_0 is the Larmor frequency (*27, 30*). If the molecular correlation time fits the equation $\omega_0\tau_c \cong 1$, the relaxation mechanism is most efficient, and the T_1 relaxation time is at the minimum (*27, 30*). The correlation time moving away from the $1/\omega_0$ point would cause an increase in the T_1 value. Temperature is a factor that modulates the molecular

correlation time. In this case, the continuous increase in the ^{31}P T_1 relaxation time above 25°C indicates the lipid's minimum T_1 for these control samples would be lower than 25°C. This is typical for phospholipids in hydrated bilayers (*27, 30*).

The incorporation of 4 mol% KIGAKI enhanced the spin-lattice relaxation and decreased the ^{31}P T_1 for all the three bilayer samples. For the POPE lipids, the ^{31}P T_1 of the bilayers are reduced to around 700 ms, and the T_1 value slightly decreases when the temperature increases. In POPG bilayers, the ^{31}P T_1 decreases to around 600 ms at 25 °C and the reduction of T_1 increases significantly as the temperature increases. At 45°C, the POPG ^{31}P T_1 is approximately 200 ms. These results suggest that a minimum T_1 would occur at higher temperatures where the molecular correlation time τ_c is equal to $1/\omega_0$. For the binary POPE/POPG bilayers, POPE ^{31}P T_1 value is reduced to 615 ms and POPG lipid ^{31}P T_1 value is reduced to 583 ms at 25 °C in the presence 4% KIGAKI. Meanwhile, the relaxation time remains consistent as the temperature increased. These results suggest that different dynamic changes of lipid headgroups occurred for the three bilayers upon association of 4% KIGAKI.

5.5 Discussion

Previous studies have indicated that compared to the antimicrobial peptide magainin and PGLa, a lower KIGAKI peptide concentration is needed to inhibit the bacterial growth while a higher peptide concentration is required to cause hemolysis (*4, 5*). Meanwhile the studies on the mimetic phospholipids bilayer membranes exhibit that the antimicrobial peptide KIGAKI exhibits high lytic activity against membranes mainly composed of POPE and lower lytic activity against POPC membranes (*4, 5*). To understand KIGAKI membrane selectivity will provide fundamental information in the design of novel, high efficacy antimicrobial peptides.

The alignment of four bilayer model membranes was compared first. The KIGAKI perturbation to POPC bilayers is finite, while the perturbation to POPC/POPG is moderate. The different effect of KIGAKI on these two bilayers can be attributed to the presence of the negatively charged POPG lipids in POPC/POPG bilayers. Comparing the alignment changes of POPE bilayers and POPE/POPG bilayers, the similar PG lipids effect can be observed. In general, the bilayers containing POPE lipids are more

susceptible to the presence of KIGAKI than the bilayers containing POPC lipids. The alignment perturbation by KIGAKI is more significant for POPE and POPE/POPG bilayers. The KIGAKI membrane selectivity manifested here seems very interesting; however, the molecular mechanism of these specific peptide-membrane interactions is still not understood.

5.5.1 The KIGAKI-POPE interaction mechanism.

POPE is major component of bacterial membranes. The interaction between KIGAKI and POPE bilayers are displayed in Figure 3(A) using phospholipid bilayer powder pattern spectra. The incorporation of KIGAKI to POPE bilayers only introduced a slight change in the ^{31}P CSA line shape, indicating minimal activity of KIGAKI with pure POPE bilayers. In addition, the ^{31}P spin-lattice relaxation time indicated a more efficient relaxation mechanism of POPE lipids in the presence of KIGAKI, suggesting that a dynamic change occurs in the POPE bilayers. The ^{31}P spin-lattice relaxation time had been previously used to study the KIGAKI-POPC interaction (*6*). The ^{31}P T_1 remained the same upon addition of KIGAKI to the POPC bilayers. ^{31}P NMR study on the same KIGAKI-POPC powder sample indicated a ^{31}P CSA line shape change. These results agree with the bilayer alignment perturbation study in this paper, which indicates that the interaction between KIGAKI and POPC bilayers is very weak. Therefore, the KIGAKI-POPE interaction is stronger than the KIGAKI-POPC interaction.

KIGAKI caused a distribution of the POPE lipid headgroup orientation on glass plates at 4 mol% concentration. However, the incorporation of KIGAKI to POPE MLVs at the same concentration only introduced a slight change in the ^{31}P CSA line shape. The inconsistency may reflect a fundamental difference in the study of these two membranes. The studies of the oriented bilayer on the glass plates are complicated by additional factors such as the ability of each individual lipid to orient on glass plates, etc. Furthermore, the hydration levels in the two samples are different. The MLV samples used here (~70% water relative to the total sample weight, calculated) have more water content than the mechanically aligned samples (usually 30~50% water by weight, FT-IR (*31, 32*)). The different hydration levels of these two bilayers may be another reason causing the perturbation difference observed on POPE bilayer introduced by KIGAKI.

5.5.2 The KIGAKI-POPG interaction mechanism.

POPG is a negatively charged phospholipid. The electrostatic interaction between the cationic peptide and the anionic lipids is important for the peptide to form the proper secondary structures (*4*). Previous reports indicate an essential role of POPG in the function of KIGAKI causing a membrane phase separation and leakage (*4, 6*). Unexpectedly, the interaction between 4 mol% KIGAKI and pure POPG bilayers didn't introduce any significant ^{31}P CSA line shape changes from the control sample (Figure 3(B)).

Meanwhile, in POPG lipids, the ^{31}P T_1 was reduced significantly in the presence of 4 mol% KIGAKI. The reduction of ^{31}P T_1 as a function of temperature suggests a minimum T_1 would be at a higher temperature where the molecular correlation time $\tau_c = 1/\omega_0$. Since the Larmor frequency of the magnetic field is fixed, the ^{31}P T_1 study proposes a much slower molecular rotation and a much longer correlation time of POPG lipids for POPG/KIGAKI sample. ^2H order parameter results indicate that the lipids acyl chain displays a higher molecular ordering and/or a slower molecular motion of POPG upon the addition of the peptide KIGAKI. This result agrees with the ^{31}P T_1 study on the lipid headgroups. One KIGAKI peptide molecule has six positive charged lysine residues. Upon interaction with POPG bilayers, the peptide forms a β-sheet structure, flanking with all six positive charges on one side (*4*). The interaction between the peptide and the lipids, mainly the electrostatic interaction, could bring the lipids closer together and/or cause the rearrangement of the lipids conformation. The space between different lipids would be decreased. Therefore, both the lipid headgroups and the lipid acyl chains exhibit restricted molecular motions. In conclusion, although KIGAKI disturbs the lipids molecular motion, and causes the leakage of the bilayers (*4*), the POPG lipids bilayer phase remains.

5.5.3 The KIGAKI-POPE/POPG interaction mechanism.

POPE/POPG is the most vulnerable model membrane against the antimicrobial peptide KIGAKI. The alignment of the bilayer on glass plates was significantly perturbed by KIGAKI. The ^{31}P and ^2H spectra line shape changes are similar to those induced by a

cyclic antimicrobial peptide RTD-1 observed in Hong's group (*9*). They propose that the micrometer-diameter lipid cylinders are formed in anionic membranes upon interaction with the antimicrobial peptide. The curvature stress introduced by RTD-1 may play a role in antimicrobial activity. The similar membrane curvature strain changes were also noticed in the research of other antimicrobial peptide such as LL-37 (*11*) and MSI-78 (*33*). However, previous study on KIGAKI using differential scanning calorimetry on DiPOPE vesicles indicates a minor increase in the bilayer-to-hexagonal phase transition temperature (*4*). Therefore, it is still under debate as to whether the change in the membrane curvature strain is important in membrane breakage upon interaction with KIGAKI. Moreover, the results obtained from the interaction with DiPOPE bilayers may not be able to generalize to other bilayers with different membrane compositions.

The interaction between KIGAKI and POPE/POPG bilayer was further investigated using POPE/POPG MLVs. The ^{31}P spectrum CSA of control POPE/POPG bilayers is close to that of POPG bilayers, but significantly different from that of POPE bilayers. Several papers have reported that the charged additives to the membrane can alter the lipid ^{31}P CSA and isotropic peak position significantly (*25, 26, 34*). In this case, the negative charge on the POPG headgroup would probably move the N^+ end of POPE headgroup towards the membrane, causing a downshift tilt. The orientational change of the POPE headgroup would probably induce a CSA change (*25*).

^2H NMR spectra of POPE/POPG bilayers exhibit larger quadrupolar splittings than that of pure POPG bilayers. Therefore, although the POPE lipid headgroup was easily affected by the charged molecules, the POPE lipids acyl chain possess a higher molecular ordering, which was indirectly demonstrated by POPG-d_{31} lipids distributed evenly within the POPE/POPG bilayers. Considering POPE lipids have a higher phase transition temperature (24°C) than POPG (-4°C), the experiment on POPE/POPG bilayers was also carried out in different temperatures (from 25°C to 45°C). ^{31}P and ^2H NMR data indicate an axially symmetry pattern spectrum similar as Figure 5.3 and 5.4, indicating the liquid-crystalline phase of POPE/POPG bilayers for all these temperatures.

Different from POPE or POPG bilayers, the association of KIGAKI to POPE/POPG binary mixed bilayers induced a big change in the ^{31}P spectrum line shape (Figure 5.3(C)). Two phases were observed, corresponding to a CSA component and an

isotropic component (Figure 5.3(F)). An isotropic component was also superimposed in a series quadrupolar splittings in POPE/POPG ^{2}H NMR spectrum in the presence of 4 mol% KIGAKI. The isotropic component could be micelles or small vesicles, which have very fast tumbling motion. No molecular order parameter changes along the lipid acyl chain upon incorporation of the peptide, suggesting that the peptide didn't penetrate inside the bilayer membranes. This is consistent with a carpet mechanism in the breakage of the membranes (*15*).

Obviously, although electrostatic interaction is very important in the interaction between KIGAKI and POPG lipids, it alone is not enough to cause a bilayer phase change. The ^{31}P T_1 relaxation study of POPE/POPG bilayers indicates a similar T_1 value for the two individual POPE and POPG lipids, suggesting that the two lipids have similar dynamic changes in the interaction with the peptide. POPG lipids were not preferentially selected in the interaction. This is different from our previous study on the interaction between KIGAKI and the POPC/POPG bilayers, where the preference of KIGAKI to interact with POPG lipids was inferred (*6*). However, both the study on the aligned bilayer sample and previous activity assays indicate that KIGAKI has selectivity against mixed bilayers in the presence of POPE lipids (*4, 5*). Therefore, the higher antimicrobial activity would depend on more than electrostatic interaction between the peptide and the POPG lipids. Both POPE and POPC lipids are zwitterionic lipids, but POPE lipid has a smaller headgroup than POPC lipid. This would probably make the interaction between the cationic peptide and the negatively charged phosphate group in the POPE lipids easier, especially with the help of POPE headgroup tilting in the addition of POPG. The capability of relatively stronger interaction between KIGAKI and POPE lipids than that between KIGAKI and POPC lipids was also supported by the ^{31}P T_1 and the bilayer alignment perturbation study on POPE and POPC bilayers. Since POPE lipids have very different dynamics from POPG lipids, indicated by significantly different ^{31}P CSA values and the ordering of lipids acyl chain, the phase separation of POPG lipids from POPE lipids in the binary POPE/POPG bilayers would be observable. No POPE and POPG phase separation was indicated after the addition of KIGAKI into the POPE/POPG bilayers. The isotropic species exhibited by ^{31}P and ^{2}H NMR spectra would likely consist of both POPE and POPG lipids in a similar proportion as the POPE/POPG bilayer

component. Alternatively, the electrostatic interaction between the antimicrobial peptide and the POPG lipids in the mixed bilayers is so strong that one would expect the cationic peptide to pull the anionic lipids close together to form a relatively separate domain. This was not the case, suggesting that the electrostatic interaction between the peptide and POPG is not so strong, and probably is comparable to the interaction between the peptide and POPE lipids, as suggested by similar POPE and POPG ^{31}P T_1 relaxation changes (Figure 5.5(B)). Therefore, the comprehensive interactions among the membranes including the lipid/lipid interaction and the interactions between the peptide and different lipids must be considered to understand the KIGAKI antimicrobial mechanism.

For the pure POPG bilayers, the membrane leakage can exist without the formation of the micelles or small vesicles. This suggests a different mechanism from the carpet mechanism, more consistent with a toroidal pore mechanism (*11, 16, 33*). KIGAKI interacts different membranes utilizing different mechanism. The different mode of action on different lipids was also observed on other lytic peptides, such as melittin (*35, 36*). For the mixed POPE/POPG bilayers, our results suggest that KIGAKI interacts with both POPE and POPG lipids in a similar fashion. In our last report, KIGAKI preferred to interact with POPG lipids in the mixed POPC/POPG bilayers (*6*). For both the mixed bilayers, the carpet mechanism is implied in the interaction between KIGAKI and membranes. Probably the mixed bilayer is more fragile. The lipids interact with each other by electrostatic interaction or hydrogen bonding etc. at the headgroup region, forming a complex network to stabilize the bilayers. Upon introduction of KIGAKI to the mixed bilayer, the interactions between the peptide and the lipids would decrease the connectivity among the lipids and permeate the membranes. This is likely the molecular basis of the KIGAKI carpet mechanism.

Acknowledgement:

This work was supported by an NSF CAREER Award (CHE-0133433) and a National Institutes of Health grant GM60259-01 to GAL and AI047165-02 to JB. The 500MHz wide-bore NMR spectrometer was obtained from a National Science Foundation grant 10116333.

5.6 References

(1) Boman, H. (1991) Antibacterial peptides: key components needed in immunity. *Cell 65*, 205-207.

(2) Boman, H. (1995) Peptide antibiotics and their role in innate immunity. *Annu. Rev. Immun. 13*, 61-92.

(3) Bradshaw, J. P. (2003) Cationic antimicrobial peptides, Issues for potential clinical use. *Biodrugs 17*, 233-240.

(4) Blazyk, J., Wiegand, R., Klein, J., Hammer, J., Epand, R. M., Epand, R. F., Maloy, W. L., and Kari, U. P. (2001) A novel linear amphipathic beta-sheet cationic antimicrobial peptide with enhanced selectivity for bacterial lipids. *J. Biol. Chem. 276*, 27899-27906.

(5) Jin, Y., Mozsolits, H., Hammer, J., Zmuda, E., Zhu, F., Zhang, Y., Aguilar, M. I., and Blazyk, J. (2003) Influence of tryptophan on lipid binding of linear amphipathic cationic antimicrobial peptides. *Biochemistry 42*, 9395-9405.

(6) Lu, J. X., Damodaran, K., Blazyk, J., and Lorigan, G. A. (2005) Solid-State NMR Relaxation Studies of the Interaction Mechanism of Antimicrobial Peptides with Phospholipid Bilayer Membranes. *Biochemistry 44*, 10208-10217.

(7) Shai, Y., and Oren, Z. (2001) From "carpet" mechanism to de-novo designed diastereomeric cell-selective antimicrobial peptides. *Peptides 22*, 1629-1641.

(8) Matsuzaki, K., Sugishita, K., Ishibe, N., Ueha, M., S., N., Miyajima, K., and Epand, R. M. (1998) Relationship of Membrane curvature to the formation of pores by magainin 2. *Biochemsitry 37*, 11856-11863.

(9) Buffy, J. J., McCormick, M. J., Wi, S., Waring, A. J., Lehrer, R. I., and Hong, M. (2004) Solid-state NMR investigation of the selective perturbation of lipid bilayers by the cyclic antimicrobial peptide RTD-1. *Biochemistry 43*, 9800-9812.

(10) Yorek, M. (1993) Biological Distribution, in *Phospholipids handbook* (Cevc, G., Ed.) pp 745-776, Marcel Dekker, Inc., New York.

(11) Wildman, K. A. H., Lee, D. K., and Ramamoorthy, A. (2003) Mechanism of lipid bilayer disruption by the human antimicrobial peptide, LL-37. *Biochemistry 42*, 6545-6558.

(12) Oren, Z., and Shai, Y. (1998) Mode of action of linear amphipathic alpha-helical antimicrobial peptides. *Biopolymers 47*, 451-463.

(13) He, k., Ludtke, S. J., Huang, H. W., and Worcester, D. L. (1995) Antimicrobial peptide pores in membranes detected by neutron in-plane scattering. *Biochemistry 34*, 15614-15618.

(14) Papo, N., and Shai, Y. (2003) Exploring peptide membrane interaction using surface plasmon resonance: differentiation between pore formation versus membrane disruption by lytic peptides. *Biochemsitry 42*, 458-466.

(15) Bechinger, B. (2005) Detergent-like properties of magainin antibiotic peptides: A 31P solid-state NMR spectroscopy study. *Biochim. Biophys. Acta 1712*, 101-108.

(16) Hallock, K. J., Lee, D. K., Omnaas, J., Mosberg, H. I., and Ramamoorthy, A. (2002) Membrane composition determines pardaxin's mechanism of lipid bilayer disruption. *Biophys. J. 83*, 1004-1013.

(17) Watts, A. (1998) Solid-state NMR approaches for studying the interaction of peptides and proteins with membranes. *Biochim. Biophys. Acta-Rev. Biomembr. 1376*, 297-318.

(18) Tiburu, E. K., Karp, E. S., Dave, P. C., Damodaran, K., and Lorigan, G. A. (2004) Investigating the dynamic properties of the transmembrane segment of phospholamban incorporated into phospholipid bilayers utilizing ^{2}H and ^{15}N solid-state NMR pectroscopy. *Biochemistry 43*, 13899-13909.

(19) Dave, P. C., Tiburu, E. K., Damodaran, K., and Lorigan, G. A. (2004) Investigating structural changes in the lipid bilayer upon insertion of the transmembrane domain of the membrane-bound protein phospholamban utilizing P-31 and H-2 solid-state NMR spectroscopy. *Biophys. J. 86*, 1564-1573.

(20) Massiot, D., Fayon, F., Capron, M., King, I., Le Calvé, S., Alonso, B., Durand, J.-O., Bujoli, B., Gan, Z., and Hoatson, G. (2002) Modelling one- and two-dimensional solid state NMR spectra. *Magn. Reson. in Chem. 40*, 70-76.

(21) McCabe, M. A., and Wassall, S. R. (1995) Fast-Fourier-Transform Depaking. *J. Magn. Reson. Ser. B 106*, 80-82.

(22) Lu, J. X., Caporini, M. A., and Lorigan, G. A. (2004) The effects of cholesterol on magnetically aligned phospholipid bilayers: a solid-state NMR and EPR spectroscopy study. *J. Magn. Reson. 168*, 18-30.

(23) Dave, P. C., Tiburu, E. K., Nusair, N. A., and Lorigan, G. A. (2003) Calculating order parameter profiles utilizing magnetically aligned phospholipid bilayers for H-2 solid-state NMR studies. *Solid State Nucl. Magn. Reson. 24*, 137-149.

(24) Aussenac, F., Laguerre, M., Schmitter, J. M., and Dufourc, E. J. (2003) Detailed structure and dynamics of bicelle phospholipids using selectively deuterated and perdeuterated labels. H-2 NMR and molecular mechanics study. *Langmuir 19*, 10468-10479.

(25) Semchyschyn, D. J., and Macdonald, P. M. (2004) Conformational response of the phosphatidylcholine headgroup to bilayer surface charge: torsion angle constraints from dipolar and quadrupolar couplings in bicelles. *Magn. Reson. in Chem. 42*, 89-104.

(26) Scherer, P. G., and Seelig, J. (1989) Electric Charge Effects on Phospholipid Headgroups - Phosphatidylcholine in Mixtures with Cationic and Anionic Amphiphiles. *Biochemistry 28*, 7720-7728.

(27) Pinheiro, T. J. T., and Watts, A. (1994) Resolution of Individual Lipids in Mixed Phospholipid-Membranes and Specific Lipid Cytochrome-C Interactions by Magic-Angle- Spinning Solid-State P-31 Nmr. *Biochemistry 33*, 2459-2467.

(28) Lindstrom, F., Bokvist, M., Sparrman, T., and Grobner, G. (2002) Association of amyloid-beta peptide with membrane surfaces monitored by solid state NMR. *Phys. Chem. Chem. Phys. 4*, 5524-5530.

(29) Lindstrom, F., Williamson, P. T. F., and Grobner, G. (2005) Molecular insight into the electrostatic membrane surface potential by $^{14}N/^{31}P$ MAS NMR spectroscopy: nociceptin-lipid association. *J. Am. Chem. Soc. 127*, 6610-6616.

(30) Pinheiro, T. J. T., and Watts, A. (1994) Lipid Specificity in the Interaction of Cytochrome-C with Anionic Phospholipid-Bilayers Revealed by Solid-State P-31 Nmr. *Biochemistry 33*, 2451-2458.

(31) Yamaguchi, S., Hong, T., Waring, A., Lehrer, R. I., and Hong, M. (2002) Solid-state NMR investigations of peptide-lipid interaction and orientation of a ss-sheet antimicrobial peptide, protegrin. *Biochemistry 41*, 9852-9862.

(32) Yamaguchi, S., Huster, D., Waring, A., Lehrer, R. I., Kearney, W., Tack, B. F., and Hong, M. (2001) Orientation and dynamics of an antimicrobial peptide in the lipid bilayer by solid-state NMR spectroscopy. *Biophys. J. 81*, 2203-2214.

(33) Hallock, K. J., Lee, D. K., and Ramamoorthy, A. (2003) MSI-78, an analogue of the magainin antimicrobial peptides, disrupts lipid bilayer structure via positive curvature strain. *Biophys. J. 84*, 3052-3060.

(34) Santos, J. S., Lee, D. K., and Ramamoorthy, A. (2004) Effects of antidepressants on the conformation of phospholipid headgroups studied by solid-state NMR. *Magn. Reson. in Chem. 42*, 105-114.

(35) Ladokhin, A. S., and White, S. H. (2001) 'Detergent-like' permeabilization of anionic lipid vesicles by melittin. *Biochim. Biophys. Acta-Biomembranes 1514*, 253-260.

(36) Rex, S., and Schwarz, G. (1998) Quantitative studies on the melittin-induced leakage mechanism of lipid vesicles. *Biochemistry 37*, 2336-2345.

Chapter 6

Phospholamban backbone dynamics and conformation study

^{15}N Solid-state NMR results on uniform ^{15}N-labeled PLB obtained in this chapter were included in the following two papers:

Abu-Baker, S., Lu, J.X., Chu, S.D. and Lorigan, G. A. "The side-chain and backbone dynamics of phospholamban in POPC bilayers utilizing ^{2}H and ^{15}N solid-state NMR spectroscopy" *Biochemistry* (in progress)

Abu-Baker, S., Lu, J.X., Chu, S.D. and Lorigan, G. A. "The structural topology of wild-type phospholamban in oriented bilayers using ^{15}N solid-state NMR spectroscopy" *Protein Science* (in progress)

6.1 Introduction

Phospholamban (PLB) is a 52 residue integral membrane protein found in the cardiac sarcoplasmic reticulum (SR) membrane that regulates the activity of calcium-ATPase (*1*). Unphosphorylated PLB inhibits the sarco(endo)plasmic reticulum calcium-ATPase (SERCA) and decreases the calcium flow into SR vesicles (*2, 3*). Phosphorylation of PLB at Ser16 by cAMP-dependent protein kinase (PKA) and/or Thr17 by CAM-kinase will increase the rate of calcium uptake into the SR leading to relaxation of the cardiac muscle (*4*). Thus, PLB plays a pivotal role in the regulation of the heartbeat. Clinical evidence indicates that naturally occurring mutations in the human PLB gene led to dilated cardiomyopathy (DCM) and heart failure (*5, 6*). Therefore, PLB has attracted extensive investigations into its function and structure (*7-9*).

Research studies have indicated that PLB exists in a dynamic equilibrium between a pentamer form and a monomer form (*10, 11*). It was first suggested that SERCA binds PLB by stripping a subunit away from the pentamer, causing the deoligomerization of PLB. The monomer PLB is the inhibitory active form (*12*). In addition, ion conductance studies also suggested pentameric PLB could act as an ion channel (*2, 13*). In the early structure models, PLB has been described as a continuous α-helix or two α-helices connected by an unstructured/β-sheet region (*14, 15*).

Extensive mutational analysis of residues within the transmembrane domain of PLB revealed that substitution of C36, C41 and C46 with either Ala or Ser stabilize the monomeric form of PLB (*16*). In order to facilitate PLB structural studies, the functional PLB mutant AFA-PLB with C36A, C41F and C46A was created; it shows only a single band on a SDS-PAGE gel (*17*). Solution NMR studies on AFA-PLB in micelles revealed that monomeric PLB is composed of three segments: cytoplasmic domain IA (residues 2-16) and cytoplasmic domain IB (residues 17-21), transmembrane domain II (residues 22-52) with helical structures for both the cytoplasmic domain IA and transmembrane domain II forming an "L" shape conformation (Figure 6.1A) (*18, 19*).

Conversely, using solid-state magic-angle sample spinning in combination with through-space and through-bond magnetization transfer techniques, the cytoplasmic domain structure of AFA-PLB incorporated into lipid bilayers was determined as a disordered random-coil (Figure 6.1B) (*20*).

Additionally, Chou's group carried out a structural study on the original pentameric form of PLB in dodecylphosphocholine micelles using solution NMR methods. They revealed that the PLB structure exists as a bellflower-like assembly held together by leucine/isoleucine zipper in the transmembrane region (Figure 6.1C). The cytoplasmic domain has a helical structure with the helix axis almost parallel to the bilayer normal (*21*).

These structural results described above are consistent in describing the PLB transmembrane domain as a helix spanning the entire membrane bilayer. However, they are inconsistent in the structure of the cytoplasmic domain. The debate on the three structural models justifies further structural and dynamic studies on PLB.

In this chapter, ^{15}N solid-state NMR spectroscopy was utilized to probe wild-type PLB backbone dynamics and orientation in its pentameric form. The study was carried out in a lipid bilayer environment, which is closer to the natural membrane environment when compared to micelles. Uniform ^{15}N labeled PLB was expressed by bacterial fermentation.

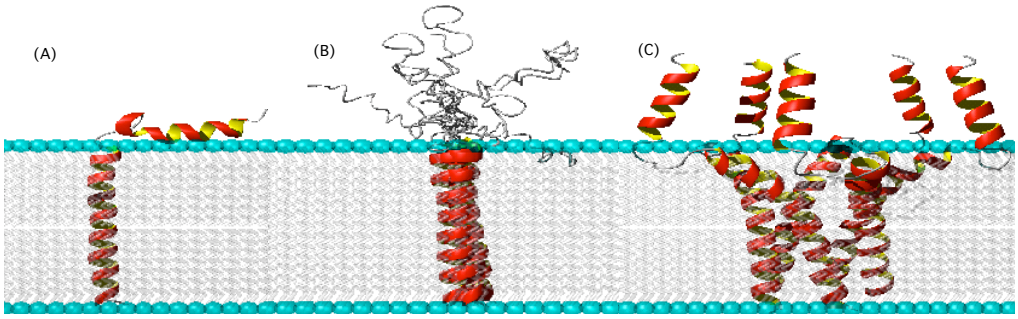

Figure 6.1 Examples of PLB structures solved using NMR spectroscopy. (A) AFA-PLB structure using solution NMR (PDB code 1N7L); (B) AFA-PLB structure using solid-state NMR; (C) pentameric wild-type PLB using solution NMR (PDB code 1ZLL). The figures were generated using MOLMOL software.

The purified PLB was first reconstructed into POPC multilamellar vesicles. PLB backbone dynamic information was obtained by analyzing ^{15}N NMR powder lineshapes.

^{15}N NMR solid-state powder lineshapes provide useful information on protein backbone dynamics, for example axially symmetry lineshape indicating restricted PLB backbone motion while isotropic lineshape indicating motional averaging. Uniform ^{15}N-labeled PLB was also incorporated into the oriented POPC bilayers and DOPC/DOPE bilayers. ^{15}N solid-state NMR spectroscopy in combination with sample alignment provides direct information regarding protein topology and orientation.

6.2 Material and methods

6.2.1 Material

1-Palmitoyl-2-oleoyl-3-*sn*-glycero-3-phospholcholine (POPC), 1, 2-Dioleoyl-*sn*-glycero-3-phospholcholine (DOPC), 1, 2-Dioleoyl-*sn*-glycero-3-phosphoethanolamine (DOPE) were purchased from Avanti Polar Lipids (Alabaster, AL) and used without further purification. The phospholipids were dissolved in chloroform and stored at -20°C prior to use. $^{15}NH_4Cl$ and deuterium-depleted water was obtained from Isotec (Miamisburg, OH). Chloroform, hexafluoro-2-propanol formic acid, HEPES, triflouroethanol (TFE) and EDTA were obtained from Sigma/Aldrich (St. Louis, MO). Microscope cover glasses (5.7 ×12 mm) were purchased from Marienfeld Laboratory Glassware (Germany).

6.2.2 Protein expression

The insertion of a constructed wild-type rabbit PLB gene into a modified pMal-c2X vector (New England Biolabs) was done at Dr. Veglia's lab in Minnesota (*22*). The Tobacco Etch Virus (TEV) recognition sequence was introduced to replace the Xa factor cleavage site. A $(His)_6$ sequence was also constructed immediately before the TEV cleavage site to allow purification by Ni-affinity chromatograpy (Figure 6.2). The gene

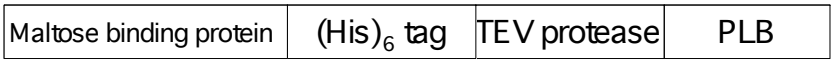

Figure 6.2 The outline of PLB fusion protein construction.

was first transformed into DH10B competent cells (Invitrogen). Plasmid DNA was isolated using a Wizard Plus miniprep kit (Promega). The plasmid DNA encoding wild-

type rabbit PLB was then transformed into *E. coli* BL21(DE3)-RIL cells (stratagene). A 3mL Luria Broth (LB) culture, supplemented with 100μg/mL ampicillin was inoculated with a single colony from a LB/amplicillin plate and incubated for 6 hr at 37 °C. A starter culture was inoculated with the LB culture and grown overnight at 37 °C in a standard M9 minimal media supplemented with vitamins (Sigma BME vitamin solution) and minerals (Minerals: 6 mg/L $FeSO_4$, 1.3 mg/L $MnSO_4$, 0.8 mg/L $CoCl_2$, 0.6 mg/L $ZnCl_2$, 0.3 mg/L $CuSO_4$, 0.02 mg/L H_3BO_3, 0.25 mg/L $(NH_4)_6$ Mo_7O_{24}, and 5 mg/L EDTA). Cells were then transferred (1:50) into fresh M9 minimal media with $^{15}NH_4Cl$ as the sole nitrogen source. Cells were induced with 1 mM isopropyl-β-D-thiogalactopyranoside (IPTG) at OD_{600} ~0.7. After 30°C overnight growth or 37°C for 6 hr, cells were harvested and stored at –20 °C. For the expression of protein without isotopic labels, the LB media was used and the culture was induced for 5 hr at 37 °C before harvesting.

6.2.3 Purification of the maltose-binding fusion protein (MBP-PLB) and PLB

Cells were resuspended using 150mL lysis buffer (20 mM TrisHCl, pH 8.0, 200 mM NaCl, 1 mM EDTA, 0.1 mM DTT, 0.5% glycerol, 2.5 μM lysozyme, 0.5 mM PMSF) for every liter of culture. The suspension was passed twice through a French Press and centrifuged at 18,000 rpm for 20 min at 4°C. The supernant with the MBP-PLB fusion protein was purified using an amylose resin (New England Biolabs). The fusion protein solution was dialyzed against TEV protease buffer and PLB was released from MBP by cleavage using active TEV protease (Ac-TEV) (Invitrogen). Approximately, one milligram of fusion protein requires 1.5 μl Ac-TEV. The subsequent mixture was first purified using Ni-affinity chromatography. However, the flow-through of Ni-affinity chromatography contains both PLB and small amounts of MBP-PLB fusion protein. The step was therefore omitted from the routine purification. The mixture after cleavage was directly purified by HPLC (Amersham Pharmacia Biotech) using a silica based C4 reverse-phase column (Vydac). PLB was eluted as a single peak at 95% solvent B (58% isopropanol, 37% acetonitrile, 5% H_2O and 0.1% TFA). Solvent A contained H_2O with 0.1% TFA. The purified PLB was confirmed by 12% SDS-PAGE and MALDI-TOF mass spectrometry.

6.2.4 Secondary structure study

Circular dichroism (CD) spectra were recorded at room temperature using a Jasco J-810 CD spectropolarimeter. The purified PLB was dissolved in an aqueous solution containing 10% TFE or 50% TFE. The final PLB concentration was 50 μM. The sample was analyzed in 0.1 cm path-length cell. Each spectrum was obtained by averaging 4 successive scans over the 180 nm-250 nm wavelength range and the blank solvent backgrounds were subtracted.

6.2.5 NMR sample preparation

Multilamellar vesicle (MLV) samples with 4 mol% peptide were prepared by mixing PLB in a minimal amount of TFE solvent with POPC (76 mg) in chloroform. The mixture was first dried under a steady stream of N_2 gas for ~ 30 minutes to remove the organic solvent. The sample was then left under a high vacuum desiccator overnight. MLVs were formed by resuspension of the dry lipids in 190 μL HEPES buffer (5mM EDTA, 20mM NaCl, and 30mM HEPES, pH 7.0) with frequent vortexing to homogenize the sample. Samples were allowed to sit in a warm water bath (50 °C) for 20 minutes before finally packed into a NMR rotor (*23*).

Mechanically aligned membranes were prepared using a procedure described previously (*24*). PLB was dissolved in a small amount TFE (≈50 μl) and mixed with POPC lipids in chloroform. The solution was spread onto 36 glass plates (~50 mg lipids) and allowed to air-dry. The glass plates were then placed in a desiccator under vacuum overnight to remove any residual solvents. The dried sample was directly hydrated using deuterium-depleted water (2 μl/plate), stacked and placed in a humidity chamber consisting of saturated ammonium monophosphate at a relative humidity of about 93% at 45°C for one day. The glass plates were sealed in a rectangular cell to prevent sample dehydration during data acquisition. The peptide accounts for around 0.5 mol% with respect to the lipids.

6.2.6 NMR spectroscopy

All experiments were recorded on a Bruker Avance 500 MHz WB solid-state NMR spectrometer. Unoriented membrane samples were studied using a 4mm triple

resonance CPMAS probe (Bruker) at both 25 °C and -25°C. A static double-resonance low-E probe (National High Magnetic Field Laboratory) was used for oriented-membrane experiments. ^{15}N NMR spectra were acquired using a standard CP pulse with TPPM proton decoupling. The spectra were referenced to an external standard of $(^{15}NH_4)_2SO_4$ at 27 ppm. ^{1}H 90° pulse was 4.7 μsec for the CPMAS probe and 5.0 μsec for the flat coil probe. The contact time was 1.5 ms and the recycle delay was 4 s. Powder-type ^{15}N NMR spectra at 25 °C were deconvoluted using two components with the DMFIT program (*25*). ^{31}P NMR spectra on oriented membrane samples were also recorded to verify the membrane alignment.

6. 3 Results and Discussion

Uniform ^{15}N-labeled PLB was purified with a best yield of 10 mg per liter of culture. A 12% SDS-PAGE gel showing the results in each purification step is in Figure 6.3. PLB fusion protein gives a band around 48 kDa. In Figure 6.3B the purified PLB gave two bands, a major band around 26 kDa and a minor band around 6 kDa, indicating that the PLB is mainly in the pentamer form under the experimental conditions. The PLB pentamer with a theoretical molecular weight around 30 kDa migrates faster than the corresponding molecular marker in the gel, which is consistent with the literature (*21*). The hydrophobic membrane protein usually migrates faster than the soluble protein in a SDS-PAGE gel because of the protein's conformation and hydrophobicity. Purified PLB in this work has 53 residues with one extra glycine at the N terminus from the TEV cleavage site. The theoretical molecular weight of each PLB subunit is 6154 Da. The corresponding MALDI-TOF result is shown in Figure 6.4A. Figure 6.4B shows the PLB molecular weight after uniform ^{15}N labeling. The peak at around 3000 Da may be from a double-charged molecular ion. CD spectrum of PLB in TFE/H_2O solution indicates that PLB is mainly in α-helix conformation (Figure 6.5).

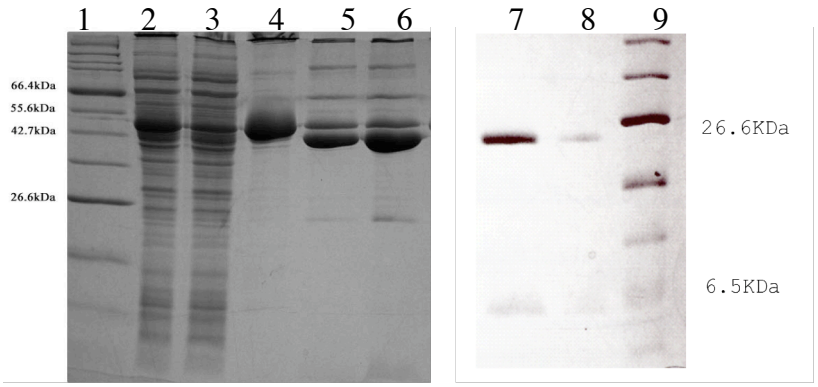

Figure 6.3 SDS-PAGE results of PLB purification in each step. (A) lane 1 is the molecular marker, lane 2 cell lysis supernant, lane 3 the flow-through from amylose column, lane 4 the elution from amylose column, lane 5 Ac-TEV cleavage for 3 hr at 1μl Ac-TEV per mg fusion protein, lane 6 addition of another 0.5μl Ac-TEV per mg fusion protein in lane 5 after overnight reaction. (B) lane 7 purified PLB using reverse phase C4 column, lane 8 1/10 dilution of lane 7, lane 9 is the molecular marker.

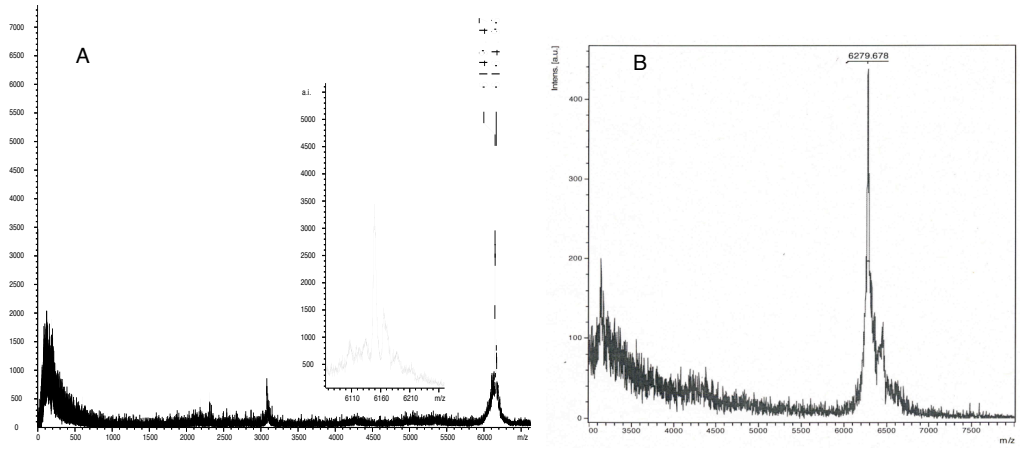

Figure 6.4 MALDI-TOF results of purified PLB (A) and ^{15}N-labeled PLB (B)

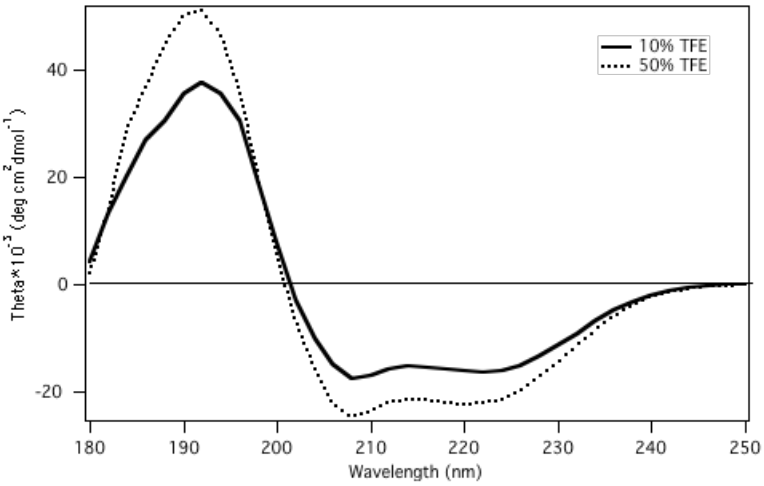

Figure 6.5 CD spectrum of purified PLB dissolved in 10% TFE or 50% TFE.

6.3.1 PLB backbone dynamics

PLB backbone dynamics were studied using ^{15}N solid-state NMR spectroscopy on a MLV sample. A ^{15}N NMR spectrum of uniform ^{15}N-labeled PLB at 25˚C is shown in Figure 6.6(A) while Figure 6.7(A) is at -25˚C. Figure 6.6(A) shows the overlap of two distinct lineshapes. The spectrum was deconvoluted using the DMFIT program, indicating a major anisotropic CSA component and a minor isotropic component. However at -25˚C, a single anisotropic CSA component was observed (Figure 6.7(A)). ^{15}N solid-state NMR spectroscopy is sensitive to molecular motion on the 10^{-4} timescale (*26*). ^{15}N anisotropic CSA lineshapes indicate restricted protein backbone motions. Conversely, a fast molecular motion will cause a significant narrowing of the CSA lineshape to an isotropic resonance. The ^{15}N NMR spectrum of uniform ^{15}N-labeled PLB indicates that at 25˚C PLB exists in two distinct dynamic populations with one rigid and the other mobile. Upon decreasing the sample temperature to -25˚C, PLB backbone motion is totally frozen and only a CSA lineshape, indicating rigid backbone motion, was observed (Figure 6.7(A)). The ^{15}N CSA tensor values of uniform ^{15}N-labeled PLB inserted into POPC bilayers at 25˚C are σ_{11} = 59.9 ppm, σ_{22} = 76.1 ppm, σ_{33} = 230.0 ppm. These values were obtained using the DMFIT fitting program.

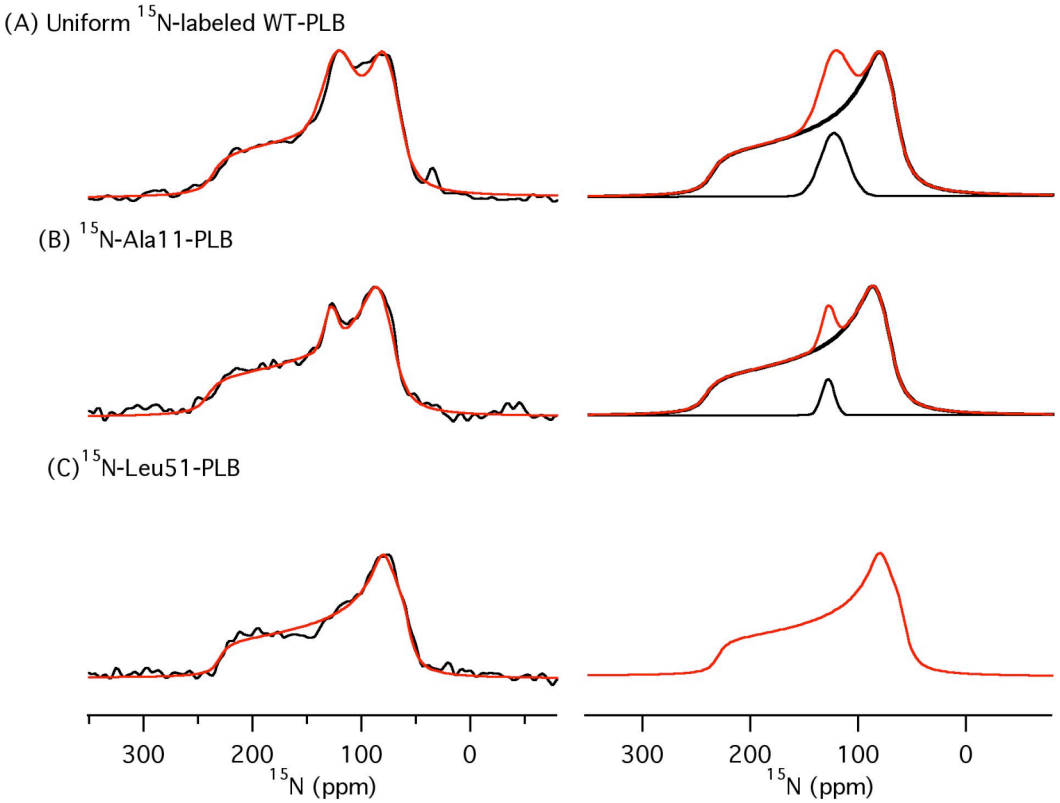

Figure 6.6 Solid-state ^{15}N NMR spectra of PLB incorporated into POPC MLVs at 25 °C. (A) Uniform ^{15}N-labeled PLB sample. (B) and (C) site-specific ^{15}N-labeled PLB at Ala11 and Leu51 respectively. Left column: black line represents the spectra obtained from experiment; red line represents the fitting using DMFIT program. Right column: black line represents the two components used in the DMFIT; red line represents the final fitting lineshape.

^{15}N NMR spectra of site-specific ^{15}N-labeled PLB at Ala11 and Leu51 were also obtained at both 25°C and -25°C in order to study PLB backbone dynamics at specific domains (site-specific ^{15}N-labeled PLB was obtained by Shadi Abu-baker.). Ala11 is located in the cytoplasmic domain of PLB. The ^{15}N NMR spectrum of Ala11-PLB shows two components at 25°C (Figure 6.6(B)) while only one component at -25°C (Figure 6.7(B)), consistent with the results obtained from uniform ^{15}N-labeled PLB. This result suggests two dynamic populations of the PLB cytoplasmic domain at room

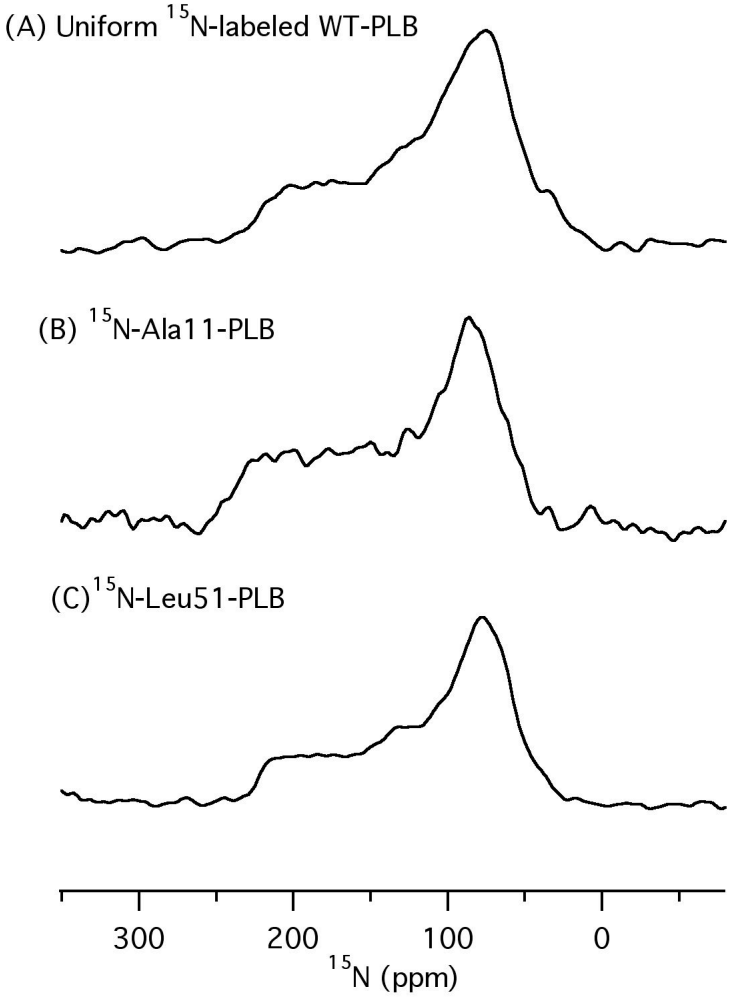

Figure 6.7 Solid-state ^{15}N NMR spectra of PLB incorporated into POPC MLVs at -25 °C. (A) Uniform ^{15}N-labeled PLB sample. (B) and (C) site-specific labeled PLB at Ala11 and Leu51 respectively.

temperature. Conversely, only one CSA component was observed in the ^{15}N NMR spectrum of Leu51-PLB at both 25°C (Figure 6.6(C)) and -25°C (Figure 6.7(C)). Leu51 is located in the transmembrane domain of PLB. This result suggests that the transmembrane domain of PLB always exists in a rigid form at both temperatures. Comparing the spectra obtained from uniform ^{15}N-labeled and site-specifically labeled PLB, it is concluded that PLB has two dynamic populations upon incorporation into POPC MLVs at room temperature, and that the difference between these two populations

is mainly in the cytoplasmic domain. The major population of PLB probably has rigid helical structures in both domains while the minor population has a higher dynamic motion in cytoplasmic domain. This result does not agree with the solid-state NMR structure study on AFA-PLB, which suggested that the cytoplasmic domain is dynamic and in a random coil structure (*20*).

EPR is more sensitive to fast molecular motions in the nanosecond range when compared to NMR. Interestingly, EPR studies probing the peptide backbone dynamics on AFA-PLB suggested that the cytoplasmic domain of PLB exhibits two resolved conformations, an ordered state and a dynamically disordered and extended state (*27*). This result is consistent with our research in that PLB has two conformations in the membrane environment with different dynamics (*28, 29*).

6.3.2 PLB backbone orientation

PLB was also incorporated into oriented POPC bilayers and DOPC/DOPE (4/1) bilayers using glass plates. The anisotropic characteristics of a solid-state ^{15}N NMR spectrum make it possible to obtain topology information on the helical tilt of PLB in an oriented sample (*30*), so that the debate on the orientation of the PLB cytoplasmic domain can be solved. ^{31}P NMR spectra of the oriented bilayer samples are shown in Figures 6.8(C) and 6.8(D). ^{31}P NMR spectra give a sharp resonance around 25 ppm indicating that the membranes were well aligned and the bilayer normal was parallel with the magnetic field. ^{15}N NMR spectra of uniform ^{15}N-labeled PLB at 25˚C are displayed in Figures 6.8(A) and 6.8(B). The spectrum shows two major resonances around 210 ppm and 74 ppm and a small isotropic peak at 115 ppm. DOPC/DOPE bilayer sample gives ^{15}N NMR spectrum with a better resolution than POPC bilayers in this case. ^{15}N chemical shift tensor values were obtained from ^{15}N NMR spectra of PLB in MLV samples (σ_{11} = 59.9 ppm, σ_{22} = 76.1 ppm, σ_{33} = 230.0 ppm). The resonance around σ_{33} (210 ppm) indicates that the protein backbone has an orientation that is slightly tilted from the magnetic field and the bilayer normal direction, corresponding to the transmembrane domain of PLB. The resonance around σ_{11} and σ_{22} (74 ppm) indicates that the protein backbone has an orientation, which is almost perpendicular to the magnetic field and bilayer normal, corresponding to the cytoplasmic domain of PLB lying on the membrane

surface. The isotropic peak at the averaged chemical shift position (close to the average of σ_{11}, σ_{22} and σ_{33}) indicates a mobile component of PLB, which has fast dynamic motion. These results suggest two dynamic populations of PLB in the membrane bilayers consistent with the results obtained from PLB incorporated into POPC MLVs. ^{15}N NMR spectra on oriented bilayers also suggests that it is impossible for the cytoplasmic domain to orient parallel to the bilayer normal, which is given in the bellflower structure (*21*). No resonance around 74 ppm was observed, which would be expected for the bellflower structure of pentameric PLB (Figure 6.1(C)).

In conclusion, our research confirmed that PLB in a lipid bilayer environment has at least two conformational populations with different dynamic motions. The cytoplasmic domain could be rigid, interacting with the bilayer surface; or dynamic, with unspecific orientation. PLB inhibits SERCA by forming a stable complex with SERCA. A dynamic

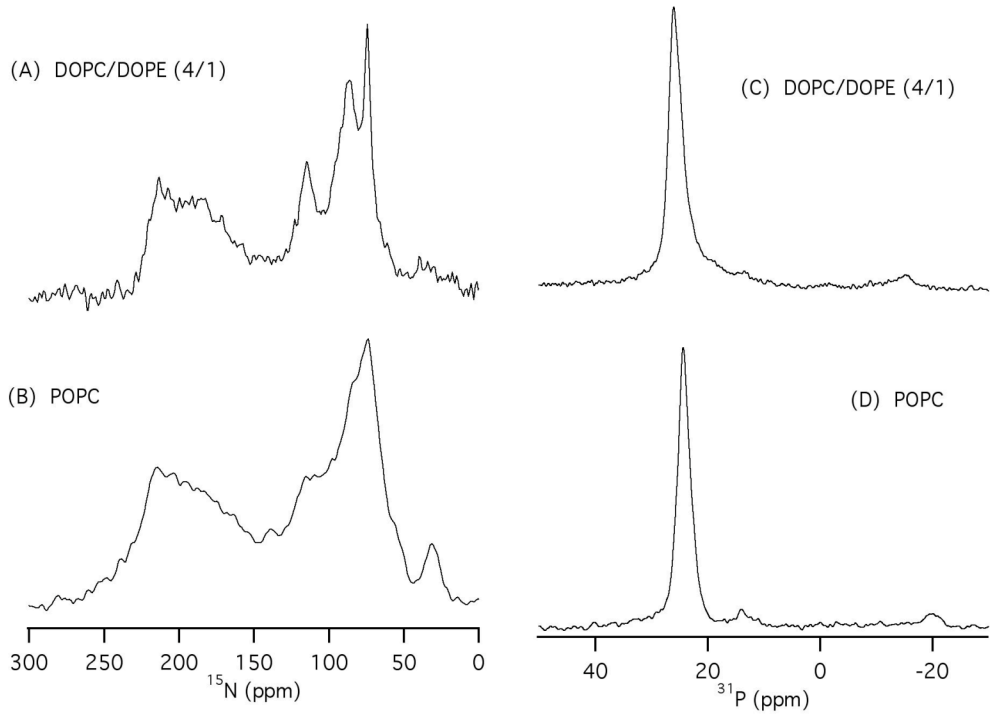

Figure 6.8 ^{15}N and ^{31}P NMR spectra of uniform ^{15}N-labeled PLB incorporated into oriented DOPC/DOPE bilayers (A), (C) and POPC bialyers (B), (D).

cytoplasmic domain of PLB will probably facilitate the initial recognition and binding of SERCA. The rigid cytoplasmic domain is close to the perpendicular orientation with respect to the bilayer normal and probably lies on the membrane surface. It agrees with previous research carried out in our group (*29*) and Middleton's group (*31*) suggesting a direct interaction between PLB and lipid headgroups (*29, 31*). Although PLB is predominantly in the pentameric form in this case, small amounts of monomer may still exist in the bilayers. We can probably relate the two oligomeric states of PLB to the two dynamic states since the pentameric form of PLB is the major component in the sample and at the same time the rigid conformation of PLB is the dominant form indicated by NMR studies. It is reasonable to propose that the dynamic component of PLB is actually in the monomer form, considering the monomer form of PLB binds SERCA. This would explain the dynamic characteristic of AFA-PLB (the monomer form) obtained by solid-state NMR (*20*). However, it is still hard to justify the inconsistency in PLB structures ("L" shape and bellflower model) obtained by solution NMR using the micelle samples (*18, 19, 21, 32*). PLB conformation could be altered in different lipids and hydration environments. It is also very important to optimize the sample preparations. The previous structural studies of PLB possibly may have only detected one of the many conformations. Therefore, a thorough structural study of PLB at different conditions and in the presence or absence of SERCA is really needed in the near future.

6.4 References

(1) Stokes, D. L. (1997) Keeping calcium in its place: Ca^{2+}-ATPase and phospholamban. *Curr. Opn. Struct. Biol. 7*, 550-558.

(2) Arkin, I. T., Adams, P. D., Brunger, A. T., Smith, S. O., and Engelman, D. M. (1997) Structural perspectives of phospholamban, a helical transmembrane pentamer. *Annu. Rev. Biophys. Biomolec. Struct. 26*, 157-179.

(3) Simmerman, H. K. B., and Jones, L. R. (1998) Phospholamban: protein structure, mechanism of action, and role in cardiac function. *Physiol. Rev 78*, 921-947.

(4) Simmerman, H. K., J.H. Collins, J.L. Theibert, A.D. Wegener, and L.R. Jones. (1986) Sequence analysis of phospholamban: identification of phosphorylation sites and two major structural domains. *J. Biol. Chem. 261*, 13333-13341.

(5) Haghighi, K., Kolokathis, F., Fan, G. C., Sato, Y., Kremastinos, D. T., and Kranias, E. G. (2004) Phospholamban mutations in human dilated cardiomyopathy. *Circulation 110*, 363-364.

(6) Haghighi, K., Kolokathis, F., Gramolini, A. O., Waggoner, J. R., Pater, L., Lynch, R. A., Fan, G. C., Tsiapras, D., Parekh, R. R., Dorn, G. W., MacLennan, D. H., Kremastinos, D. T., and Kranias, E. G. (2006) A mutation in the human phospholamban gene, deleting arginine 14, results in lethal, hereditary cardiomyopathy. *Proc. Natl. Acad. Sci. U. S. A. 103*, 1388-1393.

(7) Ying, W., Irvine, S. E., Beekman, R. A., Siminovitch, D. J., and Smith, S. O. (2000) Deuterium NMR reveals helix packing interactions in phospholamban. *J. Am. Chem. Soc. 122*, 11125-11128.

(8) Pollesello, P., and Annila, A. (2002) Structure of the 1-36 N-terminal fragment of Human phospholamban phophorylated at Ser-16 and Thr-17. *Biophys. J. 83*, 484-490.

(9) Tiburu, E. K., Dave, P. C., Vanlerberghe, J. F., Cardon, T. B., Minto, R. E., and Lorigan, G. A. (2003) An improved synthetic and purification procedure for the hydrophobic segment of the transmembrane peptide phospholamban. *Anal. Biochem. 318*, 146-151.

(10) Cornea, R. L., Jones, L. R., Autry, J. M., and Thomas, D. D. (1997) Mutation and phosphorylation change the oligomeric structure of phospholamban in lipid bilayers. *Biochemistry 36*, 2960-2967.

(11) Hughes, E., Clayton, J. C., and Middleton, D. A. (2005) Probing the oligomeric state of phospholamban variants in phospholipid bilayers from solid-state NMR measurements of rotational diffusion rates. *Biochemistry 44*, 4055-4066.

(12) Kimura, Y., Kurzydlowski, K., Tada, M., and MacLennan, D. H. (1997) Phospholamban inhibitory function is activated by depolymerization. *J. Biol. Chem. 272*, 15061-15064.

(13) Kovacs, R. J., Nelson, M. T., Simmerman, H. B. K., and Jones, L. R. (1988) Phospholamban forms calcium selective channels in lipid bilayers. *J. Biol. Chem. 263*, 18364-18368.

(14) Arkin, I. T., Rothman, M., Ludlam, C. F. C., Aimoto, S., Engelman, D. M., Rothschild, K. J., and Smith, S. O. (1995) Structural model of the phospholamban ion-channel complex in phospholipid-membranes. *J. Mol. Biol. 248*, 824-834.

(15) Tatulian, S. A., Jones, L. R., Reddy, L. G., Stokes, D. L., and Tamm, L. K. (1995) Secondary structure and orientation of phospholamban reconstituted in supported bilayers from polarized attenuated total-reflection FTIR spectroscopy. *Biochemistry 34*, 4448-4456.

(16) Mayer, E. J., E. McKenna, V.M. Garsky, C.J. Burke, H. Mach, C.R. Middaugh, M. Sardana, J.S. Smith, and R.G. Johnson Jr. (1996) Biochemical and biophysical comparison of native and chemically synthesized phospholamban and a monomeric phospholamban. *J. Biol. Chem. 271*, 1669-1677.

(17) Karim, C. B., Stamm, J. D., Karim, J., Jones, L. R., and Thomas, D. D. (1998) Cysteine reactivity and oligomeric structures of phospholamban and its mutants. *Biochemistry 37*, 12074-12081.

(18) Zamoon, J., Mascioni, A., Thomas, D. D., and Veglia, G. (2003) NMR solution structure and topological orientation of monomeric phospholamban in dodecylphosphocholine micelles. *Biophys. J. 85*, 2589-2598.

(19) Zamoon, J., Nitu, F., Karim, C., Thomas, D. D., and Veglia, G. (2005) Mapping the interaction surface of a membrane protein: Unveiling the conformational switch of phospholamban in calcium pump regulation. *Proc. Natl. Acad. Sci USA 102*, 4747-4752.

(20) Andronesi, O. C., Becker, S., Seidel, K., Heise, H., Young, H. S., and Baldus, M. (2005) Detemination of membrane protein structure and dynamics by magic-angle-spininng solid-state NMR spectroscopy. *J. Am. Chem. Soc. 127*, 12965-12974.

(21) Oxenoid, K., and Chou, J. J. (2005) The structure of phospholamban pentamer reveals a channel-like architecture in membrane. *Proc. Natl. Acad. Sci. USA 102*, 10870-10875.

(22) Buck, B., Zamoon, J., Kirby, T. L., DeSilva, T. M., Karim, C., Thomas, D., and Veglia, G. (2003) Overexpression, purification, and characterization of

recombinant Ca-ATPase regulators for high-resolution solution and solid-state NMR studies. *Protein Expr. Purif. 30*, 253-261.

(23) Dave, P. C., Tiburu, E. K., Damodaran, K., and Lorigan, G. A. (2004) Investigating structural changes in the lipid bilayer upon insertion of the transmembrane domain of the membrane-bound protein phospholamban utilizing ^{31}P and ^{2}H solid-state NMR spectroscopy. *Biophys. J. 86*, 1564-1573.

(24) Tiburu, E. K., Karp, E. S., Dave, P. C., Damodaran, K., and Lorigan, G. A. (2004) Investigating the dynamic properties of the transmembrane segment of phospholamban incorporated into phospholipid bilayers utilizing ^{2}H and ^{15}N solid-state NMR pectroscopy. *Biochemistry 43*, 13899-13909.

(25) McCabe, M. A., and Wassall, S. R. (1997) Rapid deconvolution of NMR powder spectra by weighted fast fourier transformation. *Solid State Nucl. Magn. Reson. 10*, 53-61.

(26) Colnago, L. A., Valentine, K. G., and Opella, S. J. (1987) Dynamics of fd coat protein in bacteriophage. *Biochemistry 26*, 847-854.

(27) Karim, C. B., Zhang, Z., Howard, E. C., Torgersen, K. D., and Thomas, D. D. (2006) Phosphorylation-dependent conformational switch in spin-labeled phospholamban bound to SERCA. *J. Mol. Biol 358*, 1032-1040.

(28) Abu-Baker, S., Lu, J. X., and Chu, S. D. (2007) The side-chain and backbone dynamics of phospholamban in POPC bilayers utilizing ^{2}H and ^{15}N solid-state NMR spectroscopy. *Biochemistry in progress.*

(29) Abu-Baker, S., and Lorigan, G. A. (2006) Phospholamban and its phosphorylated form interact differently with lipid bilayers: A ^{31}P, ^{2}H, and ^{13}C solid-state NMR spectroscopic study. *Biochemistry 45*, 13312-13322.

(30) Lambotte, S., Jasperse, P., and Bechinger, B. (1998) Orientational distribution of alpha-helices in the colicin B and E1 channel domains: A one and two dimensional N-15 solid- state NMR investigation in uniaxially aligned phospholipid bilayers. *Biochemistry 37*, 16-22.

(31) Clayton, J. C., Hughes, E., and Middleton, D. A. (2005) The cytoplasmic domains of phospholamban and phospholemman associate with phospholipid membrane surfaces. *Biochemsitry 44*, 17016-17026.

(32) Traaseth, N. J., Buffy, J. J., Zamoon, J., and Veglia, G. (2006) Structural dynamics and topology of phospholamban in oriented lipid bilayers using multidimensional solid-state NMR spectroscopy. *Biochemistry 45*, 13827-13834.

Chapter 7

Conclusion and future experiments

7.1 Bicelles and SAMMY technique

Bicelles have been extensively used as model membranes to align membrane proteins and facilitate membrane protein structure studies (*1-3*). However, several limitations in the application of bicelles have to be mentioned. First, the alignment temperature of bicelles is always altered when macromolecules are incorporated into the bicelles (*4*). Second, the stability and viscosity of bicelles are very sensitive to membrane additives (*5*). High concentration of additives can make the lipid mixture very viscous and in some cases bicelles wouldn't be formed or aligned (*6*). These two facts require that the amount of peptide has to be optimized while using bicelles. Also, the lipid composition and ratio in a bicelle have to be optimized to accommodate membrane proteins with different sizes (*7*). Therefore, it becomes very important to understand the effect of different membrane additives to the bicelle membranes.

In solid-state NMR, ^{31}P and ^{2}H spins are commonly used to study the bicelle alignment and lipid dynamics (*8, 9*). In this dissertation, SAMMY was applied to magnetically aligned bicelles, where both ^{1}H-^{13}C dipolar couplings and ^{13}C chemical shift values for every resolvable ^{13}C resonance of DMPC were obtained. This technique provides us an alternate way to gain information on bicelle lipid dynamic changes in local areas when bicelles interact with various membrane additives. The interaction mechanism between bicelles and membrane-associated macromolecules can also be used as a guideline to better understand the interaction between the real cell membranes and membrane additives. Based upon our research, a similar experiment has been applied to study the bicelle membrane interaction with an antidepressant molecule, desipramine (*10*). The SAMMY pulse sequence is a separated local field spectroscopy technique (*11*). Several papers have also been published developing new separated local field pulse sequences to enhance the sensitivity and resolution of this technique (*12, 13*). We expect that this approach will be applied more in the future to study the interaction between membrane-associated molecules and aligned membranes.

7.2 Membranes and membrane-associated macromolecules

7.2.1 The effect of cholesterol on bicelle membranes

Cholesterol concentration in the cell membrane varies from species to species and changes with different stages and locations of the cell (*14, 15*). Cholesterol can regulate cell membrane function (*14*). Therefore, it has been an essential component in mammalian membrane mimics (*16, 17*). Membrane proteins can assume different conformations and affect the lipids motion differently when reconstituted into model membranes with or without cholesterol (*17, 18*). For example, the bee toxin melittin has been reported to have the largest effect on DMPC mobility in DMPC/DHPC bicelles while less effect in cholesterol-doped bicelles (*18*). In this dissertation, the cholesterol effect on membrane dynamics was extensively studied. Cholesterol changes the membrane fluidity and increases the lipid acyl chain ordering above the gel-to-liquid crystalline phase transition temperature. Our results provided fundamental information on the effect of cholesterol to the bicelles and facilitated future research on membrane proteins.

7.2.2 The interaction between KIGAKI and different membrane bilayers

In the past decade, solid-state NMR has attracted people's attention as a powerful technique to study antimicrobial peptides (*10, 19*). In this dissertation, the interaction mechanisms of the antimicrobial peptide KIGAKI with different model membranes were studied using solid-state NMR techniques. Solid-state NMR proved to be a useful technique to discern the membrane lipid dynamic changes when KIGAKI was incorporated into the membranes. NMR relaxation techniques and NMR lineshape perturbation studies provided complementary lipid dynamic information. The results obtained from both techniques confirmed a carpet mechanism when KIGAKI interacts with bacterial membrane mimics. However, no detailed structure information of KIGAKI has been obtained till now. It will be ideal to carry out further experiments on the structure and conformation of KIGAKI in the same membrane mimics used in this dissertation. The REDOR (Rotational echo double resonance) technique combined with site-specific ^{15}N, ^{13}C-labeled peptides can be used to distinguish between an α-helix or a β-sheet structure (*20, 21*). The structural constraints of Alzheimer's β-amyloid fibril have been obtained using 2D solid-state NMR ^{13}C-^{13}C or ^{13}C-^{15}N correlation spectroscopy (*22, 23*). Similar techniques can also be applied to the antimicrobial peptide KIGAKI.

7.2.3 The structure of PLB

Structural studies on the membrane peptide phospholamban (PLB) in our lab started with a short version of PLB that only contains the transmembrane segment (*24, 25*). Recently, the full-length form of PLB was obtained and studied (*26*). The interaction of PLB with membrane bilayers was first carried out using ^{31}P and ^{2}H NMR spectroscopy (*26*). However, structural studies of the full-length PLB in our lab have to be extended. In this dissertation, ^{15}N solid-state NMR studies were carried out when PLB was reconstituted into membrane bilayers. PLB backbone dynamic information was obtained from unoriented lipid bilayer membrane samples. The backbone orientation of PLB was obtained from aligned bilayer membrane samples. We also found out that the ^{15}N NMR spectrum of PLB in aligned DOPC/DOPE bilayers had a better resolution than that obtained from aligned POPC bilayers. This result indicated the importance to optimize the bilayer membrane samples, including the choice of the lipids, the sample hydration, and the concentration of the peptide in the sample, etc. The inconsistency of the PLB structure in the literature may be caused by these factors (*27, 28*). It will be interesting to know what kind of structural changes occur with PLB upon interaction with SERCA and what is the difference in the structure between native PLB and PLB mutants that cause heart disease. All these comparisons have to be based on a correct native PLB conformation. Therefore, the native conformation of PLB has to been obtained before any further experiments. PISEMA (Polarization inversion spin-exchange at the magic angle) type NMR techniques can be used on uniform or site-specific ^{15}N-labeled PLB to gain more structure information (*29*). PISEMA experiments yield a 2D NMR spectrum with one dimension consisting of the ^{15}N chemical shift, the other dimension the ^{1}H-^{15}N dipolar coupling. If possible, a group of PLB samples should be prepared using bilayers with different types of lipids. Bicelles probably can also be used to reconstitute PLB, since they are the membrane system closer to the natural membrane (*13*). Data from these experiments will be used to compare the structures obtained from different sample preparations and to gain a thorough understanding of the PLB structure.

7.3 References

(1) Marassi, F. M. (2002) NMR of peptides and proteins in oriented membranes. *Concepts Magn. Resonance 14*, 212-224.

(2) Marassi, F. M., and Opella, S. J. (2002) Using Pisa pies to resolve ambiguities in angular constraints from PISEMA spectra of aligned proteins. *J. Biomol. NMR 23*, 239-242.

(3) Opella, S. J., and Marassi, F. M. (2004) Structure determination of membrane proteins by NMR spectroscopy. *Chem. Rev. 104*, 3587-3606.

(4) Lu, J.-X., Caporini, M. A., and Lorigan, G. A. (2004) The Effects of Cholesterol on Magnetically Aligned Phospholipid Bilayers: A Solid-State NMR and EPR Spectroscopy Study. *J. Mag. Res*, in press.

(5) Park, S. H., De Angelis, A. A., Nevzorov, A. A., Wu, C. H., and Opella, S. J. (2006) Three-dimensional structure of the transmembrane domain of Vpu from HIV-1 in aligned phospholipid bicelles. *Biophys. J. 91*, 3032-3042.

(6) Lu, J. X., Damodaran, K., and Lorigan, G. A. (2006) Probing membrane topology by high-resolution H-1-C-13 heteronuclear dipolar solid-state NMR spectroscopy. *J. Magn. Reson. 178*, 283-287.

(7) Tiburu, E. K., Moton, D. M., and Lorigan, G. A. (2001) Development of magnetically aligned phospholipid bilayers in mixtures of palmitoylstearoylphosphatidylcholine and dihexanoylphosphatidylcholine by solid-state NMR spectroscopy. *Biochim. Biophys. Acta-Biomembr. 1512*, 206-214.

(8) Vold, R. R., and Prosser, R. S. (1996) Magnetically oriented phospholipid bilayered micelles for structural studies of polypeptides. Does the ideal bicelle exist? *J. Magn. Reson. 113*, 267-271.

(9) Dave, P. C., Tiburu, E. K., Damodaran, K., and Lorigan, G. A. (2004) Investigating structural changes in the lipid bilayer upon insertion of the transmembrane domain of the membrane-bound protein phospholamban utilizing ^{31}P and ^{2}H solid-state NMR spectroscopy. *Biophys. J. 86*, 1564-1573.

(10) Dvinskikh, S. V., Durr, U. H. N., Yamamoto, K., and Ramamoorthy, A. (2007) High-resolution 2D NMR spectroscopy of bicelles to measure the membrane interaction of ligands. *J. Am. Chem. Soc. 129*, 794-802.

(11) Nevzorov, A. A., and Opella, S. J. (2003) A "Magic Sandwich" pulse sequence with reduced offset dependence for high-resolution separated local field spectroscopy. *J. Magn. Reson. 164*, 182-186.

(12) Dvinskikh, S., Durr, U., Yamamoto, K., and Ramamoorthy, A. (2006) A high-resolution solid-state NMR approach for the structural studies of bicelles. *J. Am. Chem. Soc. 128*, 6326-6327.

(13) Dvinskikh, S. V., Yamamoto, K., Durr, U. H. N., and Ramamoorthy, A. (2007) Sensitivity and resolution enhancement in solid-state NMR spectroscopy of bicelles. *J. Magn. Reson. 184*, 228-235.

(14) Alberts, B., Johnson, A., Lewis, J., Roberts, K., and P., W. (2002) *Molecular biology of the cell*, 4th ed., Garland Science, New York.

(15) Yeagle, P. L. (1985) Cholesterol and the cell membrane. *Biochim. Biophys. Acta 822*, 267-287.

(16) Mani, R., Buffy, J. J., Waring, A. J., Lehrer, R. I., and Hong, M. (2004) Solid-state NMR investigation of the selective disruption of lipid membranes by protegrin-1. *Biochemistry 43*, 13839-13848.

(17) Akech, J., Roy, S. S., and Das, S. K. (2005) Modulation of cholinephosphotransferase activity in breast cancer cell lines by Ro5-4864, a peripheral benzodiazepine receptor agonist. *Biochemical and Biophysical Research Communications 333*, 35-41.

(18) Andersson, A., Biverstahl, H., Nordin, J., Danielsson, J., Lindahl, E., and Maler, L. (2007) The membrane-induced structure of melittin is correlated with the fluidity of the lipids. *Biochim. Biophys. Acta-Biomembranes 1768*, 115-121.

(19) Ramamoorthy, A., Thennarasu, S., Lee, D. K., Tan, A. M., and Maloy, L. (2006) Solid-state NMR investigation of the membrane-disrupting mechanism of antimicrobial peptides MSI-78 and MSI-594 derived from magainin 2 and melittin. *Biophys. J. 91*, 206-216.

(20) Chan, J. C. C., Oyler, N. A., Yau, W. M., and Tycko, R. (2005) Parallel beta-sheets and polar zippers in amyloid fibrils formed by residues 10-39 of the yeast prion protein Ure2p. *Biochemistry 44*, 10669-10680.

(21) Gordon, D. J., Balbach, J. J., Tycko, R., and Meredith, S. C. (2004) Increasing the amphiphilicity of an amyloidogenic peptide changes the beta-sheet structure in the fibrils from antiparallel to parallel. *Biophys. J. 86*, 428-434.

(22) Paravastu, A. K., Petkova, A. T., and Tycko, R. (2006) Polymorphic fibril formation by residues 10-40 of the Alzheimer's beta-amyloid peptide. *Biophys. J. 90*, 4618-4629.

(23) Petkova, A. T., Yau, W. M., and Tycko, R. (2006) Experimental constraints on quaternary structure in Alzheimer's beta-amyloid fibrils. *Biochemistry 45*, 498-512.

(24) Tiburu, E. K., Dave, P. C., Damodaran, K., and Lorigan, G. A. (2004) Investigating Leucine Side-Chain Dynamics and Backbone Conformations of Phospholamban Incorporated in Phospholipid Bilayers Utilizing ^{2}H and ^{15}N Solid-State NMR Spectroscopy. *Biochemistry 43*, 13899-13909.

(25) Tiburu, E. K., Dave, P. C., Vanlerberghe, J. F., Cardon, T. B., Minto, R. E., and Lorigan, G. A. (2003) An improved synthetic and purification procedure for the hydrophobic segment of the transmembrane peptide phospholamban. *Anal. Biochem. 318*, 146-151.

(26) Abu-Baker, S., and Lorigan, G. A. (2006) Phospholamban and its phosphorylated form interact differently with lipid bilayers: A ^{31}P, ^{2}H, and ^{13}C solid-state NMR spectroscopic study. *Biochemistry 45*, 13312-13322.

(27) Zamoon, J., Mascioni, A., Thomas, D. D., and Veglia, G. (2003) NMR solution structure and topological orientation of monomeric phospholamban in dodecylphosphocholine micelles. *Biophys. J. 85*, 2589-2598.

(28) Oxenoid, K., and Chou, J. J. (2005) The structure of phospholamban pentamer reveals a channel-like architecture in membrane. *Proc. Natl. Acad. Sci. USA 102*, 10870-10875.

(29) Nevzorov, A. A., and Opella, S. J. (2003) Structural fitting of PISEMA spectra of aligned proteins. *J. Magn. Reson. 160*, 33-39.